Adsorption and co-precipitation behavior of antimony with ferrihydrite and their silica effects

A dissertation submitted in partial fulfillment
of the requirements for the degree of
Doctor of Philosophy in Engineering

By

Shuang Zhou

Division of Sustainable Resources Engineering
Graduation School of Engineering, Hokkaido University, Japan

2019

Acknowledgement

I would like to express my sincere gratitude to my supervisor, Prof. Tsutomu Sato who provided me the chance to study and doing research at Hokkaido University. It has been an honor to be his Ph.D. student. I am grateful for his continuous support of my Ph.D. study and related research, for his patience, motivation and immense knowledge. His guidance helped me in all the time of research and writing of this thesis. I could not have imagined having a better advisor and mentor for my Ph.D. study.

Besides my supervisor, I would like to extend my particular appreciation to Associate Prof. Tsubasa Otake, for his kindness, academic assistance and valuable insights for my thesis. The door to his office was always open whenever I ran into a trouble spot or had a question about my research or writing. The advices he gave me not only helped my research but also impacted my daily life.

My sincere thanks also goes to Kumiko Kinoshita and Junko Hasegawa, who taught me to use the laboratory analytical instruments. Without they precious support it would not be possible to conduct this research. A very special gratitude goes out to our lab secretary Yoshie Hoshi who kept us organized and was always ready to help.

In my study of triple layer modeling fitting at Kanazawa University, I am particularly indebted to Associate Prof. Keisuke Fukushi. He taught me to use the extended triple layer model and set up the framework for fitting the model to adsorption data. His kindness and patience helped me a lot, I cannot finish this research without his precious help. It was fantastic to have the opportunity to work of my research in his facilities.

My sincere thanks also goes to the Chinese Government who have provided me the scholarship that enables me to study and accomplish my doctoral studies at Hokkaido University, who provided me an opportunity to see a big world. None of this could have happened without they precious support.

The members of the environment geology group have contributed immensely to my personal and professional time at Hokkaido University. The group has been a source of friendships as well as good advice and collaboration. I am grateful to my lab mates for their support and assistance of

my experiments especially to Ryohei Kawakita, Khamphila Khandala, Paul Clarence Francisco and Unguana Cornelio de Jesus Armindo. Many thanks also to Akane Ito, Kanako Toda, Frances Chikanda and those who helped me dealing with difficulties. It was great sharing laboratory with all of you during last three and a half years.

My time at Hokkaido University was made enjoyable in large part due to the many friends and groups that became a part of my life. I am grateful for time spent with friends, for my backpacking buddies and our memorable trips around Hokkaido, and for many other people and memories.

Last but by no means least, I must express my very profound gratitude to my family for all their love and providing me with unfailing support and continuous encouragement throughout my years of study. This accomplishment would not have been possible without them.

Thanks for all your encouragement!

Abstract

Antimony(Sb) is a natural occurring element widely dispersed in the lithosphere. Elevated antimony concentrations in aqueous environments from anthropogenic sources such as mining and smelting are becoming of global concern. In this respect ferrihydrite are known to strongly adsorb aqueous antimony species with different oxidation states, but the effect of silica on the removal characteristics is not well understood despite being a common component in the environment. A further important process, co-precipitation with ferrihydrite, does not appear to have been reported. In this study, first, the adsorption of antimonite (Sb(III)) and antimonate (Sb(V)) onto ferrihydrite were investigated as a function of initial pH, ionic strength, initial concentration and adsorbent dosage. It was further studied the adsorption process under the dissolved silica (Si) effect. Second, the surface complexation modeling was applied for the adsorption mechanism, the surface Sb(III) and Sb(V) species at different chemical conditions were evaluated. Finally, the adsorption and co-precipitation behavior of Sb(III) and Sb(V) with ferrihydrite and Si-bearing ferrihydrite was investigated.

Chapter 1 refers to the background of this study and the reviews the literature on the chemistry speciation of Sb, its distributions, the remediation from the natural environment as well as current knowledge on adsorption mechanism. This chapter describes iron oxides and hydroxides minerals such as goethite, hematite, and ferrihydrite, which are excellent scavengers for Sb adsorption due to their ubiquitous distribution in the surface, large specific surface area and unique surface characteristics. As iron minerals are closely associated with silica, one of the most common ligands present in natural environments, this could mean that silica may affect the crystallization behavior as well as the capacity of ferrihydrite to regulate hazardous element recycling.

Chapter 2 presents the literature review on surface complexation model of antimony and research objectives of this study, the drawbacks of the current using surface complexation model are identified. To gain knowledge on the adsorption mechanism of Sb on ferrihydrite, it is useful to develop a predictive model for the adsorption behaviors of Sb(III) and Sb(V) on ferrihydrite, which can predict both the adsorption effectiveness and surface speciation under variable solution conditions.

Chapter 3 refers to the adsorption of Sb on ferrihydrite and their silica effect. In this work, the X-ray diffraction (XRD) analyses of the precipitates showed two broad diffraction features at approximately 35° and 62° 2θ, which are characteristics of 2-line ferrihydrite, but no significant shifts in peak positions in the ferrihydrite regardless of the Si/Fe ratios. The infrared spectra showed a sharp band at ~930 cm^{-1}, corresponding to asymmetric stretching vibrations of Si-O-Fe bonds which increased in intensity with increasing Si/Fe molar ratios. Further, the surface charge on the precipitates became more negative with increasing Si/Fe molar ratios. The adsorption experiments indicated that Sb(V) was preferentially adsorbed under acidic conditions which decreased dramatically with increasing pH while the adsorption rate of Sb(III) was independent of pH. However, the presence of Si suppressed the adsorption of both Sb(III) and Sb(V).

Chapter 4 focuses on the adsorption mechanism of Sb(III) and Sb(V) on ferrihydrite. Adsorption data were modelled using an extended triple-layer model (ETLM) to infer Sb(III) and Sb(V) adsorption reactions and equilibrium constants. The two principal reactions of Sb(III) adsorption forming bidentate binuclear inner-sphere surface species were found to be consistent with the experimental data. Solution pH and ionic strength showed little effects on the adsorption of Sb(III). The adsorption of Sb(V) was represented by the formation of a monodendate-mononuclear outer-sphere and a bidentate-binuclear inner-sphere species. The Sb(V) adsorption on ferrihydrite decreases continuously with increasing pH and ionic strength. The predicted model speciation of Sb(V) on ferrihydrite showed that the inner-sphere species increase concomitantly with increasing pH and ionic strength and solid concentration. The outer-sphere species distribute over a wider range of pH conditions and are more important at lower ionic strengths.

Chapter 5 investigates the adsorption and co-precipitation behavior of Sb(III) and Sb(V) with ferrihydrite and Si-bearing ferrihydrite. The adsorption experiments indicated that Sb(V) was preferentially adsorbed under acidic conditions which decreased dramatically with increasing pH while the adsorption rate of Sb(III) was independent of pH. However, the presence of Si suppressed the adsorption of both Sb(III) and Sb(V). The results showed that Sb(III) and Sb(V) ions were significantly inhibited by co-precipitation with ferrihydrite even in the presence of Si by isomorphous substitution in the ferrihydrite crystal structure. Both adsorption and co-precipitation samples were analyzed by XRD for mineralogical characterization. In the

adsorption samples of the Si/Fe molar ratios precipitates series, all of the XRD patterns were almost identical to that of pure two-line ferrihydrite, and any other peaks and peak shift were not observed for both Sb(III) and Sb(V) loading. While the co-precipitation samples showed that the peak of ferrihydrite around 30° and 60° gradually shifted to a lower angle with Si/Fe ratio. In addition to these noticeable features, broadening of both peaks was also observed on co-precipitation samples. They suggest that the shift and broadening can be attributed to the differences in ionic radius and charge between Fe(III) and guest Sb in ferrihydrite.

Chapter 6 presents the summary and concluding remarks as well as a short outlook for future necessities and suggestions of research. Overall, this study investigated adsorption and co-precipitation of Sb on ferrihydrite and their silica effect to gain knowledge on Sb remediation mechanism. The establishment of ETLM for antimony adsorption may help to understand not only prediction of the environmental behavior but also to provide the effective countermeasure for the contamination. This study also has important implications for determining the role of ferrihydrite in controlling the final state of Sb in the environments in which it is released. Although ferrihydrite is an excellent substance for capturing Sb, its use as a medium in a natural Si-rich system should be considered with caution because it will tend towards inhibition of Sb capture induced by the Si-rich environment. However, this may be different in the case of co-precipitation processes. In the present study, we found that silica and Sb(III) and Sb(V) can be incorporated into ferrihydrite and that these three are structurally compatible with ferrihydrite. The co-precipitation process of Sb(III) and Sb(V) would not be greatly influenced by the silica factor. Thus, Sb(III) and Sb(V) co-precipitation with ferrihydrite would be more efficient than Sb(III) and Sb(V) adsorption by ferrihydrite. This finding will be important when making predictions of the final state of Sb associated with ferrihydrite in natural Si-rich systems. In order to further develop and apply the ferrihydrite in adsorption and co-precipitation process. The efficiency of ferrihydrite to remove Sb should be studied in different water matrices since the natural environment is a more complex condition.

Table of Contents

List of tables

List of figures

1. General introduction

Antimony (Sb) is a natural occurring element and situated fourth in the Group 15 of the periodic table. It is widely dispersed in the lithosphere and often present together with Arsenic (As). Sb is widely used in industry as a catalyst in plastics, flame retardants, storage batteries, and ammunition (Filella et al., 2002a)(Carlin Jr, 2000)(Herbst et al., 1985). It is the ninth most mined metal for industrial uses worldwide (Krachler et al., 2001)(Filella et al., 2002b), and one result of this is elevated concentrations of Sb in many soils and waters, especially around mining and smelting areas (Scheinost et al., 2006)(He, 2007)(Wang et al., 2011)(Westerhoff et al., 2008)(Mitsunobu et al., 2006)(Lichti et al., 2015)(Okkenhaug et al., 2012). There has been a growing concern over the adverse effect of Sb on human health due to its toxicity. Sb has been increasingly identified as a toxic heavy metal with implications for it being a carcinogen (Gebel, 1997). This has caused Sb and its compounds to be listed as a leading pollutant by the United States Environmental Protection Agency (USEPA, 1979) and the Council of the European Union (CEC, 1976). In 1993, the WHO set a guideline of Sb in drinking water as a permissible level as 5.0 μg/L (Organization, 2004). However, unlike As, Sb first attracted public attention in the mid-1990 (Filella et al., 2009). In contrast to As, less information is available on Sb.

Recent studies have shown that both Sb(III) and Sb(V) appear to adsorb strongly onto iron oxides (Mitsunobu et al., 2006)(Mitsunobu et al., 2010)(Leuz et al., 2006)(Okkenhaug et al., 2013), which thereby strongly influence the speciation, mobility, and final states of Sb in the environment. Sb is preferentially associated with iron(III) (Fe(III)) oxyhydroxide in soils and sediments on the basis of direct evidence using extended X-ray absorption fine structure spectroscopy (EXAFS) (Scheinost et al., 2006)(Mitsunobu et al., 2006)(Ackermann et al., 2009). This would suggest that adsorption and incorporation processes into the Fe(III) oxyhydroxide phases would be able to control the mobility of Sb in natural environments. However, the surface structure of Sb(III) and Sb(V) binding with Fe(III) oxyhydroxide is still unclear. A further important process, co-precipitation with Fe(III) oxyhydroxide, does not appear to have been reported. In natural systems, Fe(III) (hydro)oxides are often identified in precipitates from the oxidation of iron(II) (Fe(II)) in the presence of the relevant anions. Thus, the precipitation process may be as important as adsorption, as a sequestration process of Sb species by Fe(III)

oxyhydroxide when groundwater with natural or added Fe comes in contact with air or oxygenated water takes place.

Further, as iron minerals are closely associated with silica (Si), one of the most common ligands present in natural environments, pure ferrihydrite is not, strictly speaking, present in nature. Silica always associates with ferrihydrite in the structure or on the ferrihydrite surface. This could mean that silica may affect the crystallization behavior as well as the capacity of ferrihydrite to regulate hazardous element recycling. The effect of silica on As adsorption has been reported for ferrihydrite (Swedlund and Webster, 1999), but no reports of the effect of silica on Sb adsorption or co-precipitation have been reported for other oxides.

1.1 Chemistry, speciation and toxicity

Sb, metalloid, fourth element of VA group of periodic table, has both inorganic and organic species in natural systems. Among them, inorganic species predominate over organic species for Sb in most environmental systems (Andreae et al., 1983)(Sun et al., 1999)(Ellwood and Maher, 2002). For inorganic speciation, Sb may be present in a variety of oxidation states (−III, 0, III, V) because of its s^2p^3 outer orbital electron configuration, however it is mainly found in the two oxidation states (III and V) in environmental, biological, and geochemical environments (Filella et al., 2002a)(Filella et al., 2002b). The Eh-pH diagram of Sb is shown in **Figure 1-1**. These two inorganic forms of Sb are subjected to hydrolysis in aquatic systems by forming hydroxide species. For example, $Sb(OH)_6^-$ is the only major form of Sb(V) over a wide range of pH, which is different with As(V) having the successive deprotonation steps over a similar range of pH. The dominant Sb(III) species is the uncharged pyramidal antimonous acid $Sb(OH)_3$ in a wide pH range from 2 to 11, and exists as $Sb(OH)_2^+$ in acidic media and as $Sb(OH)_4^-$ in basic media. The stability and structure of aqueous complexes formed by Sb(III) and Sb(V) with simple organic ligands were determined (Tella and Pokrovski, 2009), which showed that stable complexes could be formed between $Sb(OH)_3$ and oxalic, citric and lactic acids. Organic Sb species are less well understood than inorganic species but are known to exist. Attempts to understand Sb methylation have generally been inconclusive or contradictory (Dodd et al., 1992)(Gürleyük et al., 1997). Despite this, biologically mediated reduction and methylation of Sb compounds in *Pseudomonas fluorescens* bacterial cultures and soil samples has been confirmed (Gürleyük et al., 1997). The

biological production of trimethylantimony under reducing conditions, Jenkins (Jenkins et al., 1998) suggests that biomethylation of Sb may occur in environments such as in waterlogged soils. Conversely, mono-, dimethyl and trimethyl Sb compounds have been detected in oxidized seawaters (Andreae et al., 1981) and urban soils (Duester et al., 2005), and Brannon and Patrick (Brannon and Patrick, 1985) reported that unidentified Sb volatiles could be lost from sediments regardless of oxygen status. The toxicity of these volatile Sb species is not yet understood and little is known about their environmental chemistry.

Sb as a genotoxic element, is gaining increasing environmental concern due to its more toxic behavior to plants and animals than expected. Sb and its compounds to be listed as a leading pollutant by the United States Environmental Protection Agency (USEPA, 1979) and the Council of the European Union (CEC, 1976). In 1993, the WHO set a guideline of Sb in drinking water as a permissible level as 5.0 μg/L (Organization, 2004). Sb is on the list of hazardous substances under the Basel convention concerning the restriction of transfer of hazardous waste across borders (UNEP, 2001). Sb has no known biological function and like As, the toxicity of Sb in the environment strongly depend upon speciation (Filella et al., 2002a). There is still little knowledge about antimony toxicology and impact on the environment and human health. However, over the last decade, it is visible the growing interest on the research about this metalloid. Elemental Sb is more toxic than its salts; inorganic forms more toxic than organics; and, trivalent species more toxic than pentavalent forms (Stemmer, 1976), similar to the case of As (Oorts et al., 2008). Compared to Sb(V), Sb(III) reaches easily critical biological targets, and tends to be retained for longer periods of time in the body (Ceriotti and Amarasiriwardena, 2009). Sb(III) oxides had been shown to cause lung cancer in rats (Gebel, 1997). Both chronic exposure and long-term inhalation of Sb have undoubtedly harmful effects to eyes, skin and lungs (Cooper and Harrison, 2009). The accumulation of Sb in crops is a potential threat to human health and well-being.

1.2 Sources and distributions in natural systems

Sb occurs naturally in the environment at trace levels but it is less common in nature than As, the significance for human health and for the environment is equally important. Antimony and its compounds have distinct properties that can be used for a variety of purposes. Diantimony

trioxide (Sb_2O_3) is used as a catalyst in the production of polyethylene terephthalate (PET) and as a flame retardant in the production of plastics, textiles and rubber (Reimann et al., 2010). About 60% of antimony is consumed in flame retardants and 20% used in alloys (Biswas et al., 2009). Sb is used in brake linings, semiconductor components, battery grids, bearing and power transmission equipment, sheet and pipe and in pigments for paints. It is also applied as addictive in glassware and ceramics, as an active ingredient in the treatment of Leishmaniasis disease (Ceriotti and Amarasiriwardena, 2009) and, as elemental Sb, in ammunition (Guo et al., 2009). Antimony contamination is found in areas affected by mining activities, copper smelters or power plants. A significant input of Sb into the environment occurs at shooting ranges, since most bullets contain substantial amounts of Sb (Johnson et al., 2005). Due to antimony use in auto brake linings and disks, Sb release, as antimony trioxide (a potential carcinogen), occurs during braking (Ceriotti and Amarasiriwardena, 2009). China has the most rich Sb resources in the world and plays an important role in global anthropogenic emissions, leading to severe environmental contamination (He et al., 2012).

The abundance of Sb in the Earth's crust is approximately 0.2 mg/kg (Anderson, 2012). It is observed that more than 100 natural minerals contain Sb. Similar to As, Sb can be found in natural waters, sediments and soils, and in atmosphere as a result of natural processes and human activities (Filella et al., 2002a). Regarding to antimony, speciation and distribution in freshwater have not been extensively studied. Total Sb dissolved concentrations in groundwater have been reported in the range 0.010 - 1.5 mg/L (Filella et al., 2002a), but anthropogenic sources can be responsible for much higher levels. Sb levels in geothermal groundwater (Izmir, Turkey) were reported in the range of 0.06 - 26 mg/L (Aksoy et al., 2009). Groundwater in the vicinity of abandoned antimony mines in Slovakia presented Sb level up to1000 mg/L (Hiller et al., 2012). Moreover, Sb distribution in surface water has been reported from several studies, Sb levels in freshwaters have been reported in the range from ng/L to a few mg/L (Reimann et al., 2010)(Wang et al., 2011), with the average Sb concentration in world rivers being 1 mg/L (Wang et al., 2011). Higher concentrations related to localized anthropogenic sources can be found. In Stampede and Slate Creek watersheds, Kantishna Hills mining district (Alaska, USA) Sb concentrations of 239 μg/L were found (Ritchie et al., 2013) and high levels of Sb (2 - 6384 mg/L) were found in rivers around the world largest antimony mine at Xikuangshan area of

Hunan Province (China) (Wang et al., 2011). Antimony concentrations in sediments and soils are of the order of a few μg/g. Higher concentrations are directly related to anthropogenic sources, mainly proximity to smelting plants (Ainsworth et al., 1990)(Asami et al., 1992). Elevated concentrations in sediments near the outfalls of sewage and fertilizer facilities have also been reported (Papakostidis et al., 1975)(Grimanis et al., 1977). Antimony compounds are rather volatile and they are released into the atmosphere during the incineration of waste, fossil combustion, and during the smelting of metals. Antimony is one of the elements that show higher enrichments in aerosols over the concentrations expected from sea salt and from crustal sources (Steinnes, 1990)(Kersten et al., 1991)(Cutter, 1993)(Arimoto et al., 1995). For example, analysis of aerosol samples from Cape D'Aguilar, Hong Kong Island, China, showed that Sb concentrations in the total suspended particulates and the PM 10 (particles measuring 10 μm or less) fraction ranged from 0.032 to 17.0 and from 0.023 to 9.50 ng/m^3, respectively (Cheng et al., 2000). Thus, the distribution of Sb in the natural systems has largely affected by the human actives which resulted in a serious Sb contamination by releasing a large quantity of Sb into the environment (He et al., 2012)(Wilson et al., 2004).

1.3 Remediation of Sb from natural waters

The contamination of Sb in natural waters is a serious and worldwide problem and has become a challenge for scientists, considering legal limits and toxic effects, the removal of these metalloid from natural water is mandatory. Publications about antimony removal from water are limited compare to that of arsenic removal. Only in the last few decades antimony had gain particular interest probably as consequence of its toxic and carcinogenic nature as well as the elevated concentrations in the vicinity of smelters, chemical plants, and mining and mineralized areas (Tighe et al., 2005). A variety of technologies have been used and proposed to remove this toxic element from aqueous media, including oxidation, bioremediation, membrane separation, electrochemical methods, coagulation/flocculation and adsorption. In anoxic groundwater or even in wastewaters, Sb(III) can be quantitative significant in solution. A re-oxidation, to convert Sb(III) to the higher valence sate Sb(V), can be required prior to coagulation, adsorption processes or membrane filtration, to enhance the treatment efficiency. Leuz (Leuz and Johnson, 2005) concluded that O_2 was unlikely to be a significant oxidant in homogenous solution, but

that H_2O_2 might be responsible for the oxidation of Sb(III) in natural waters. In a recently study, bioremediation of antimony using sulfate-reducing bacteria was found effective (Wang et al., 2013). Sulfate-reducing bacteria convert sulfate ions in Sb mine drainage into sulfides that reduce Sb(V) to Sb(III) with formation of Sb_2S_3. Research on the removal of antimony by membrane processes is scarce and not published recently. However, Kang assumed that the removal of Sb in drinking water by reverse osmosis membranes has a higher efficiency than that of arsenic compounds, regardless of pH changes (Kang et al., 2000). For membrane separation technique, membrane contaminated, clogged and decay of membrane flux are the disadvantages of Sb removal. Electrodepositing (electrolytic reduction) was investigated for Sb removal from copper electrorefining and spent battery solutions (1500 and 3500 mg Sb/L) (Koparal et al., 2004) and from flotation water from an antimony mine (approx. 10 and 29 mg Sb/L) (Zhu et al., 2011). The effects of operation parameters such as current density, pH and standing time on the Sb removal efficiency were studied. Although high efficiencies were obtained (96-100%), further studies on this technique have to be done to evaluate the economical aspect of the process. Research of coagulation and flocculation showed that 80-90% Sb in the solution was removed with $FeCl_3$ as coagulant in specific controlled pH (Nakamura and Tokunaga, 1996). It was reported that 98% of Sb(V) was removed with proper pH and the proper dose of ferric coagulants. The removal of Sb(III) needed less ferric coagulant dose and certain pH range between 4.0 and 10.0. Comparing behaviors between Sb(III) and Sb(V) during coagulation, the removal efficiency of Sb(III) was higher than Sb(V) during ferric coagulation. In addition, Sb(III) was less affected by the interfering components like phosphate and humic acids (Guo et al., 2009). However, the toxic by-products and large amount of coagulant demand are regarded as the disadvantages of Sb removal.

Among these methods, adsorption is regarded as a promising technology for removing metalloids from water/wastewater in terms of the simplicity of operation, cost effectiveness and the regeneration capability e.g. (Ali and Gupta, 2007)(Ungureanu et al., 2015). The chemical properties of adsorbents and adsorbates are vital to the adsorption process. Numerous adsorbents were used for the removal of Sb, for example, aluminum oxides (Ilgen and Trainor, 2012)(Xu et al., 2001), manganese oxides (Wang et al., 2012), activated carbon (Navarro and Alguacil, 2002), resins (Riveros, 2010), clay minerals (Rakshit et al., 2015), as well as natural and synthetic iron

oxides (Kolbe et al., 2011)(Mittal et al., 2013). Fe is a ubiquitous element in the earth surface and often occurs as iron oxides and iron hydroxides. They are widespread in natural system and play an important role in many geological and biological processes. The iron oxide under the surface conditions including goethite, hematite, lepidocrocite, maghemite, ferrihydrite and schwertmannite (Schwertmann and Cornell, 2008). Among them, ferrihydrite is the mineral name identifying poorly ordered hydrous ferric oxide precipitates, it is a common product of low-temperature geochemical processes at the earth's surface; it has been identified in weathering crusts (Jackson and Keller, 1970), in precipitates from the oxidation of emerging Fe^{2+}-bearing waters (Fuller and Davis, 1989)(Carlson and Schwertmann, 1981), in the water column of lakes (Tipping et al., 1981), in bog and lake sediments (Schwertmann et al., 1982), and in various soil horizons (ADAMS and KASSIM, 1984).

Because of its reactivity and large specific surface area, ferrihydrite is believed to be one of the most important adsorbents of minor elements in surface and groundwater systems (Davis and Kent, 1990). This premise is based on studies of its absorptivity in natural environments as well as numerous laboratory studies of cation adsorption and anion adsorption. In natural systems, iron(III)(hydro)oxides are often identified in precipitates from the oxidation of iron(II) in the presence of the relevant anions. Thus, the precipitation process may be as important as adsorption, as a sequestration process of Sb species by iron (III) (oxyhdr)oxides when groundwater with natural or added Fe comes in contact with air or oxygenated water takes place. Precipitation of metals as insoluble hydroxides, carbonates, or sulfides is widely practiced for treating industrial wastewaters prior to discharge to the environment. But the co-precipitation of antimony on ferrihydrite, which is the simultaneous removal of a foreign ion (e.g. Sb(III) or Sb(V)) during the formation of ferrihydrite has not been previously studies. Further, as iron minerals are closely associated with silica, one of the most common ligands present in natural environments, pure ferrihydrite is not, strictly speaking, present in nature. Silica always associates with ferrihydrite in the structure or on the ferrihydrite surface. This could mean that silica may affect the crystallization behavior as well as the capacity of ferrihydrite to regulate hazardous element recycling. The effect of silica on arsenic adsorption has been reported for ferrihydrite (Swedlund and Webster, 1999), but no reports of the effect of silica on Sb adsorption or co-precipitation have been reported for other oxides.

1.4 Adsorption and co-precipitation behavior of Sb on iron oxides

The adsorption behavior of Sb was studied on different types of iron oxides, for example, on goethite (Leuz et al., 2006), hematite (Shan et al., 2014) and magnetite (Mittal et al., 2013). It was observed that the factor of pH had an evident influence on the adsorption behavior of Sb. The adsorption of Sb(V) was favored at acidic pH while the adsorption of Sb(III) was constant over a broad range of pH on iron hydroxides (Guo et al., 2014)(Leuz et al., 2006). It was also reported that Sb(III) adsorption was independent on pH and ionic strength on the red earth soil with rich iron oxides while the highest Sb(V) adsorption occurred at lowest pH and affected by the ionic strength (Vithanage et al., 2013). Shan (Shan et al., 2014) pointed out that the removal of trace Sb(III) by hematite modified magnetic nanoparticles was not obviously affected by the solution pH, the ionic strength and the coexisting anions (chloride, nitrate, sulfate and phosphate). Zhao (Zhao et al., 2014) evaluated Sb(III) and Sb(V) removal by zero-valent iron nanoparticles coated with PVA. The maximum adsorption capacity of both Sb(III) and Sb(V) was obtained at pH less than 5, but as pH increased Sb(III) adsorption dropped slightly while Sb(V) adsorption dropped significantly. The coexistence of oxyanions also could affect the removal efficiency of Sb. It was reported that the presence of nitrate, sulfate and phosphate had a slight effect on the adsorption of Sb(III), but sulfate, phosphate and carbonate inhibited the adsorption of Sb(V) (He et al., 2015)(Wu et al., 2010)(Xi et al., 2011). It was observed that the presence of phosphate significantly decreased Sb(III) adsorption on goethite and the presence of nitrate and sulfate had no effect on the adsorption of Sb(III)(Xi et al., 2014). However, to the best of our knowledge, there were no reports about the silica effect on the adsorption of Sb(III) and Sb(V) on ferrihydrite in previous studies. Sb adsorption by hydrous oxide surfaces is widely reported as we mentioned, However, direct detailed comparison of adsorption and co-precipitation is rare, especially for Sb and ferrihydrite. More specifically, few have explored these processes from the perspective of achieving low residual Sb levels using ferrihydrite.

1.5 Adsorption mechanism of Sb

Adsorption is the accumulation of a chemical species at the interface between a solid phase and a fluid phase. Adsorption processes of Sb have been described using a variety of approaches. For example, the adsorption mechanisms of Sb were assessed by the empirical adsorption models

such as Langmuir and Freundlich isotherms. He (He et al., 2015) have illustrated that the Freundlich model was better than the Langmuir model to describe the adsorption of Sb(III) and Sb(V) on the *in-situ* FeO_xH_y. While Zhao (Zhao et al., 2014) have also demonstrated that the Langmuir model fitted the experimental data better than the Freundlich model for both Sb(III) and Sb(V) adsorption by a polyvinyl alcohol-stabilized granular adsorbent containing nanoscale zero-valent iron. However, empirical adsorption models provide descriptions of experimental adsorption data without any theoretical basis, which are of limited use in describing geochemical systems with changing solution or mineral chemistry. This is because they do not account explicitly for the development of electrical charge on mineral surfaces with the addition (or removal) of surface species. Furthermore, these models do not include any structural information regarding adsorbed species. Because the structure of an adsorbed species largely determines its reactivity, this is particularly limiting when a species may adsorb at a mineral surface with different structures, depending on solution or mineral surface conditions. Many of the shortcomings of the isotherm to modeling adsorption may be overcome by explicitly representing the chemical structure of the mineral-water interface, as is done in 'surface complexation models' (SCMs). There are only a few studies using surface complexation models (Guo et al., 2014)(Vithanage et al., 2013). To the best of our knowledge, no surface complexation modeling approach of Sb adsorption on ferrihydrite has been published. Thus, the study of the surface complexation modeling of antimony adsorption on ferrihydrite is more meaningful. The potential for predicting the competitive adsorption mechanism of Sb using modeling methods needs further studies.

Spectroscopy methods are extensively used to study the adsorption mechanisms of ions on surfaces, including Fourier transform infrared (FTIR), extended X-ray absorption fine structure spectroscopy (EXAFS), X-ray photoelectron spectroscopy (XPS), and Raman spectroscopy. Spectroscopy techniques are also used to determine the adsorption mechanism of Sb, which was mainly adsorbed in an inner-sphere mode on the surface sites of iron oxides (McComb et al., 2007)(Mitsunobu et al., 2010)(Vithanage et al., 2013), aluminum oxides (Ilgen and Trainor, 2012), Fe-modified aerobic granules (Wang et al., 2015). However, the data from either macroscopic or spectroscopic of Sb adsorption on ferrihydrite in natural systems investigations

are scarce. Liking sophisticated hydrologic models to spectroscopy evidence offers great potential in furthering our understanding of adsorption processes.

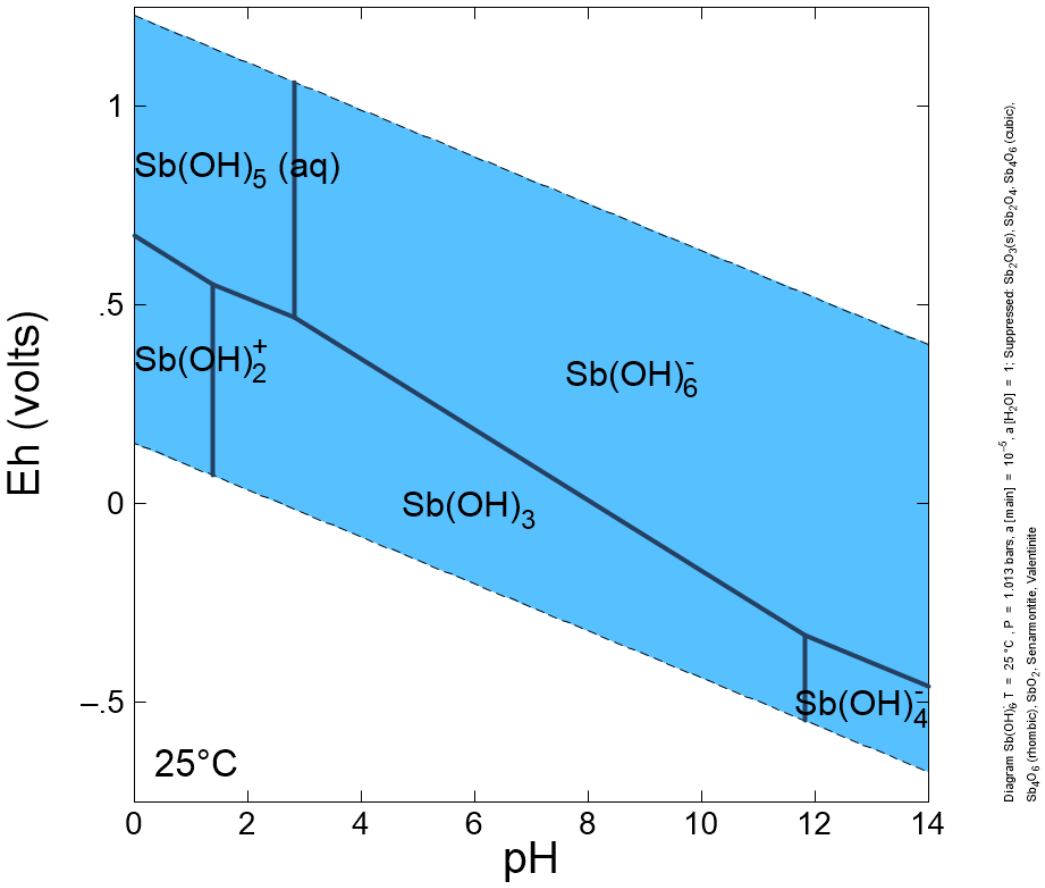

Figure 1-1 Eh-pH diagram of Sb in the Sb-H_2O system at Sb activity of 10^{-6} M and at 1 bars.

2. Review of surface complexation modeling of antimony adsorption and objectives

2.1 Surface complexation modeling

As mentioned in the previous chapter, many of the shortcomings of the isotherm approaches to modeling adsorption may be overcome by explicitly representing the chemical structure of the mineral-water interface, as is done in "surface complexation models" (SCMs). SCMs, which are based on thermodynamics and which are analogous to aqueous speciation models, are a powerful approach to surface reaction modeling (Sposito and others, 1984)(Sposito, 1990)(Davis and Kent, 1990)(Dzombak and Morel, 1990)(Morel et al., 1993)(Schindler, 1990)(Stumm, 1992)(Stumm and Morgan, 2012). Various chemical surface complexation models have been developed to describe potentiometric titration and metal adsorption data at the oxide-mineral solution interface. Surface complexation models provide molecular descriptions of metal adsorption using an equilibrium approach that defines surface species, chemical reactions, mass balances, and charge balances. Thermodynamic properties such as solid-phase activity coefficients and equilibrium constants are calculated mathematically. The major advancement of the chemical surface complexation models is consideration of charge on both the adsorbate metal ion and the adsorbent surface. In addition, these models can provide insight into the stoichiometry and reactivity of adsorbed species.

As emphasized by Dzombak and Koretsky (Dzombak and Morel, 1990)(Koretsky, 2000), surface complexation models of the solid-solution interface share at least six common assumptions: (1) surfaces can be described as planes of constant electrical potential with a specific surface site density; (2) equations can be written to describe reactions between solution species and the surface sites; (3) the reactants and products in these equations are at local equilibrium and their relative concentrations can be described using mass law equations; (4) variable charge at the mineral surface is a direct result of chemical reactions at the surface; (5) the effect of surface charge on measured equilibrium constants can be calculated; and (6) the intrinsic (i.e., charge and potential independent) equilibrium constants can then be extracted from experimental measurements (Dzombak and Morel, 1990)(Koretsky, 2000).

Three of the most commonly chemical surface complexation models that have been applied to metal and metalloid adsorption by reference minerals or soil systems are described. The constant capacitance model, the diffuse double layer model, and the triple layer model, they use the same approach in writing chemical reactions between the bulk solution and the solid surface. Each of these models assumes that all of the sites on a solid surface can be described by average surface site characteristics. If two or more surface site types are used to fit adsorption data with these models, the site types are still generic in nature, with no specific correlation to the solid surface structure. The three models differ in their approach and level of detail used to describe the charge and electric potential gradients at the solid-solution interface. In all three models, the surface sites are amphoteric surface hydroxyl groups that pronate and deprotonate as a function of pH.

Table 2-1 summarizes the three SCMs in terms of the adjustable parameters, the allowed surface chemical reactions, and the charge potential relationships. Surface charge-balance and mass-balance equations for each of the models are given in **Table 2-2. Figure 2-1**, **Figure 2-2** and **Figure 2-3** depicts the physical-chemical structure of the interfacial region and the interfacial charge and potential relationships for each of these models.

2.2 Surface complexation models of antimony adsorption

Surface complexation models (SCMs) have emerged as one of the most promising tools for predicting metal(loid) ion sorption to oxides and clay materials and have been well studied (S. Korichi, A. Elias, A. Mefti, 2009)(Pakzadeh and Batista, 2011)(Pokrovsky et al., 2012). SCMs have been used successfully to predict the adsorption of several different ions onto a wide range of adsorbents over a fairly extensive set of aqueous solution conditions. As a consequence, SCMs will be effective in understanding the basic characteristics of Sb adsorption and in predicting its behavior in the environment. To our knowledge, SCMs have not been widely applied to Sb adsorption in aqueous solutions (Leuz et al., 2006)(Rakshit et al., 2011), especially to assess Sb adsorption on ferrihydrite. Very few studies to date have reported surface complexation of Sb (V) on ferrihydrite using the above SCM approaches, although there are few data reported the Sb adsorption on other natural minerals. For example, Guo (Guo et al., 2009) employed DLM for both Sb(III) and Sb(V) adsorption at various pH during ferric chloride coagulation but the data can only be roughly predicted and there are still some discrepancies

between the theoretical model and the real experimental results. The modified triple-layer model was use to describe the Sb(V) adsorption on goethite, but the influence of ionic strength on the sorption of Sb(V) could not be predicted by the modified TLM using either outer-sphere surface complexes alone or a combination of inner-sphere and outer-sphere surface complexes (Leuz et al., 2006). Guo (Guo et al., 2014) used DLM to simulated Sb(III) and Sb(V) adsorption edges on goethite, the adsorption capacity was drastically overestimated at alkaline pH. And some discrepancy for Sb(III) adsorption on goethite and Sb(V) adsorption at lower pHs. All these results shown that the moderate agreement between the modeling fits and experimental data was obtained with significant discrepancy ant relatively lower or higher pH.

Hence, it is useful to develop a predictive model for the adsorption behaviors of Sb(III) and Sb(V) on ferrihydrite, which can predict both the adsorption effectiveness and surface speciation under variable solution conditions. The extended triple-layer model (ETLM), which is a SCM, has predicted the surface complexes as a function of pH, ionic strength and solid concentration independently, consistent with spectroscopic results in many anion-mineral systems, such as sulfate, selenate, arsenite and arsenate (Sverjensky, 2005)(Sverjensky and Fukushi, 2006a)(Sverjensky and Fukushi, 2006b)(Fukushi and Sverjensky, 2007a)(Fukushi and Sverjensky, 2007b)(Kanematsu et al., 2010). Recently studies have attempted to characterize Sb adsorption surface speciation based on spectroscopic techniques such as X-ray photoelectron spectroscopy (XPS), Fourier transform infrared (FT-IR) spectroscopy, and extended X-ray absorption fine structure (EXAFS) (Ilgen and Trainor, 2012)(Wu et al., 2010)(Mitsunobu et al., 2010)(McComb et al., 2007). But the spectroscopic studies of surface speciation have not been intergraded with surface complexation models at all. Integration of both surface complexation model and spectroscopic techniques would be useful to characterize the Sb(V) adsorption mechanism. Thus, employing the ETLM to predict the adsorption of Sb on ferrihydrite is more meaningful.

2.3 Scopes and objectives

This study mainly focused on investigating the adsorption properties of Sb on ferrihydrite and co-precipitation process of Sb with ferrihydrite under silica effect. So far, most studies have been involved in the adsorption of Sb on iron oxides individually. However, in natural systems, Fe(III)

oxyhydroxides are often identified in precipitates from the oxidation of Fe(II) in the presence of the relevant anions. Thus, the precipitation process may be as important as adsorption, as a sequestration process of Sb species by Fe(III) oxyhydroxides when groundwater with natural or added Fe comes in contact with air or oxygenated water takes place. Further, as iron minerals are closely associated with silica, one of the most common ligands present in natural environments, pure ferrihydrite is not, strictly speaking, present in nature. Silica always associates with ferrihydrite in the structure or on the ferrihydrite surface. This could mean that silica may affect the crystallization behavior as well as the capacity of ferrihydrite to regulate hazardous element recycling. Thus it is more meaningful to study the adsorption and co-precipitation behavior of Sb with ferrihydrite under silica effect. This study also contributes to better understand the fate, mobility and transport of Sb in the environment. This project mainly involved:

1) Batch experiments were carried out to investigate the adsorption behavior of Sb(III) and Sb(V) on ferrihydrite, by varying pH adsorbent dosage, initial concentrations and ionic strength. The dissolved Si effect on the adsorption of Sb(III) and Sb(V) on ferrihydrite has also been conducted.

2) The Extended Triple Layer Modeling (ETLM), which is a SCM. Has been used for prediction of the Sb(III) and Sb(V) adsorption on ferrihydrite in different chemical conditions.

3) The adsorption and co-precipitation of Sb with ferrihydrite was evaluated under varies Si/Fe ratios. The post-adsorption samples and co-precipitation samples of Sb(III) and Sb(V) were studies. The difference of the adsorption and co-precipitation of Sb with ferrihydrite were discussed.

Specifically, three papers are presented in this thesis. The first paper “Adsorption of antimony on ferrihydrite and their silica effect” (Chapter 3), gives an overview about the adsorption behavior of Sb(III) and Sb(V) on ferrihydrite and their silica effect. The main objective in this study was to compare the relative adsorption capabilities of Sb(III) and Sb(V) onto ferrihydrite, (2) to evaluate the effect of dissolved silica during the adsorption of Sb(III) and Sb(V) on ferrihydrite.

Chapter 4 with the title of “Surface complexation modeling for antimony adsorption on ferrihydrite and their silica effect” was a subsequent study of the adsorption behavior of Sb(III) and Sb(V) by ferrihydrite in different chemical conditions such as pH, ionic strength, and solid

concentration. Adsorption data were analyzed using an extended triple-layer modeling (ETLM) for surface complexation modeling to infer Sb(III) and Sb(V) reactions and equilibrium constants.

Chapter 5 is about “Difference between antimony adsorption onto ferrihydrite and antimony co-precipitated with ferrihydrite and their silica effect”. In this study, ferrihydrite was synthesized at various Si/Fe molar ratios to investigate its adsorption and co-precipitation behaviors with aqueous antimony anionic species, Sb(III) and Sb(V). This study showed that both the adsorption experiments indicated that Sb(V) was preferentially adsorbed under acidic conditions which decreased dramatically with increasing pH while the adsorption rate of Sb(III) ions was independent of pH. However, the presence of silica suppressed the adsorption of both Sb(III) and Sb(V). The results showed that Sb(III) and Sb(V) ions were significantly inhibited by co-precipitation with ferrihydrite even in the presence of silica by isomorphous substitution in the ferrihydrite crystal structure.

Table 2-1 Surface complexation reactions and model parameters (modified from (Hayes et al., 1991))

CCM	DLM	TLM
	Proteolysis reaction	
$SOH + H^+ = SOH_2^+ \quad K^+$ $SOH = SO^- + H^+ \quad K^-$	Same as CCM	Same as CCM
	Surface complexation reactions	
	Coordination Complexes	
$SOH + Me^{2+} = SOMe^+ + H^+ \; K_{Me}$ $SOH + L^- = SL + OH^- \quad K_L$	Same as CCM	Same as CCM
	Ion-pair complexes	
Not allowed	Not allowed	$SOH + Cat^+ = SO\_Cat^+ + H^+ \; K_{Cat}$ $SOH + An^- + H^+ = SOH_2^+ \_ An^- \quad K_{An}$
	Charge-potential relationships	
$\sigma_0 = C_1 \psi_0$	$-\sigma_0 = \sigma_d = -0.1174\sqrt{I}\sinh(zF\psi_d/2RT)$ $\psi_0 = \psi_d$	$\sigma_d = -0.1174\sqrt{I}\sinh(zF\psi_d/2RT)$ $\sigma_0 = (\psi_0 - \psi_\beta)C_1$ $\sigma_0 + \sigma_\beta = (\psi_\beta - \psi_d)C_2 = -\sigma_d$
	Adjustable model parameters	
K^+, K^-, N_s, C_1	K^+, K^-, N_s	$K^+, K^-, K_{Cat}, K_{An}, N_s, C_1, C_2$

Table 2-2 Surface charge and mass balance equations [a]

Model	Surface charge balance equations [b]	Surface mass balance equations
CCM	$\sigma_0 = B([SOH_2^+] - [SO^-])$	$S_T = [SOH] + [SOH_2^+] + [SO^-] + [SL] + [SOMe^+]$
DLM	Same as for CCM	Same as for CCM
TLM	$\sigma_0 = B([SOH_2^+] + [SOH_2^+\_An^-] + [SOMe^+] - [SO^-] - [SOH_2^+\_Cat^-])$ $\sigma_\beta = B(+ [SOH_2^+\_Cat^-] - [SOH_2^+\_An^-])$	$S_T = [SOH] + [SOH_2^+] + [SO^-] + [SOH_2^+\_An^-] + [SOH_2^+\_Cat^-] + [SL] + [SOMe^+]$

[a] Equations written for systems described in ***Table 2-1***.

[b] The constant, B, converts surface charge from mole/liter to C/m^2; $B=F/C_S S_A$ where F is Faraday's constant, C_S is the solids concentrations in g/liter, and S_A is the specific surface area of the solid in m^2/g.

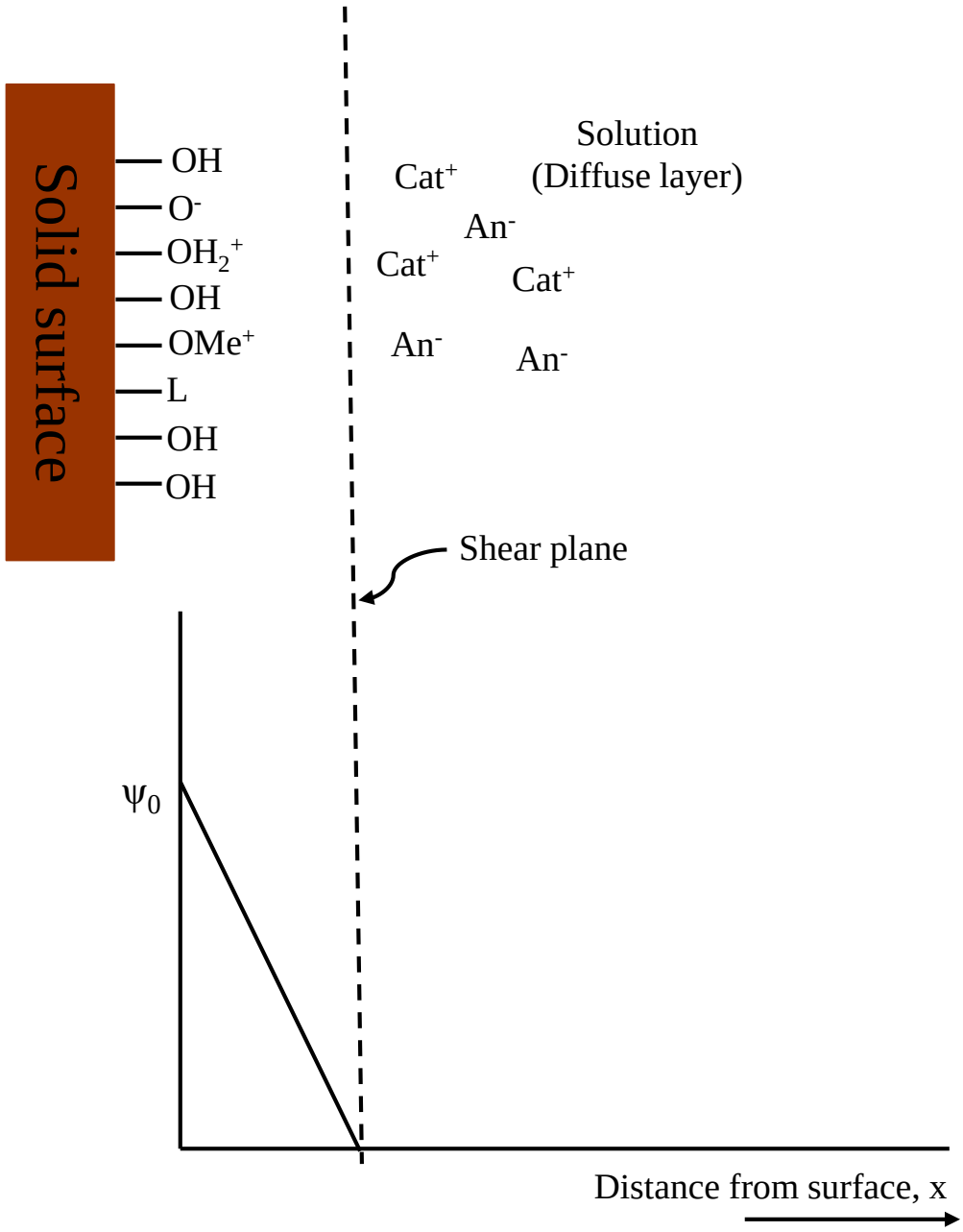

Figure 2-1 Schematic representation of physical-chemical structure of the interfacial region and interfacial charge and potential relationships for CCM (Modified from (Hayes et al., 1991)).

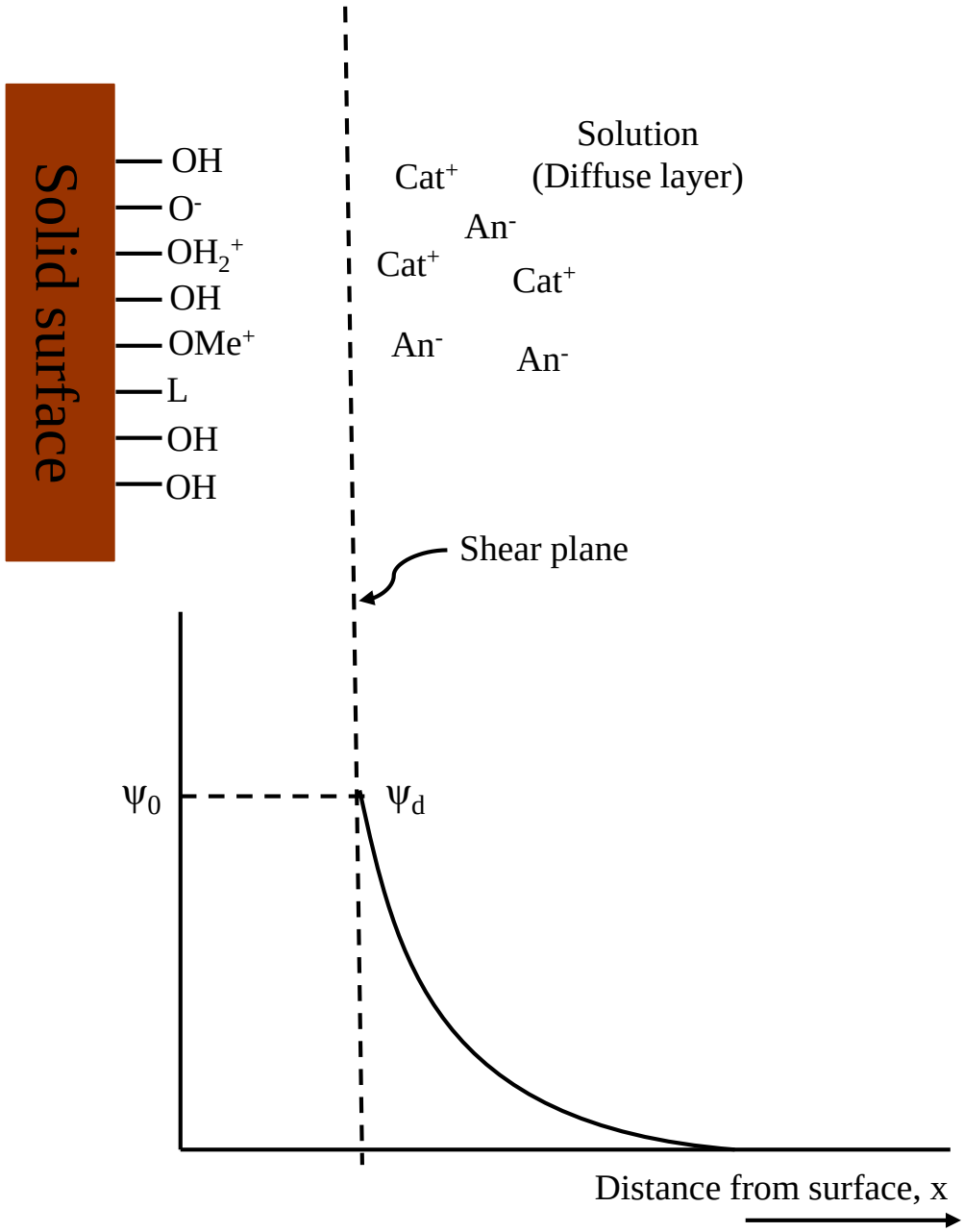

Figure 2-2 Schematic representation of physical-chemical structure of the interfacial region and interfacial charge and potential relationships for DLM (Modified from (Hayes et al., 1991)).

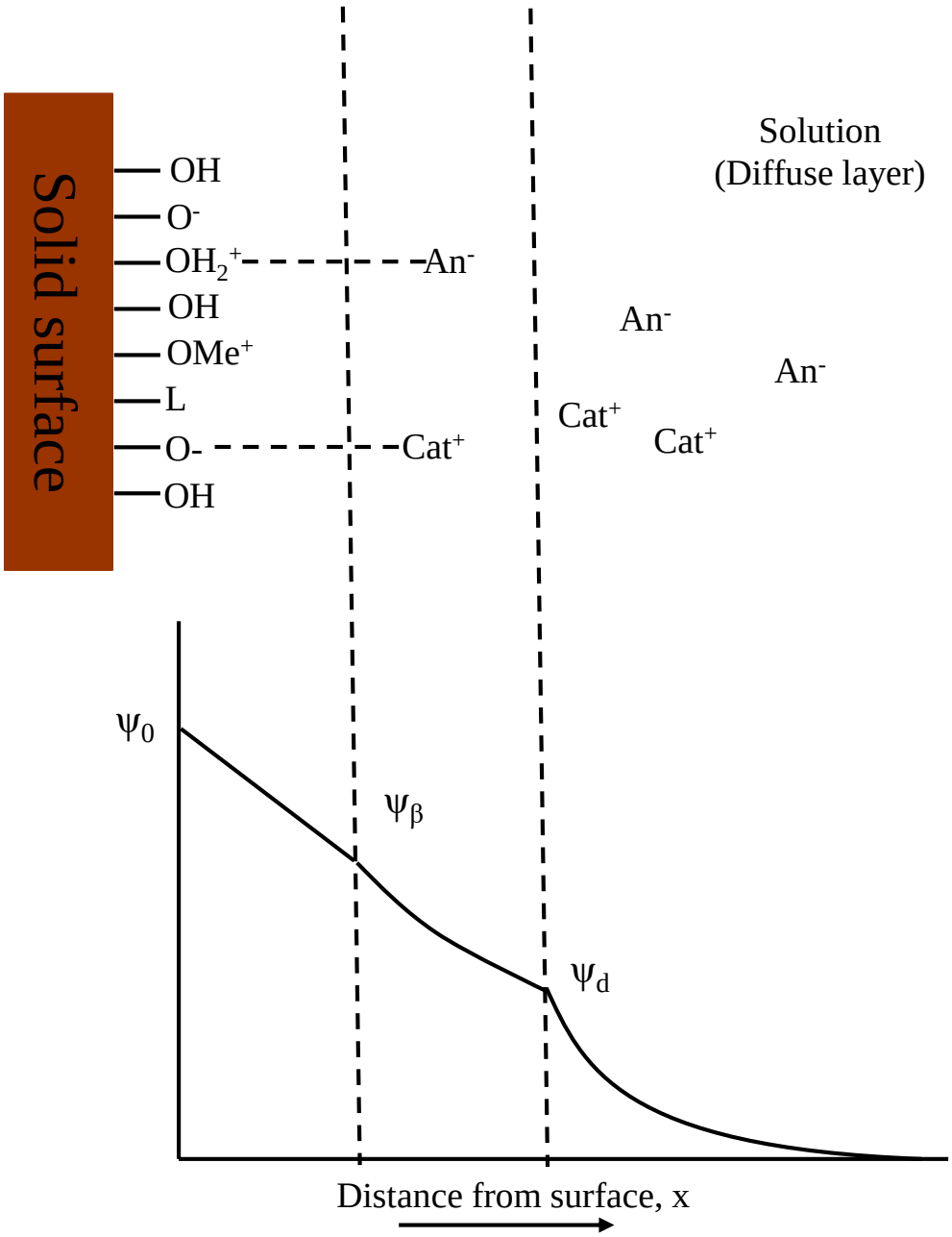

Figure 2-3 Schematic representation of physical-chemical structure of the interfacial region and interfacial charge and potential relationships for TLM (Modified from (Hayes et al., 1991)).

3. Adsorption of antimony on ferrihydrite and their silica effect

Abstract

Elevated antimony concentrations in aqueous environments from anthropogenic sources are becoming of global concern. In this respect iron oxides are known to strongly adsorb aqueous antimony species with different oxidation states, but the effect of silica on the removal characteristics is not well understood despite being a common component in the environment. In this study, ferrihydrite was synthesized at various Si/Fe molar ratios to investigate its adsorption and co-precipitation behaviors with aqueous antimony anionic species, Sb(III) and Sb(V). The X-ray diffraction (XRD) analyses of the precipitates showed two broad diffraction features at approximately 35° and 62° 2θ, which are characteristics of 2-line ferrihydrite, but no significant shifts in peak positions in the ferrihydrite regardless of the Si/Fe ratios. The infrared spectra showed a sharp band at ~930 cm^{-1}, corresponding to asymmetric stretching vibrations of Si-O-Fe bonds which increased in intensity with increasing Si/Fe molar ratios. Further, the surface charge on the precipitates became more negative with increasing Si/Fe molar ratios. The adsorption experiments indicated that Sb(V) was preferentially adsorbed under acidic conditions which decreased dramatically with increasing pH while the adsorption rate of Sb(III) ions was independent of pH. However, the presence of silica suppressed the adsorption of both Sb(III) and Sb(V) ions.

3.1 Introduction

Antimony (Sb) is widely used in industry as a catalyst in plastics, flame retardants, storage batteries, and ammunition (Filella et al., 2002a)(Carlin Jr, 2000)(Herbst et al., 1985). It is the ninth most mined metal for industrial uses worldwide (Krachler et al., 2001)(Filella et al., 2002b), and one result of this is elevated concentrations of Sb in many soils and waters, especially around mining and smelting areas (Scheinost et al., 2006)(He, 2007)(Wang et al., 2011)(Westerhoff et al., 2008)(Mitsunobu et al., 2006)(Lichti et al., 2015)(Okkenhaug et al., 2012). There has been a growing concern over the adverse effect of Sb on human health due to

its toxicity. Sb has been increasingly identified as a toxic heavy metal with implications for it being a carcinogen (Gebel, 1997). This has caused Sb and its compounds to be listed as a leading pollutant by the United States Environmental Protection Agency (USEPA, 1979) and the Council of the European Union (CEC, 1976).

Sb may be present in a variety of oxidation states (−III, 0, III, V) because of its s^2p^3 outer orbital electron configuration, however it is mainly found in the two oxidation states (III and V) in environmental, biological, and geochemical environments (Filella et al., 2002a)(Filella et al., 2002b). The toxicity of Sb depends strongly on its oxidation state, and reduced Sb(III) species are ten times more poisonous than oxidized Sb(V), similar to the case of arsenic (Oorts et al., 2008). In spite of the widespread usage and the substantial toxicity, the geochemical behaviors of antimony in soil and aquatic systems are poorly understood (Krupka and Serne, 2002)(Mitsunobu et al., 2010).

Recent studies have shown that both Sb(III) and Sb(V) appear to adsorb strongly onto iron oxides (Mitsunobu et al., 2006)(Mitsunobu et al., 2010) (Leuz et al., 2006)(Okkenhaug et al., 2013), which thereby strongly influence the speciation, mobility, and final states of Sb in the environment. Sb is preferentially associated with iron(III) oxyhydroxide in soils and sediments on the basis of direct evidence using extended X-ray absorption fine structure spectroscopy (EXAFS) (Scheinost et al., 2006)(Mitsunobu et al., 2006)(Ackermann et al., 2009). This would suggest that adsorption and incorporation processes into the iron(III) (oxyhydr)oxide phases would be able to control the mobility of Sb in natural environments. Several experimental studies have investigated the Sb adsorption mechanism on iron(III) oxyhydroxides, focusing on Sb speciation at the solid-liquid (water) interface using EXAFS (Mitsunobu et al., 2006)(Guo et al., 2014). However, the surface structure of Sb(III) and Sb(V) binding with iron(III) oxyhydroxides is still unclear. Further, as iron minerals are closely associated with silica, one of the most common ligands present in natural environments, pure ferrihydrite is not, strictly speaking, present in nature. Silica always associates with ferrihydrite in the structure or on the ferrihydrite surface. This could mean that silica may affect the crystallization behavior as well as the capacity of ferrihydrite to regulate hazardous element recycling. The effect of silica on arsenic adsorption has been reported for ferrihydrite (Swedlund and Webster, 1999), but no reports of the effect of silica on Sb adsorption or co-precipitation have been reported for other oxides.

Based on the above, the objectives of this study were to (1) to compare the relative adsorption capabilities of Sb(III) and Sb(V) onto ferrihydrite, (2) to evaluate the effect of dissolved silica during the adsorption and co-precipitation of Sb(III) and Sb(V) on ferrihydrite.

3.2 Materials and methods

3.2.1 Synthesis

A stock solution of ferric iron (Fe(III), 0.05 mol/L), was prepared by dissolving reagent grade $Fe(NO_3)_3 \cdot 9H_2O$ (Kanto,99%, Tokyo, Japan) in ultrapure water (18M·W·cm). Tetraethylorthosilicate (TEOS; Alfa Aesar, 98%, Heysham, United Kingdom) was then added to 500 mL of the Fe solution to achieve silica concentrations of 0 to 20×10^{-3} mol/L (i.e., Si/Fe = 0.4). These solutions containing both silica and Fe(III) were stirred for about 30 min to dissolve the TEOS completely before pH adjustment. The initial pH of the solution was about 1.8, which was adjusted to about 7.0±0.1 by titrating 1.0 M NaOH (Kanto, 97%, Tokyo, Japan). Addition of the NaOH hydrolyzes the Fe(III) in the solution resulting in formation of a slurry of dark brown precipitate. The slurries were stirred for an additional 15 min to allow the pH to stabilize. The resulting 500 mL slurries were then equally divided into 50 mL polypropylene bottles and then washed in the bottles at least four times with deionized water to remove the salts and freeze-dried for at least 24 h. Samples with different silica concentrations were replicated to evaluate the reproducibility of the experimental results.

3.2.2 Adsorption experiments

Stock solutions of Sb(V) were prepared by dissolving $KSb(OH)_6$ powder (Wako, 50%, Tokyo, Japan) into deionized water, and of Sb(III) by dissolving Sb2O3 powder (Wako, 98%, Tokyo, Japan) into 2 mol/L HCl (Kanto, 37%, Tokyo, Japan) solution. The initial concentration of both the Sb(III) and Sb(V) was 100 μM. A control experiment showed that neither Sb(III) nor Sb(V) precipitated under this initial concentration. The adsorption experiments with both Sb(III) and Sb(V) were conducted at a solid concentration of 0.5 g/L with a background ionic strength of 0.01 M NaCl. Triplicates of 40 mL suspensions with a fixed amount of solids (20 mg) and 100 μM solute concentrations were prepared in 50 mL polypropylene bottles. The experiments were conducted at a pH range of 3-12. The pH of the suspensions was adjusted using small volumes of

0.5 M HCl or 0.5 M NaOH during the experiments. Suspensions were agitated on a rotary shaker (110 rpm) for 24 h at 20.5 °C. After the reaction, the suspensions were centrifuged and then filtered through a 0.2 μm cellulose membrane filter for further analysis.

3.2.3 Analytical methods

The powder X-ray diffraction (XRD) analyses were conducted to determine the mineralogy of the dark brown precipitates. Synthesized precipitates were analyzed by XRD using a Rigaku RINT2000 (Rigaku Co., Tokyo, Japan) X-ray diffractometer operated at 40 kV and 40 mA, equipped with a Cu target and graphite monochromator, and diffraction profiles were collected from 10° to 70° 2θ.

To identify the chemical bonds in the initial adsorbents, Fourier transform infrared spectroscopy (FTIR) analyses were conducted. The FTIR spectra were recorded from 400 to 4000 cm^{-1} by a JASCO FTIR-4100 spectrometer (JASCO international Co., Ltd., Tokyo, Japan) with a 1.0 cm^{-1} spectral resolution. The potassium bromide (KBr) used to prepare the sample was heated at 110 °C for two hours prior to analysis to remove water. The blank KBr sample (i.e., pure KBr only, in pellet form) was measured first in order to account for the matrix background. Pellets for analyzing were prepared by pulverizing the precipitates and mixing with KBr at a 1.5 mg precipitate to 250 mg KBr ratio.

To examine the surface charge properties of the initial adsorbents, the ζ-potential measurements at different pH were conducted. The ζ-potential of the samples was measured using a Zetasizer Nano ZS90 (Malvern Zetasizer Nano series Nano-ZS90, Malvern Instruments Ltd., Malvern, United Kingdom). Freeze-dried precipitates were re-suspended in 10 mL deionized water to obtain a final mineral concentration of 100 mg/L. The auto-titration was initiated at pH values from 2 to 12 (in 0.5 pH increments) adjusting the pH with dilute HNO3 or NaOH solution.

To measure the concentration of Sb, Inductively Coupled Plasma (ICP)-Atomic Emission Spectroscopy (AES) analyses were conducted. Filtrates were analyzed for Sb(III) and Sb(V) as total Sb by ICP-AES (ICPE-9000). The detection limit of this method was 0.1 μg/L. The pH of the solutions was measured with a pH meter (HORIBA, D-55) calibrated by using commercial pH 4.0, 7.0, and 10.0 buffer solutions. The amount of solute adsorbed was calculated using the difference between the initial and final dissolved solute concentrations.

The XRD data were processed by Match (version 3.3.0) software (Crystal Impact. Bonn, Germany), FTIR data were processed by Spectra Manager^{TM} software (JASCO international Co., Ltd. Tokyo, Japan). All the graphs were exported by Sma4 (Version 1.47) software (T. Suzuki, Kyoto, Japan) and Microsoft office 2013.

3.3 Results

3.3.1 Characterization of initial adsorbents

XRD. The XRD analyses were conducted to determine the mineralogy of the dark brown precipitates. In all of the samples with the various initial ratios of Si/Fe, the XRD analyses of the dark brown precipitates, which were used as adsorbents in the following adsorption experiments, were characterized by two broad maxima centered at approximately 35° and 62° 2θ (**Figure 3-1**), consistent with the presence of 2-line ferrihydrite (Russell, 1979)(Cornell and Schwertmann, 2003). No significant shifts or changes in the width of the ferrihydrite peaks in these precipitates were observed in the range of silica concentration studied.

FTIR Spectroscopy. To identify the chemical bonds in the initial adsorbents, FTIR analyses were conducted, and the infrared spectra of the initial adsorbents were generally consistent with published data on ferrihydrite (Russell, 1979). Two distinct regions can be identified in the spectra (**Figure 3-2**). First, the area from ~1300 to ~1700 cm^{-1}, where relatively sharp adsorption bands at ~1350, ~1480, and ~1650 cm^{-1} corresponding to the vibrations of adsorbed water are observed. The most significant changes with increasing Si concentration are observed in the second region, where a relatively sharp band at ~930 cm^{-1} corresponding to asymmetric stretching vibrations of Si-O-Fe bonds appears and increases in intensity with increasing concentration of silica (Doelsch et al., 2003). Swedlund (Swedlund et al., 2010) reported that the presence of a small amount of polymeric silica could be observed at ~1060 cm^{-1} in high Si/Fe ratio. However, no peaks were observed at this position in this study, this may be explained by the relatively higher background in high Si/Fe ratio, which masks the vibrations in this region.

ζ-Potential. To examine the surface charge properties of the initial adsorbents, the ζ-potential measurements at different pH were conducted. The ζ-potentials of the initial precipitates are shown as a function of pH in **Figure 3-3**. In general, the pH_{pzc} (point of zero charge) of ferrihydrite

decreases with increasing silica content during the synthesis. For instance, the pH_{pzc} of ferrihydrite in the absence of silica was 8.2 and that of ferrihydrite at Si/Fe = 0.4 was 4.8, suggesting that the surface of the initial precipitates was more negatively charged after the silica loading.

The XRD results indicate that the Si/Fe of the precipitating solution does not influence the mineralogy of the initial precipitates. Rapid hydrolysis of the Fe(III) in solution due to the addition of NaOH resulted in the co-precipitation of silica and Fe into poorly ordered ferrihydrite. The FTIR data show that silica became closely associated with the ferrihydrite via the formation of Si-O-Fe groups, indicating that silica was incorporated into the structure of ferrihydrite. Pokrovski (Pokrovski et al., 2003) demonstrated that aqueous silica may form stable iron silicate aqueous complexes with polymeric ferric oxy-hydroxide species. However, recent studies have shown that silica could also occur on the surface (Seehra et al., 2004)(Dyer et al., 2010)(Cismasu et al., 2014). Detailed infrared spectra studies of adsorbed silica on ferrihydrite surfaces show the formation of bidentate surface complexes composed of monomeric silicate species at low silica ratios, similar to the concentrations used in this study (Swedlund et al., 2009). Formation of these silica surface complexes results in a net release of protons that decreases the positive charge on the precipitate surface (Hiemstra et al., 2007). This is consistent with the changes in the ζ-potential observed with increasing Si/Fe ratios (**Figure 3-3**). At high silica ratios, the surface can be expected to become more negative as the silica polymerizes and creates more acidic surface complexes (Swedlund et al., 2010).

3.4 Discussion

3.4.1 Sb(III) and Sb(V) adsorption in the absence of Silica

The adsorbed ratios of Sb(III) and Sb(V) ions onto ferrihydrite in 0.01 M NaCl solutions is shown as a function of pH in **Figure 3-4**. The adsorption rate of Sb(V) was over 90% between pH 3 and 6. With increasing pH, from 6 to 12, the adsorption rate of Sb(V) rapidly decreased from 90% to 10%. A strong pH dependence on Sb(V) adsorption was reported when goethite and ferrihydrite were used as adsorbents ((Guo et al., 2014)(Qi and Pichler, 2016)). The effect of pH on Sb(III) adsorption however was much weaker, showing a constant adsorbed fraction ~95% over the whole of the pH range investigated here, from 3 to 12. This is in good agreement with

earlier studies (Leuz et al., 2006)(Guo et al., 2014). The difference in adsorption efficiency of Sb(III) and Sb(V) ions may mainly be due to differences in the electrostatic interactions between the sorbent surface and Sb oxyanions present in the solutions. The $Sb(OH)_6^-$ is the dominant Sb(V) species over the wide pH range, here pH 3-10 (Filella et al., 2002a). The surface charge of ferrihydrite is positive below pH ~8.2, pH_{pzc} (point of zero charge), and electrostatic attraction between the $Sb(OH)_6^-$ and the surface of ferrihydrite can be expected to be stronger under acidic conditions since $Sb(OH)_6^-$ is negatively charged under the conditions here, leading to electrostatic forces playing an important role in the Sb(V) adsorption. For Sb(III), a trihydroxy neutral species, $Sb(OH)_3$, is the dominant species over a wide pH range of 2-11 (Filella et al., 2002a), and only minor or no electrostatic effects may be expected for the Sb(III) adsorption.

A specific interaction (so-called surface complexation) may also play an important role between the adsorbate and adsorbent in addition to the electrostatic effect. To evaluate the effects of surface complexation reactions of Sb(III) and Sb(V) on ferrihydrite, ζ-potential measurements were carried out after the adsorption experiments at different pH values. A ζ-potential analysis is able to indirectly discriminate between inner- and outer-sphere surface complexes on mineral solid surfaces, as the formation of charged inner-sphere surface complexes changes the ζ-potential values and the pH_{pzc} because the ion adsorption occurs inside the shear plane (Stumm and Morgan, 2012). The ζ-potential over a wide pH range, from 3 to 12, and a significant pH_{pzc} shift was observed (**Figure 3-5**) for both Sb(III) and Sb(V) adsorption on ferrihydrite. The pH_{pzc} of the ferrihydrite after adsorbing Sb(V) is 7.1, which is higher than the 6.1 of Sb(III) (**Figure 3-5**). The shifts in pH_{pzc} are likely due to negative charges generated by inner-sphere complexation of Sb ions on the surface of ferrihydrite, and the results of the ζ-potential measurements suggest that Sb(V) ions are adsorbed on the ferrihydrite surface but not as strongly as Sb(III) ions. The strong pH dependence on Sb(V) adsorption (**Figure 3-4**) suggests that electrostatic interactions play an important role for Sb(V) ions, and the strong pH dependence and shifts in pH_{pzc}. Together, these results imply that both outer- and inner-sphere complexes rather than only inner-sphere complexes contribute to the adsorption of Sb(V) ions on the ferrihydrite. Wang (Wang et al., 2015) reported a combination of outer and inner-sphere complexes for Sb(V) adsorption on iron modified aerobic granules, which is consistent with the results for Sb(V) adsorption here.

At the same time, the steep decrease in the pH_{pzc} by Sb(III) adsorption on ferrihydrite suggests that the uncharged Sb(III) is bound strongly to the surface of ferrihydrite by inner-sphere complexation, and the surface complexation between Sb(III) and Fe species is likely the dominating mechanism for Sb(III) adsorption, which would also be consistent with the pH independence of Sb(III) adsorption (**Figure 3-4**). An inner-sphere formation for bidentate mononuclear edge-sharing between Sb(III) and HFO was reported by using extended X-ray absorption fine structure (EXAFS) (Guo et al., 2014). However, further spectroscopic evidence is necessary to understand the adsorption mechanism of Sb(III) and Sb(V) on the mineral surface in more detail.

All of the above results suggest that Sb(III) showed a higher adsorption efficiency toward ferrihydrite than Sb(V) in the pH range 6-12. Previous studies also reported more effective removal of Sb(III) than Sb(V) by ferric chloride over a broad pH range and under a variety of competing ions such as phosphate and humic acid (Guo et al., 2009). The comparison in mobility between the two Sb species appears to be different from that for the As(III) and As(V) species despite Sb and As belonging to the same group of the periodic table. Here the relatively stronger adsorption of Sb(III) compared to As(III) could be attributed to antimonite being a stronger Lewis base than arsenite (Leuz et al., 2006) having a higher pKa value ($pKa1(H_3AsO_3)$ = 9.22; $pKa(Sb(OH)_3)$ = 11.9). Ferrihydrite is frequently amphoteric, and if considering the surface sites of ferrihydrite as Lewis acids, this would explain the stronger binding of Sb(III).

3.4.2 Sb(III) and Sb(V) adsorption in the presence of Silica

The effect of silica on the adsorption of Sb was investigated by varying the Si/Fe ratio of the precipitates at pH 7. The results demonstrated that both Sb(III) and Sb(V) are significantly affected by the presence of silica, with the adsorbed fraction decreasing with increasing Si/Fe ratios (**Figure 3-6**). Both Sb(III) and Sb(V) adsorption were suppressed in the presence of silica. The adsorbed fractions of Sb(III) and Sb(V) ions decreased from >96% at Si/Fe = 0 to 60% at Si/Fe = 0.4 and from >75% at Si/Fe = 0 to 30% at Si/Fe = 0.4, respectively. This shows that Sb(V) was affected more significantly by silica than Sb(III). The drop in Sb(V) adsorption efficiency is likely a result of decreased electrostatic interactions between Sb(V) ions and the surface of ferrihydrite by the decreased surface charge of ferrihydrite due to the presence of

silica on the ferrihydrite surface (**Figure 3-3**), as discussed in the previous Section 3.3.1. Swedlund (Swedlund and Webster, 1999) also suggested that the decreasing surface charge of ferrihydrite by increasing silica concentrations could be an important factor in inhibiting As adsorption. Besides the effect of silica to decrease the surface charge, silica may also suppress adsorption of Sb by occupying surface sites by inner sphere complexation. No apparent pH_{pzc} shift was observed after adsorption of either Sb(III) or Sb(V) on ferrihydrite synthesized at Si/Fe = 0.2 (**Figure 3-7**). This suggests that Sb(III) or Sb(V) ions could not make enough inner-sphere complexes with surface ≡FeOH groups on ferrihydrite to change the ζ-potential because potential surface sites were already occupied by silica. This effect would be more important with Sb(III) ions since inner-sphere complexation is the dominating adsorption mechanism for Sb(III) ion onto ferrihydrite. Jordan (Jordan et al., 2009) also showed that silicic acid could inhibit the retention of oxyanions of selenium onto hematite surfaces by competition with the surface sites of hematite. This suggests that a competition for surface sites on ferrihydrite could be a possible mechanism for inhibition of Sb adsorption.

3.5 Conclusions

This study examined dissolved silica effects on the adsorption and co-precipitation of Sb(III) and Sb(V) with ferrihydrite. The Sb(V) adsorption onto ferrihydrite increased under more acidic conditions. Overall, Sb(III) adsorption was constant over a broad pH range. The adsorption of Sb(III) and Sb(V) appeared to be significantly affected by the presence of silica.

Our findings on the behavior of Sb(III) and Sb(V) adsorption on ferrihydrite and Si-ferrihydrite have important implications for determining the role of ferrihydrite in controlling the final state of Sb in the environments in which it is released. Although ferrihydrite is an excellent substance for capturing Sb, its use as a medium in a natural Si-rich system should be considered with caution because it will tend towards inhibition of Sb capture induced by the Si-rich environment.

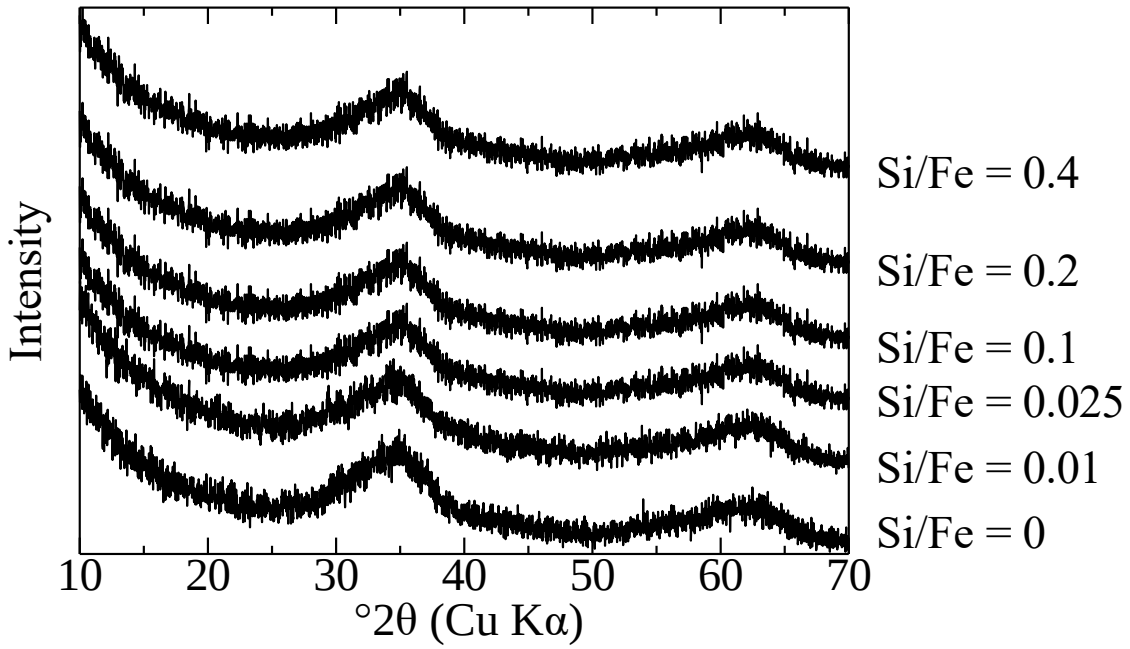

Figure 3-1 X-ray diffraction (XRD) spectra of the initial synthetic precipitates with different Si/Fe ratios.

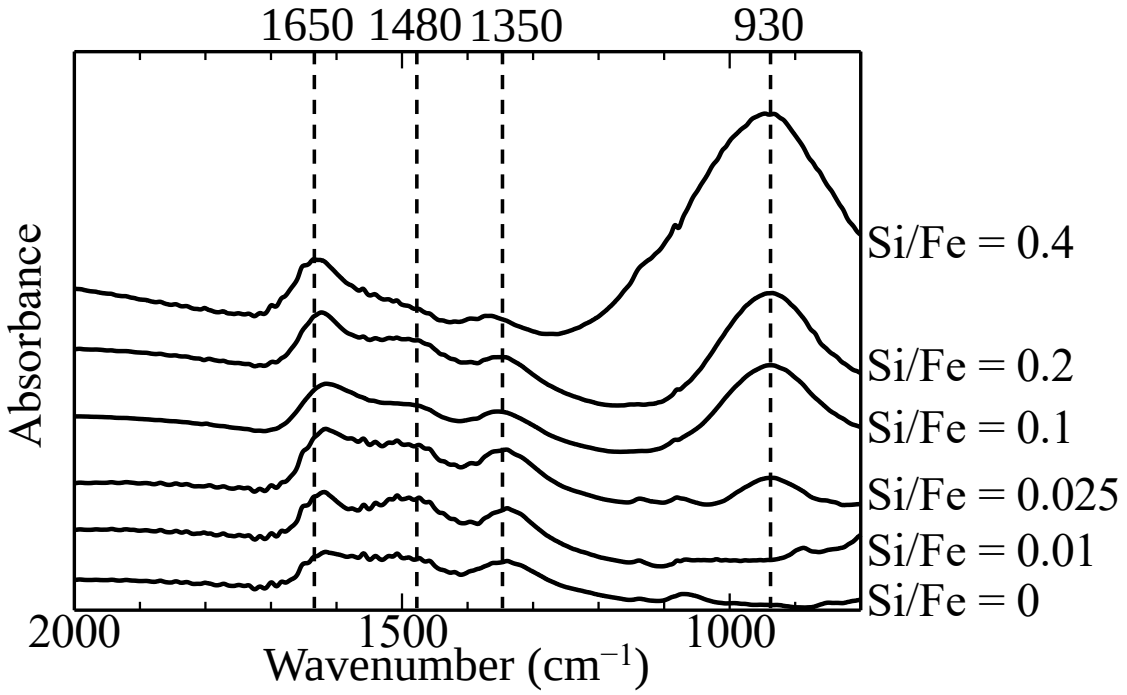

Figure 3-2 Fourier transform infrared (FTIR) spectra of the initial synthetic precipitates with different Si/Fe ratios.

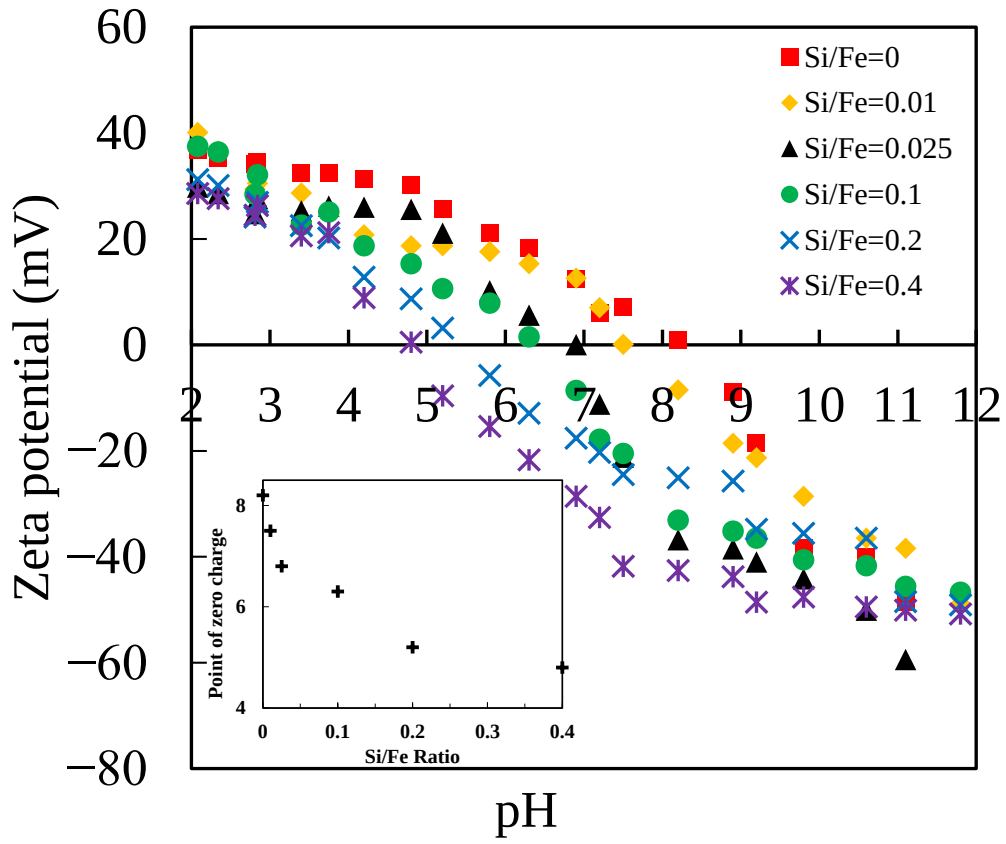

Figure 3-3 Changes in the ζ-potential of ferrihydrite at different Si/Fe ratios as a function of pH in 0.01 M NaCl.

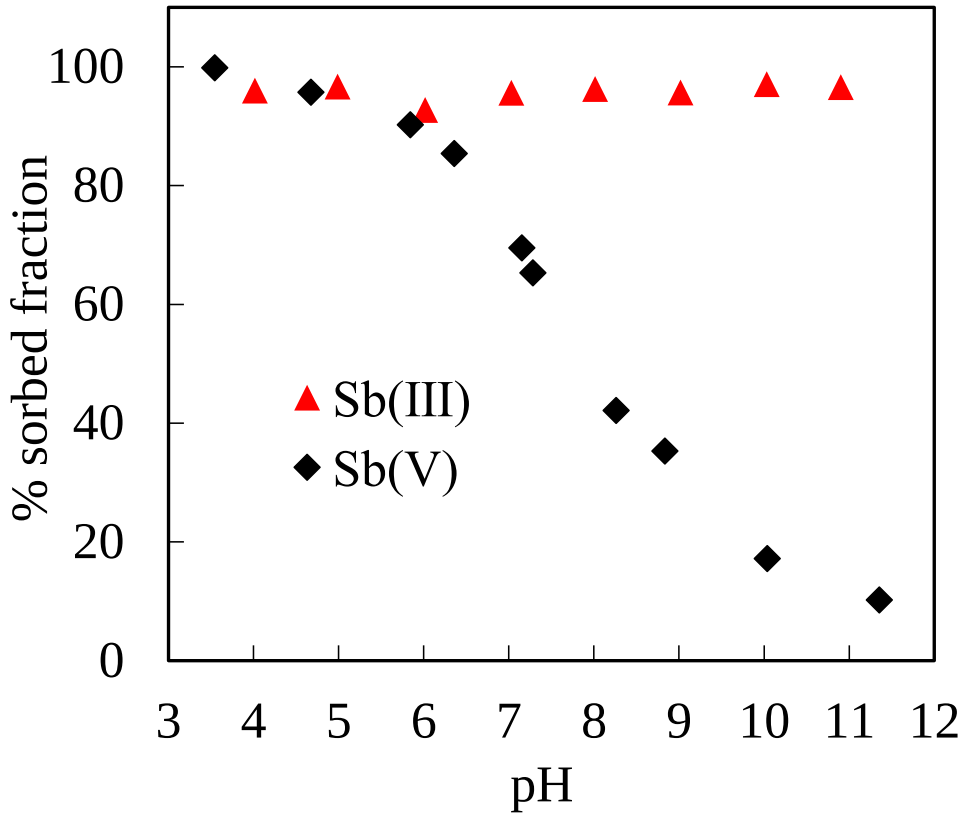

Figure 3-4 Adsorption of Sb(III/V) onto ferrihydrite as a function of the pH in 0.01 M NaCl solutions. The initial Sb(III/V) concentration were 100 µM for each sample. The concentrations of suspended solids were 0.5 g/L.

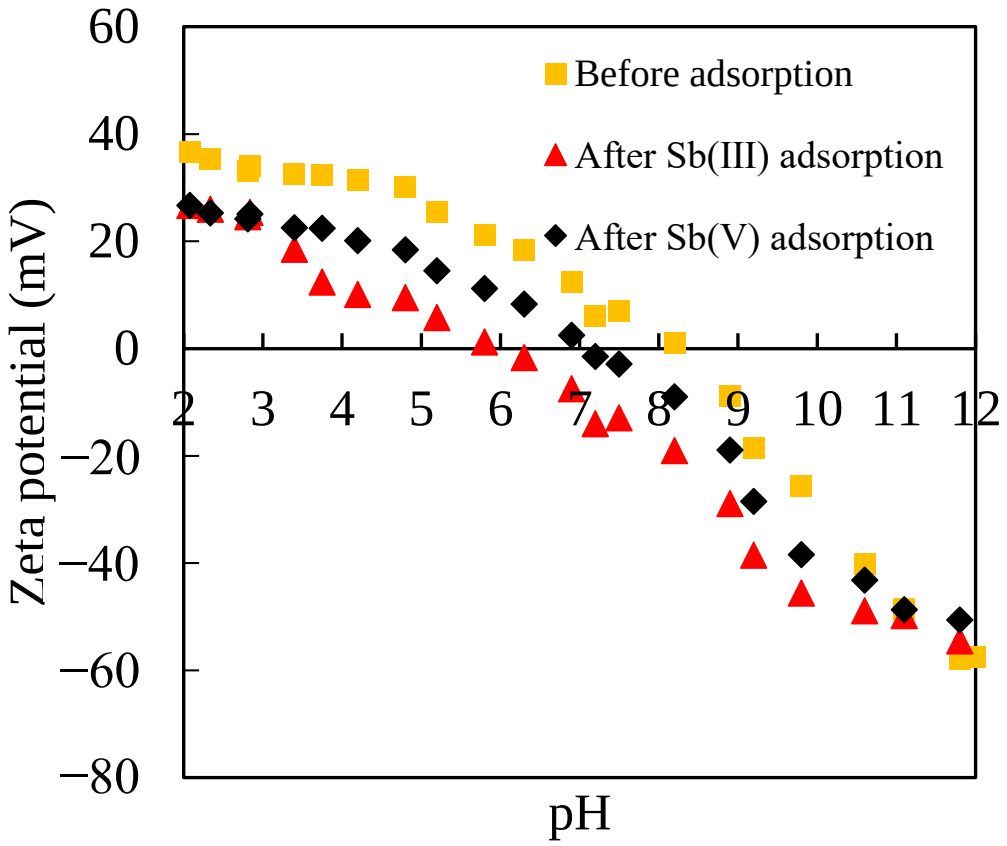

Figure 3-5 Changes in the ζ-potential of ferrihydrite after adsorbing Sb(III/V) as a function of pH in 0.01 M NaCl. The initial Sb(III/V) concentrations were 100 μM for all samples. The concentrations of suspended solids were 0.5 g/L.

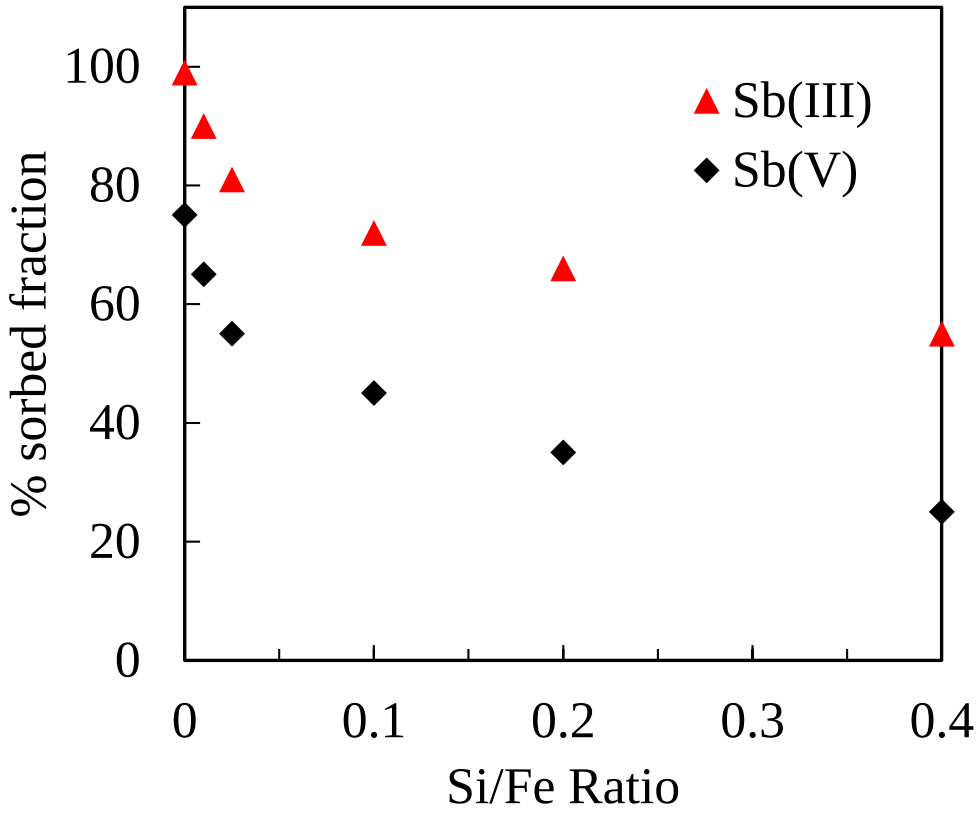

Figure 3-6 Adsorption of Sb(V) onto ferrihydrite with different Si/Fe ratios in 0.01 M NaCl solution at pH 7. The initial Sb(III) concentration were 100 µM. The concentrations of suspended solids were 0.5 g/L.

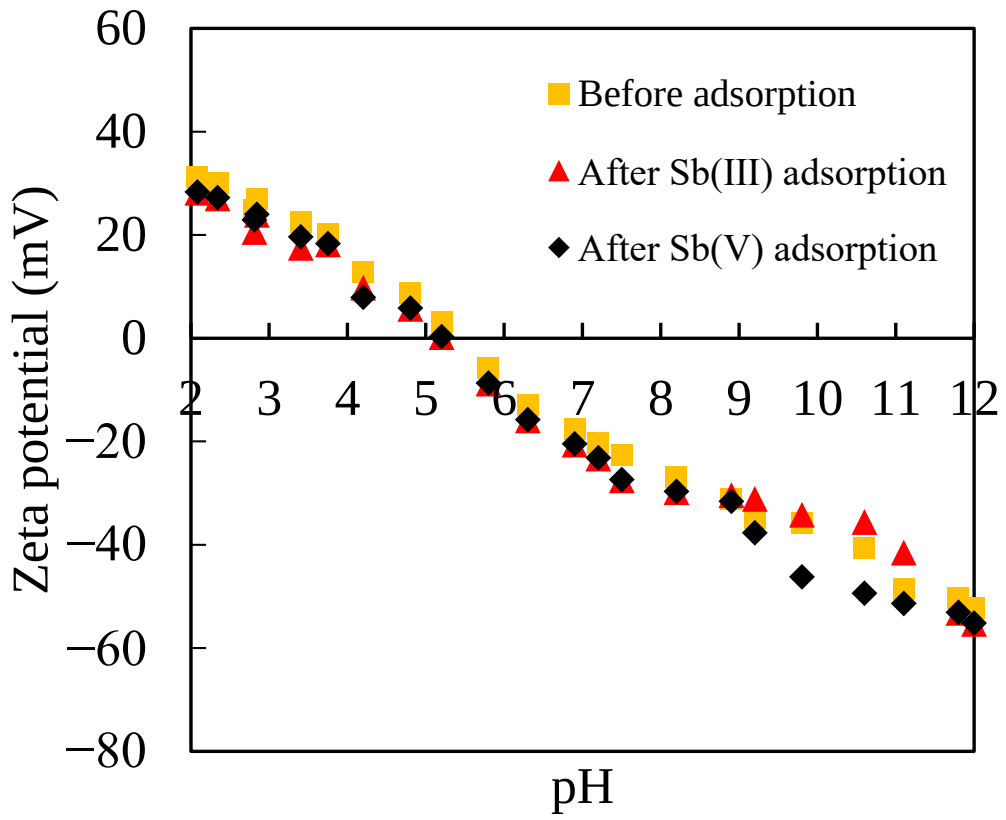

Figure 3-7 Changes in the ζ-potential of Si-ferrihydrite (Si/Fe = 0.2) after adsorbing Sb(III/V) as a function of pH in 0.01 M NaCl. The initial Sb(III/V) concentrations were 100 µM for all samples. The concentrations of suspended solids were 0.5 g/L.

4. Surface complexation modeling of antimony adsorption on ferrihydrite and their silica effect

Abstract

Antimony is a contaminant of emerging concern in natural environment. Ferrihydrite appears to be an important sorbent for antimony in soil and sediments, while the adsorption process of antimony adsorption on ferrihydrite is largely unexplored in a variety of environments. In this study, the adsorption behavior of antimonite (Sb(III)) and antimonate (Sb(V)) by ferrihydrite was examined as functions of pH, ionic strength, and solid concentration. Adsorption data were analyzed using an extended triple-layer modeling (ETLM) for surface complexation modeling to infer Sb(V) reactions and equilibrium constants. Results of ETLM analysis suggest that adsorption of Sb(V) on ferrihydrite occurs as both an outer-sphere and an inner-sphere process, expressed by the following complexation reactions:

$$>FeOH + H^+ + Sb(OH)_6^- => FeOH_2^+\_Sb(OH)_6^-$$

$$2>FeOH + 2H^+ + Sb(OH)_6^- => Fe_2Sb(OH)_6^+ + 2H_2O$$

And the adsorption of Sb(III) on ferrihydrite occurs as two main bidentate-binuclear inner sphere species and one outer sphere species, expressed by the following complexation reactions:

$$2>FeOH + Sb(OH)_3 => (FeO)_2Sb(OH)_2 + 2H_2O$$

$$2>FeOH + Sb(OH)_3 => (FeO)_2SbO^- + H^+ + 2H_2O$$

$$>FeOH + Sb(OH)_3 => FeOH_2^+\_SbO(OH)_2^-$$

where >FeOH denotes surface hydroxyl. The predicted model speciation of Sb(V) on ferrihydrite showed that the inner-sphere species increase concomitantly with decreasing pH, surface Sb(V) loading and increasing solid concentration. The outer-sphere species distribute over a wider range of pH conditions and are more important at lower ionic strengths. Additionally, the outer-sphere species are dominant for pH>5, whereas the inner-sphere species are dominant for pH<5. While the predicted model of Sb(III) on ferrihydrite showed that no pH-dependence and liner

isotherm founded for low surface coverage speciation, the Sb(III) inner-sphere surface complex at the surface confirmed by the weak ionic strength effect on Sb(III) adsorption. Batch adsorption data from this study were reasonably reproduced using ETLM with the predicted equilibrium constants, thereby validating this approach.

4.1 Introduction

Antimony (Sb) and its compounds are considered as pollutants of priority interest because of its reported toxicological effects (Filella et al., 2002b)(USEPA, 1979). Contaminations of antimony in soils and water have been detected around mining and smelter areas, at shooting ranges and along roadsides (Scheinost et al., 2006)(Duester et al., 2011)(Mathys et al., 2007). Two frequently observed oxidation states of Sb in the environment are antimonite (Sb(III)) and antimonate (Sb(V)) (Leuz and Johnson, 2005). Sb(V) species predominantly occurs as $Sb(OH)_6^-$ in oxic waters while Sb(III) occurs as $Sb(OH)_3$ in aqueous solutions and is more stable under anoxic conditions (Baes and Mesmer, 1976).

A solubility study in shooting-range soil from Switzerland showed that a major amount of Sb is distributed to oxalate soluble fractions (Johnson et al., 2005). These findings were confirmed by an EXAFS study (Scheinost et al., 2006), which reported that Sb occurs as Sb(V) bound to iron-oxide phases. Thus the mobility of Sb on the surface environment is governed by adsorption reactions between water and iron hydroxides. More evidences have been found by analysis on sediments and sorption experiment studies (He et al., 2015)(Guo et al., 2014)(Daus and Wennrich, 2014)(Tighe et al., 2005)(Leuz et al., 2006). Ferrihydrite, which is a common iron hydroxides found in the earth's surface environment, is considered one of the most important materials for anionic species adsorption (Dzombak and Morel, 1990)(Davis and Kent, 1990), because of its large surface area and high zero point of charge (ZPC). Therefore, it is quite important to understand the adsorption behavior of Sb on ferrihydrite to predict the migration of Sb in the earth's surface environments. Several macroscopic (batch adsorption) and microscopic (spectroscopic) studies have been conducted to ascertain the adsorption behaviors of Sb(V) on mineral surfaces (Guo et al., 2014)(Mitsunobu et al., 2010)(Leuz et al., 2006)(Mitsunobu et al., 2013)(Scheinost et al., 2006). Among them, batch adsorption experiments were conducted to elucidate the efficiency of Sb(V) adsorption on minerals under the given solution conditions

(Guo et al., 2014)(Mitsunobu et al., 2010)(Leuz et al., 2006), although with not investigated effect of surface coverage or pH on the surface complex species. Whereas spectroscopic studies were conducted to clarify the speciation of Sb on mineral surfaces such as goethite and hematite (Mitsunobu et al., 2013)(Scheinost et al., 2006). However, the integration of both macroscopic and spectroscopic techniques has not been used to characterize the Sb adsorption mechanism.

Both the adsorption efficiency and the surface speciation of Sb on variable charged minerals depend on solution conditions such as pH, electrolyte type, ionic strength, and metal loadings. Therefore, any experimental attempt can obtain the fragmental information of the adsorption behavior only under specific solution conditions. Water chemistries in the surface water and groundwater may vary depending on various factors, such as geological conditions and pollution sources (Drever, 1997)(Appelo and Postma, 2004). Therefore, it is useful to develop a generalized model for the adsorption behaviors of Sb, which can predict both the adsorption efficiency and surface speciation under variable solution conditions. Currently, a number of empirical models including Langmuir (He et al., 2015) and Freundlich isotherm models (Zhao et al., 2014) of Sb adsorption are in wide use. Such models must be calibrated in the laboratory before being applied to a system of interest, they cannot be readily extrapolated beyond strict experimental conditions such as pH, ionic strength, electrolyte composition, hence they may be tricky to apply to natural systems with variable environmental conditions (Reviewers may doubt that SCM can really apply to field-scale system). Surface complexation models (SCMs), which are very much analogous to aqueous speciation models, represent a significant improvement over strictly empirical models because they are based on the thermodynamic principles and calculations are valid over wide rangers of solution composition, which, in turn, enables prediction of the adsorption efficiency and surface speciation under any given solution conditions for minerals (Nagata and Fukushi, 2010)(Fukushi et al., 2013). The diffuse-layer model (DLM) which is one of sub-model of SCM has been applied for Sb removal by ferric chloride coagulation (Guo et al., 2009). However, employing DLM for Sb removal at various pH during ferric chloride coagulation can only be roughly predicted, there are still some significant discrepancies between the theoretical model and the real experimental results. The extended triple-layer model (ETLM), which is a SCM, has predicted the surface complexes as a function of pH, ionic strength and solid concentration independently, consistent with spectroscopic results

in many anion-mineral systems, such as sulfate, selenate, arsenite and arsenate (Sverjensky, 2005)(Sverjensky and Fukushi, 2006a)(Sverjensky and Fukushi, 2006b)(Fukushi and Sverjensky, 2007a)(Fukushi and Sverjensky, 2007b)(Kanematsu et al., 2010). ETLM has not been applied to assess Sb adsorption on ferrihydrite. Hence, the speciation, equilibrium constants and adsorption data are scarce for Sb adsorption on ferrihydrite. Integration of both adsorption data and surface complexes speciation will be useful to characterize the Sb adsorption mechanism.

The objective of this study was to predict the adsorption behavior and surface speciation of Sb on ferrihydrite under various solution conditions with ETLM. To construct ETLM that predict the adsorption behavior in a wide range of conditions, reliable ETLM parameters must be estimated from experimental data for solute-oxide surface interactions. However, few macroscopic adsorption data of Sb are available for various solution parameters on ferrihydrite, as described above. Therefore, in this study, we conducted both Sb(III) and Sb(V) adsorption experiments as a function of pH, ionic strength, and solid concentration for ferrihydrite and also measured the surface charge behavior of the ferrihydrite. Then, the reaction equations and equilibrium constants for Sb(III) and Sb(V) adsorption on ferrihydrite were estimated using ETLM and the adsorption behavior and surface speciation of Sb(III) and Sb(V) on ferrihydrite are predicted using the estimated parameters.

4.2 Materials and methods

4.2.1 Materials

Ferrihydrite was synthesized using the procedure of Schwertmann (Schwertmann and Cornell, 2008). A stock solution of ferric iron (Fe(III), 0.05 mol/L), was prepared by dissolving reagent grade $Fe(NO_3)_3 \cdot 9H_2O$ (Kanto, 99%, Tokyo, Japan) in ultrapure water (18 M Ω·cm). The initial pH of the solution was about 1.8, then 1.0 M NaOH (Kanto, 97%, Tokyo, Japan) solution was titrated to the stock solution to adjust the solution pH to 7.0 ± 0.1. Addition of the NaOH hydrolyzes the Fe(III) in the solution resulting in formation of a slurry of dark brown precipitate. The freshly prepared ferrihydrite suspension were stirred and stabled for 4h before use for the titration and adsorption experiments.

4.2.2 Potentiometric acid-base titrations

The surface acid-base properties of ferrihydrite was examined using potentiometric acid-base titrations at 25℃. Titrations were performed in a closed polycarbonate vessel equipped with a magnetic stirrer. After the stabling period described above, NaCl electrolyte was added to the ferrihydrite suspension to yield an ionic strength of 0.01, 0.05, or 0.1. The acid and base titrations were conducted independent from each other. The ionic strength of the ferrihydrite suspensions did not change during the course of all the titration runs. A change of less than 0.01 pH units over 3 min was used as the criterion for equilibrium. The surface charge, σ_0 (C/m^2), was calculated from titration data by means of the following equation:

$$\sigma_0 = (F/S)\,(C_A - C_B + [OH^-] - [H^+]) \quad (1)$$

In this equation, F is Faraday's constant (96485 C/mol), S is the total surface area of the suspension (m^2/L), and $C_A - C_B$ is the net concentration of acid or base added to the solution (mol/L). The specific surface area of ferrihydrite was assumed to be 600 m^2/g, as reported by Dzombak, Davis and Nagata (Dzombak and Morel, 1990)(Davis and Kent, 1990)(Nagata et al., 2009).

4.2.3 Adsorption experiments

The Sb(V) stock solution (500 μM) was prepared by dissolving $KSb(OH)_6$ powder (Wako, 50%, Tokyo, Japan) into deionized water, and the Sb(III) stock solution (100 μM) was prepared by dissolving Sb_2O_3 powder (Wako, 98%, Tokyo, Japan) into 2 mol/L HCl (Kanto, 37%, Tokyo, Japan) solution. The adsorption experiments were conducted on a rotary shaker (110 rpm) at 25℃. Reaction times for equilibration were determined from the preliminary kinetic experiments as follows. Solid concentrations were 0.5 g/L for ferrihydrite. The Sb(III) and Sb(V) concentration was adjusted to 1 μM by addition of a small volume of Sb(III) and Sb(V) stock solution, respectively. The ionic strength of the suspensions was adjusted to 0.01 using a NaCl background electrolyte. The suspension pH was adjusted to pH 7.0. After pH adjustment, the suspensions were stirred for 0.5, 1, 2, 4, 6, 10, 18 and 24 h. At the end of the reaction time, each suspension pH was measured. The suspensions were filtered through a 0.2 μm cellulose membrane. The filtered solution was acidified using 60% ultrapure HNO_3. The Sb concentrations

in the filtrates were measured using Inductively Coupled Plasma (ICP)-Atomic Emission Spectroscopy (AES) (ICPE-9000, Shimadzu Corp., Kyoto, Japan). The detection limit of this method was 0.1 μg/L. **Figure 4-1** and **Figure 4-2** presents the kinetics of Sb(V) and Sb(III) adsorption on ferrihydrite. The percentage of adsorbed Sb(V) remained constant after 12 h within the examined reaction times up to 24 h, which suggests that adsorption equilibria were attained within 24 h. While the percentage of adsorbed Sb(III) reached its maximum after 4 h, which means side reactions such as diffusion of Sb to the particle interior did not occur. Hereafter, we conducted all the adsorption experiments for 24 h with the assumption that the adsorption equilibria were attained.

Adsorption edges were obtained as a function of pH, Sb concentration, solid concentration, and ionic strength. The Sb(V) concentrations were 10, 100 or 500 μM and the Sb(III) concentrations were 1, 10 or 100 μM. Solid concentrations were 0.5 or 2 g/L. The ionic strength of the suspensions was adjusted to be 0.01, 0.1, and 1 M using NaCl electrolytes. The suspension pH was adjusted using 0.1 M or 1 M HCl or HNO_3 and NaOH solutions to the final pH of 3-10. After pH adjustment, the suspensions were stirred on a rotary shaker (110 rpm) at 25℃ for 24 h. At the end of the reaction time, each suspension pH was measured. Then the suspensions were filtered through a 0.2 μm cellulose membrane. The Sb concentrations in the filtrates were measured using ICP-AES. The adsorption amount was calculated from the differences of initial and final Sb concentrations as

$$\text{Adsorption} = \frac{[\text{Sb}]_0 - [\text{Sb}]_{eq}}{[\text{Sb}]_0} \times 100(\%) \quad (2)$$

,where $[\text{Sb}]_0$ and $[\text{Sb}]_{eq}$ represent the initial and final Sb concentrations, respectively.

4.2.4 Estimation of ETLM basic parameters for ferrihydrite

Aqueous speciation calculations were conducted with consideration of aqueous ionic activity coefficients appropriate to single electrolytes up to high ionic strengths calculated using the extended Debye–Hückel equation (Criscenti and Sverjensky, 1999). Aqueous antimony protonation reaction was consistent with those reported from an earlier study (Baes and Mesmer, 1976).

$$Sb(OH)_5 + H_2O = Sb(OH)_6^- + H^+ \qquad \log K = -2.47$$

$$Sb(OH)_3 + H_2O = Sb(OH)_4^- + H^+ \qquad \log K = -11.82$$

$$Sb(OH)_2^+ + H_2O = Sb(OH)_3 + H^+ \qquad \log K = -1.42$$

The ETLM calculations were performed with GEOSURF (Sahai and Sverjensky, 1998) which adopts the hypothetical 1.0 M standard state relative to >SOH species for surface species. The ETLM application requires the following basic parameters: surface protonation equilibrium constants (K_1^θ and K_2^θ), the stoichiometry of the electrolyte adsorption equations, the electrolyte adsorption equilibrium constants ($K_{Na^+}^\theta$ and $K_{Cl^-}^\theta$), surface site density (N_s), specific surface area (A_s), and the inner-layer and outer-layer capacitance (C_1 and C_2). The specific surface area (A_s) of ferrihydrite is assumed to be 600 m^2/g (Davis and Kent, 1990)(Dzombak and Morel, 1990)(Nagata et al., 2009). The surface site density (N_s) of 3.8 (sites/nm^2) was adopted for ferrihydrite based on the relation between the surface area and site density of ferrihydrite, as reported by (Sverjensky, 2005) and (Nagata et al., 2009). For ferrihydrite, an inner-layer capacitance (C_1) of 1.0 F/m^2, and an outer-layer capacitance (C_2) of 0.2 F/m^2 were obtained from Fukushi and Sverjensky (Fukushi and Sverjensky, 2007b). The values of these parameters in the present study are summarized in **Table 4-1**. The surface protonation reactions and the equilibrium constants K_1^θ and K_2^θ, corresponding to site-occupancy standard states (denoted by the superscript "θ") are given by

$$>\mathrm{FeOH} + \mathrm{H^+} => \mathrm{FeOH_2^+} \qquad (3)$$

$$\mathrm{K_1^\theta} = \frac{\mathrm{a}_{>\mathrm{FeOH_2^+}}}{\mathrm{a}_{>\mathrm{FeOH}}\mathrm{a}_{\mathrm{H^+}}} 10^{\frac{\mathrm{F}\psi_0}{2.303\mathrm{RT}}} \qquad (4)$$

and

$$> FeO^- + H^+ => FeOH \quad (5)$$

$$K_2^\theta = \frac{a_{>FeOH}}{a_{>FeO^-} a_{H^+}} 10^{\frac{F\psi_0}{2.303RT}} \quad (6)$$

In those equations, >FeOH denotes surface sites; R and T represent the universal gas constant and absolute temperature (K), respectively. ψ_0 denotes the electrical potential at the 0-plane where H^+ and/or OH^- adsorb on surface sites. The surface protonation equilibrium constants were calculated from pH_{ZPC} (ZPC: zero point of charge) and ΔpK_n^θ (Sverjensky, 2005) as

$$\log K_1^\theta = pH_{ZPC} - \frac{\Delta pK_n^\theta}{2} \quad (7)$$

$$\log K_2^\theta = pH_{ZPC} + \frac{\Delta pK_n^\theta}{2} \quad (8)$$

The value of pH_{ZPC} of ferrihydrite was taken from (Nagata et al., 2009). Values of ΔpK_n^θ were predicted theoretically (Fukushi et al., 2013)(Sverjensky, 2005). The equilibrium constants based on a site-occupancy standard state are independent of the surface area and site density (Sverjensky, 2003). For convenience, the surface protonation equilibrium constants referring to the hypothetical 1.0 M standard state (denoted by the superscript "0") are also given in **Table 4-1**. The relations between the two standard states are given as

$$\log K_1^0 = \log K_1^\theta - \log\left(\frac{N_s A_s}{N^\ddagger A^\ddagger}\right) \quad (9)$$

and

$$\log K_2^0 = \log K_2^\theta - \log\left(\frac{N_s A_s}{N^\ddagger A^\ddagger}\right) \quad (10)$$

where N_s and A_s represent the surface site density and specific surface area of the *s*th solid, respectively. $N^\ddagger$ and $A^\ddagger$ correspond to values for the same properties at the hypothetical standard state. In this study, $N^\ddagger$ values of 10 sites/nm^2 and $A^\ddagger$ values of 10 m^2/g were selected for all solids (Sverjensky, 2003).

Other parameters, i.e., electrolyte adsorption equilibrium constants were estimated from ETLM analysis of surface charge data obtained from three different ionic strengths in NaCl solutions (**Figure 4-3**). Both Na^+ and Cl^- are assumed to absorb on ferrihydrite on β-plane in ETLM (outer-sphere). The NaCl electrolyte adsorption equations are given as shown below.

$$>FeO^- + Na^+ => FeO^-\_Na^+ \quad (11)$$

$$>FeOH_2^+ + Cl^- => FeOH_2^+\_Cl^- \quad (12)$$

Equilibrium constants $K^{\theta}_{Na^+}$ and $K^{\theta}_{Cl^-}$, corresponding to site-occupancy standard states are derived as presented below.

$$K^{\theta}_{Na^+} = \frac{a_{>FeO^-\_Na^+}}{a_{>FeO^-}a_{Na^+}} 10^{\frac{F\psi_\beta}{2.303RT}} \quad (13)$$

$$K^{\theta}_{Cl^-} = \frac{a_{>FeOH_2^+\_Cl^-}}{a_{>FeOH_2^+}a_{Cl^-}} 10^{\frac{-F\psi_\beta}{2.303RT}} \quad (14)$$

The relations between the site-occupancy standard states, $\log K^{\theta}_{Na^+}$ and $\log K^{\theta}_{Cl^-}$, and the hypothetical 1.0 M standard state, $\log {}^{*}K^{0}_{Na^+}$ and $\log {}^{*}K^{0}_{Cl^-}$ (where superscript "*" signifies a reaction relative to the >FeOH species), are givens as shown below.

$$\log {}^{*}K^{0}_{Na^+} = \log K^{\theta}_{Na^+} - pH_{ZPC} - \Delta pK^{\theta}_{n} - \log\left(\frac{N_s A_s}{N^{\ddagger} A^{\ddagger}}\right) \quad (15)$$

and

$$\log {}^{*}K^{0}_{Cl^-} = \log K^{\theta}_{Cl^-} + pH_{ZPC} - \Delta pK^{\theta}_{n} - \log\left(\frac{N_s A_s}{N^{\ddagger} A^{\ddagger}}\right) \quad (16)$$

The ETLM with the above parameters generally reproduces well the surface charge data of ferrihydrite used in this study as a function of pH and ionic strength in NaCl electrolyte (**Figure 4-3**). The ETLM analysis of surface charge as a function of ionic strength produced the values of $\log K^{\theta}_{Na^+} = 4.3$ and $\log K^{\theta}_{Cl^-} = 4.5$. These basic parameters for ETLM are also presented in **Table 4-1**.

4.3 Results and discussion

4.3.1 Surface charge of ferrihydrite in NaCl solutions

The obtained proton surface charge on ferrihydrite as a function of pH from potentiometric titrations in NaCl solutions are shown in **Figure 4-3**. The surface charges increased with salt concentrations in NaCl solutions, of which behaviors are consistent with the variable charge minerals. Meanwhile, the titration curves of ferrihydrite in NaCl electrolyte solutions at various ionic strengths (I = 0.01, 0.05, and 0.1) exhibit a common intersection point (i.e., points of zero salt effect (PZSE)) at pH 7.9 (**Figure 4-3**). This pH_{PZSE} is almost identical to values previously reported for ferrihydrite in NaCl solutions (Ching-kuo Daniel Hsi and Langmuir, 1985)(Nagata et al., 2009). The solid lines in **Figure 4-3** are regression curves calculated by ETLM. The parameters used in the calculations are given in **Table 4-1**. ETLM analysis resulted in values of $\log K^{\theta}_{Na^+} = 4.3$ and $\log K^{\theta}_{Cl^-} = 4.5$. This agreement of the adsorption equilibrium constants for both reactions indicates that no asymmetry occurred in binding, ascertaining the above assumption that pH_{PZSE} = pH_{ZPC} (Sverjensky, 2005). Criscenti and Sverjensky (Criscenti and Sverjensky, 2002) analyzed the titration data obtained by Davis (Davis et al., 1978) for ferrihydrite and obtained adsorption equilibrium constants of 4.3 and 4.5 for $\log K^{\theta}_{Na^+}$ and $\log K^{\theta}_{Cl^-}$, respectively. The similarity between these values and our obtained values indicates that the surface properties of the present ferrihydrite were almost identical to those of Davis's samples (Davis et al., 1978). Therefore, the assumed ferrihydrite specific surface area of 600 m^2/g used in the present study is justified.

4.3.2 Sb(V) and Sb(III) adsorption reaction stoichiometries

The stoichiometry of adsorption reaction(s) and the adsorption equilibrium constant(s) for Sb(V) and Sb(III) on ferrihydrite were estimated from ETLM regression calculations for both the proton surface charge of ferrihydrite and pH adsorption edges as functions of ionic strength and Sb loading as well as solid concentration. For Sb(V) adsorption, all adsorption data were fitted reasonably by assuming the two adsorption reactions. They are formations of monodentate, mononuclear outer-sphere species and bidentate, binuclear inner-sphere species as shown below.

$$> FeOH + H^+ + Sb(OH)_6^- => FeOH_2^+\_Sb(OH)_6^- \quad (17)$$

$$2 > FeOH + 2H^+ + Sb(OH)_6^- => Fe_2Sb(OH)_6^+ + 2H_2O \quad (18)$$

While for that of Sb(III) adsorption, they are formations of two main bidentate, binuclear inner-sphere species and one outer-sphere species as shown below.

$$2 > FeOH + Sb(OH)_3 => (FeO)_2Sb(OH)_2 + 2H_2O$$

$$2 > FeOH + Sb(OH)_3 => (FeO)_2SbO^- + H^+ + 2H_2O$$

$$> FeOH + Sb(OH)_3 => FeOH_2^+\_SbO(OH)_2^-$$

Michel (Michel et al., 2007) proposed a structure for ferrihydrite with δ-Keggin entities. According to the structure, most of the Fe-Fe distance in ferrihydrite, which can be approximated as the distance between the two surface hydroxyls in ferrihydrite, is equal to or less than 3.0 Å, except for that between tetrahedral Fe and octahedral Fe (Manceau, 2012). The ionic radius of antimonate is 0.6 Å. The diameter of antimonate is 1.2 Å. Therefore, the spontaneous formations of two adjacent bidentate antimonate species on the surface in ferrihydrite might be possible because of the spatial constraint. In fact, Mitsunobu (Mitsunobu et al., 2010) observed that Sb(V) is absorbed on ferrihydrite with the formation of inner-sphere surface complexes including edge-sharing and double corner-sharing complexes from X-ray absorption fine structure (XAFS) analysis of adsorption samples. Vithanage (Vithanage et al., 2013) reported that the Sb(III) adsorption was mainly adsorbed in an inner-sphere model on the surface sites of iron oxides. Our previous study (Zhou et al., 2018) also interpreted Sb(V) adsorption by zeta-potential analysis as attributable to the formation of the outer-sphere complex and inner-sphere complex formed by ligand exchange processes, Sb(III) adsorption was attributable to the formation of inner-sphere complex. Another research from Leuz (Leuz et al., 2006) suggested that the inner-sphere complex of Sb(V) is dominant at lower pH on the goethite surface, and the outer-sphere complex relatively increases at pH>6. Therefore, the estimated reactions for both Sb(V) and Sb(III) of outer-sphere complex and inner-sphere complex involving ligand exchange process, which are consistent with previous spectroscopic and electrophoresis studies.

Here, we show the detailed methodology for estimation of the ETLM equilibrium constants for Sb(V) adsorption. For that of the Sb(III) adsorption, the methodology is the same with that of Sb(V) adsorption.

The corresponding adsorption equilibrium constants of Eqs. (17) and (18) can be written as presented below:

$$ {}^{*}K^{\theta}_{>FeOH_2^+\_Sb(OH)_6^-} = \frac{a_{>FeOH_2^+\_Sb(OH)_6^-}}{a_{>FeOH}a_{H^+}a_{Sb(OH)_6^-}} 10^{\frac{F(\Delta\psi_{\gamma,17})}{2.303RT}} \tag{19} $$

$$ {}^{*}K^{\theta}_{>Fe_2Sb(OH)_6^+} = \frac{a_{>Fe_2Sb(OH)_6^+}a^2_{H_2O}}{a^2_{>FeOH}a^2_{H^+}a_{Sb(OH)_6^-}} 10^{\frac{F(\Delta\psi_{\gamma},18)}{2.303RT}} \tag{20} $$

In those equations, $\Delta\psi_{\gamma}$ is the electrostatic factor related to the work done in an electric field when the species in the reaction move on or off the changed surface. For the outer-sphere species in Eq. (17), the electrostatic factor $\Delta\psi_{\gamma,17}$ is evaluated in the traditional way in the triple-layer model (Davis et al., 1978) as

$$ \Delta\psi_{\gamma,16} = \psi_0 - \psi_{\beta} \tag{21} $$

where the term ψ_0 represents changes in the potential experienced by the H^+ adsorbing to the 0-plane. The term $-\psi_{\beta}$ refers to changes in the potential experienced by the $Sb(OH)_6^-$ adsorbing to the β-plane. For the inner-sphere species in Eq. (18), $\Delta\psi_{\gamma,18}$ was estimated using the procedure described by Sverjensky and Fukushi (Sverjensky and Fukushi, 2006a). Inner-sphere anion adsorption is thought to proceed by a ligand exchange mechanism involving the release of water dipoles (Zhang and Sparks, 1990)(Stumm, 1992)(Grossl et al., 1997). To show clearly how the electrostatics of this process are treated in ETLM, we disaggregate Eq. (18) into two reactions. The first reaction, in which surface sites are protonated and $Sb(OH)_6^-$ is adsorbed to the β-plane of the TLM, can be represented as follows:

$$ 2>FeOH + 2H^+ + Sb(OH)_6^- = (>FeOH_2^+)_2\_Sb(OH)_6^- \tag{22} $$

The electrostatic factor associated with Eq. (22), $\Delta\psi_{\gamma,22}$ is evaluated traditionally as:

$$\Delta\psi_{\gamma,22} = 2\psi_0 - \psi_\beta \tag{23}$$

In the second reaction, water is desorbed from the 0-plane and an inner-sphere complex is formed:

$$(>FeOH_2^+)_2\_Sb(OH)_6^- => Fe_2Sb(OH)_6^+ + 2H_2O \tag{24}$$

The magnitude of the electrostatic work associated with desorption of n moles of water dipoles from the 0-plane in the ETLM is given as:

$$\delta w \approx nF(\psi_0 - \psi_\beta) \tag{25}$$

where F is the Faraday constant (F = 96485 C/mol), and where ψ_0 and ψ_β, respectively, signify the potentials at the 0-plane and b-plane of TLM (Sverjensky and Fukushi, 2006a)(Sverjensky and Fukushi, 2006b). Applying Eq. (25) to the reaction shown in Eq. (24) yields:

$$\delta w_{23} \approx 2F(\psi_0 - \psi_\beta) \tag{26}$$

The electrostatic work of dipole desorption shown in Eq. (26) can be expressed in equilibrium constant form as presented below:

$$K_{23} = 10^{\frac{2F(\psi_0 - \psi_\beta)}{2.303RT}} \tag{27}$$

That is to say, the electrostatic factor for Eq. (24), $\Delta\psi_{\gamma,24}$, is given as:

$$\Delta\psi_{\gamma,23} = 2(\psi_0 - \psi_\beta) \tag{28}$$

The overall reaction in Eq. (18) represents the sum of the reactions in Eqs. (22) and (24). Consequently, the overall electrostatic factor for Eq. (18), $\Delta\psi_{\gamma,18}$, is given as the sum of Eqs. (23) and (28):

$$\Delta\psi_{\gamma,17} = \Delta\psi_{\gamma,21} + \Delta\psi_{\gamma,23} = 2\psi_0 - \psi_\beta - 2(\psi_0 - \psi_\beta) = \psi_\beta \tag{29}$$

The solid lines in Figs. Show ETLM regressions of the adsorption data. The ETLM analysis uses $\log K^{\theta}_{>Fe_2Sb(OH)_6^+} = 21.5$ and $\log K^{\theta}_{>FeOH_2^+\_Sb(OH)_6^-} = 12.3$ for ferrihydrite.

The relation of equilibrium constants between the site-occupancy standard state and the hypothetical 1.0 M standard state relative to >FeOH is given as

$$\log {}^{*}K^{0}_{>Fe_2Sb(OH)_6^+} = \log K^{\theta}_{>Fe_2Sb(OH)_6^+} + 2pH_{ZPC} - \Delta pK_n^{\theta} - \log\left(\frac{(N_s A_s)^2}{N^{\ddagger} A^{\ddagger}} C_s\right) \quad (30)$$

where C_s is the solid concentration of the system (g/L). For convenience the Sb(V) adsorption equilibrium constants referring to the hypothetical 1.0 M standard state relative to >FeOH species are also given in **Table 4-2**.

4.3.3 Prediction of adsorption of Sb(V) and Sb(III) on ferrihydrite in NaCl solutions

Figure 4-4 portrays the adsorption edges on ferrihydrite as a function of Sb(V) loading in 0.01 M NaCl solutions (**Figure 4-4a**), and as a function of ionic strength in constant Sb(V) concentration (**Figure 4-4b**), and as a function of solid concentration (**Figure 4-4c**). In all examined conditions, Sb(V) adsorption were almost 100% at around pH 3.5. The amounts of adsorption decreased concomitantly with increasing pH. The pH dependence of the adsorption is consistent with that of the anionic species on variable charge minerals (Dzombak and Morel, 1990)(Stumm, 1992). The strong pH dependence of Sb(V) adsorption and the fact that adsorption was favored at acidic pH were reported for kaolinite and goethite (Rakshit et al., 2015)(Leuz et al., 2006). The adsorption behavior of Sb(V) in terms of pH is firstly attributed to the electrostatic attraction between $Sb(OH)_6$ and the surface of ferrihydrite (Zhao et al., 2014). A surface complexation may also play an important role between the adsorbate and adsorbent in addition to the electrostatic effect (Zhou et al., 2018). In all examined conditions, Sb(V) adsorptions were over 80% between pH 3 and 6. As expected, Sb(V) adsorption was dependent on pH, which the amounts of adsorption decreased concomitantly with increasing pH. The adsorption edge shifted to higher pH with decreased Sb(V) loading.

The adsorption data depicted in **Figure 4-4b** shows Sb(V) adsorption edge on ferrihydrite as a function of the electrolyte concentrations of NaCl. The adsorption decreases concomitantly with increased ionic strength in NaCl solutions at pH>5. The ionic strength dependence suggests that the adsorption of Sb(V) on ferrihydrite is suppressed in the presence of high concentrations of

electrolytes in solutions. In addition, these results infer a differing strength of bonding, there has been relatively little mention in the literature of the molecular basis for these observations. Ionic strength shows effect on the macroscopic adsorptive performances, which provide valuable information on formation of surface complexes (Hayes et al., 1988). In detail, the formation of outer-sphere complexes was relative in that the adsorptive capacity decreases with increasing ionic strength. On the contrary, in cases where ionic strength has little effect on the adsorption capacity, the formation of inner-sphere complexes may be inferred. Consistency between the experimental and modeling results on the ionic-strength dependence suggests that the ETLM has a plausible molecular basis, i.e., the formation of inner- vs outer-sphere surface complexes.

The adsorption data depicted in **Figure 4-4c** are related to Sb(V) adsorption edges on ferrihydrite as a function of solid concentrations and 10 μM Sb(V) concentration in 0.01 M NaCl solutions. The solid curves in **Figure 4-4c** represent regression calculation on ferrihydrite using two reactions. It is apparent that the calculated curves provide a close description of the Sb(V) adsorption data over a range of experimental conditions. The estimated values of $\log K^{\theta}$ of bidentate species and monodentate species are 21.5 and 12.3. The higher equilibrium constants suggest higher affinity of ferrihydrite to Sb(V).

Figure 4-5 presents the adsorption edges on ferrihydrite as a function of Sb(III) loading in 0.01 M NaCl solutions (**Figure 4-5a**), and as a function of ionic strength in constant Sb(III) concentration (**Figure 4-5b**), and as a function of solid concentration (**Figure 4-5c**). In all examined conditions, Sb(III) adsorption were almost 100% over a broad pH range except that with the lower solid concentration shown in **Figure 4-5c**. The pH dependence of Sb(III) adsorption was less pronounced than that of Sb(V), showing a constant adsorption capacity to the pH at which adsorption was almost complete. This was in good agreement with the earlier studies, which showed that Sb(III) adsorption by iron oxides can be optimized over a broad pH range (Guo et al., 2014)(Shan et al., 2014) (Leuz et al., 2006).

The adsorption data depicted in **Figure 4-5b** shows Sb(III) adsorption edge on ferrihydrite as a function of the electrolyte concentrations of NaCl. Good agreement with the experimental data is obtained using the inner-sphere species reactions. The formation of inner-sphere complexes can be inferred since ionic strength has little effect on the adsorption capacity. McComb (McComb et

al., 2007) has reported that Sb(III) can be bound strongly to the surface sites by formation of inner-sphere surface complexes, which consist with present study.

The adsorption data depicted in **Figure 4-5c** are related to Sb(III) adsorption edges on ferrihydrite as a function of solid concentrations in 0.01 M NaCl solutions. The solid curves in **Figure 4-5c** represent regression calculation on ferrihydrite using Sb(III) reactions. It is apparent that the calculated curves provide a close description of the Sb(III) adsorption data over a range of experimental conditions.

4.3.4 Prediction of surface Sb(V) and Sb(III) species on ferrihydrite in NaCl solutions

The predicted surface speciation on ferrihydrite as a function of Sb(V) loading in 0.01 M NaCl solutions is shown in **Figure 4-6a-c**. The lower surface loading also results in the higher contribution of bidentate inner-sphere species over monodenate outer-sphere species at lower pH. Scheinost (Scheinost et al., 2006) reported the dominant Sb(V) surface species in shooting-range soils is a bidentate inner-sphere species in their investigation using XAFS. The prediction of surface species as a function of pH and surface coverage is consistent with their findings.

The predicted surface speciation of Sb(V) on the surface of the ferrihydrite with different electrolyte concentrations in constant Sb(V) concentration is shown in **Figure 4-7a-c**. The ionic strength dependence suggests that the adsorption of Sb(V) on ferrihydrite is suppressed in the presence of high concentrations of electrolytes in solutions. Specifically, the inner-sphere species is the predominant species at pH<5 for all the ionic strengths, which is consistent with the discussion above. The contribution of the outer-sphere species appears at slightly acidic to alkaline conditions, and decreases concomitantly with increased ionic strength, of which the behavior is consistent with the discussed above.

The predicted surface speciation on ferrihydrite as a function of solid concentrations and 10 μM Sb(V) concentration in 0.01 M NaCl solutions is given in **Figure 4-8a-c**. The proportion of the inner-sphere species to outer-sphere species clearly depends on the surface solid concentration. The low solid concentration results in the higher contribution of outer-sphere species over inner-sphere species at pH>5. The speciation also shows that the contribution of outer-sphere species increases with pH, whereas that of inner-sphere species decreases monotonously with pH. The

adsorption speciation showed that the inner-sphere species values obtained from 2 g/L of solid concentrations at low pH conditions (pH<6) were markedly higher than those from 0.5 g/L solid concentration, although those from 2 g/L were almost identical to those from 0.5 g/L at high pH conditions (**Figure 4-8b-c**). Comparison of the surface speciation between 0.5 and 2 g/L of solid concentration clarifies that the difference of distribution of the inner-sphere species.

The predicted surface speciation on ferrihydrite as a function of Sb(III) loading in 0.01 M NaCl solutions is shown in **Figure 4-9a-c**. The lower surface loading also results in the higher contribution of two bidentate inner-sphere species over monodenate outer-sphere species over all range of pH.

The predicted surface speciation of Sb(III) on the surface of the ferrihydrite with different electrolyte concentrations in constant Sb(III) concentration is shown in **Figure 4-10a-c**. The predicted two bidentate binuclear inner-sphere species dominate over the pH ranges as a function of electrolyte concentrations, which is consistent with the discussion above.

The predicted surface speciation on ferrihydrite as a function of solid concentrations in 0.01 M NaCl solutions is given in **Figure 4-11a-c**. The proportion of the inner-sphere species to outer-sphere species clearly depends on the surface solid concentration. The low solid concentration results in the lower inner-sphere species. The adsorption speciation showed that the inner-sphere species values obtained from 0.5 g/L and 2 g/L of solid concentrations at low pH conditions (pH<7) were markedly higher than those from 0.01 g/L solid concentration. Sverjensky (Sverjensky, 2003) revealed that the binuclear inner-sphere complexes depend on the amount of solid. Here we observed the bidentate binuclear inner-sphere species increasing with solid concentrations, which was consistent with the reported conditions. Comparison of the surface speciation between 0.01 g/L and 2 g/L of solid concentration clarifies that the difference of distribution of the inner-sphere species.

4.3.5 Application to Sb(V) and Sb(III) adsorption

Figure 4-12 represents the adsorption of Sb(V) on HFO from (Guo et al., 2014). The solid curves in **Figure 4-12** represent regression calculations using the same reactions as in **Figure 4-4**, i.e., involving the species of bidentate binuclear inner-sphere species and outer-sphere species. It can be seen that the calculated curves provide a close description of the bulk of the experimental data

of all kinds. The predicted model speciation of antimonate on HFO showed that outer-sphere species dominated a wide pH range, while the inner-sphere species only presented at pH < 5.

Figure 4-13 represent the adsorption of Sb(III) on HFO from (Guo et al., 2014). The solid curves in **Figure 4-13** represent regression calculations using the same reactions as in **Figure 4-5**, i.e., involving the species of two bidentate binuclear inner-sphere species. It can be seen that the calculated curves provide a close description of the bulk of the experimental data of all kinds. The predicted model speciation of antimonite on HFO showed that the $(>FeO)_2Sb(OH)_2$ species dominated at pH < 6, and the other inner-sphere species $(>FeO)_2SbO^-$ increasing with increased pH.

4.3.6 Application to Sb(V) and Sb(III) adsorption under silica effect

Figure 4-14 and **Figure 4-15** represent the adsorption of Sb(V) and Sb(III) on ferrihydrite under silica effect at 0.01 M NaCl solution. It can be seen from **Figure 4-14**, with increasing Si/Fe ratio the adsorption efficiency of Sb(V) decreased and shifted to lower pH value. While in **Figure 4-15**, the silica decreasing the Sb(III) efficiency on ferrihydrite and the pH showed on effect on the adsorption. It is apparently that the ETLM curve can reproduce the experimental data for the whole range of pH. Thus the ETLM could allow us to predict Sb adsorption on ferrihydrite under silica effect without taking extensive experiment. Using the ETLM theory, it is possible to estimate adsorption equilibrium constants of Sb ions for ferrihydrite despite the presents of silica. The application of ETLM theory to ferrihydrite will enable us to understand how those ions macroscopically and thermodynamically interact with each other on the common adsorbent in water treatment systems in a way consistent with spectroscopic and molecular evidence.

4.4 Conclusions

The adsorption data of Sb on ferrihydrite were obtained from this study, conducted under widely various pH, Sb loadings, ionic strength and solid concentrations in NaCl solutions, which were analyzed using ETLM. The adsorption of Sb(V) on ferrihydrite decreased concomitantly with pH, which is consistent with other anionic species on iron oxides, and decreased with ionic strength. The ETLM analysis of the adsorption date suggest that Sb(V) adsorbs to ferrihydrite via

formation of monodentate, mononuclear outer-sphere species and bidentate binuclear inner-species, as shown below:

$$>FeOH + H^+ + Sb(OH)_6^- => FeOH_2^+\_Sb(OH)_6^-$$

$$2>FeOH + 2H^+ + Sb(OH)_6^- => Fe_2Sb(OH)_6^+ + 2H_2O$$

The prediction of the surface speciation of Sb(V) on ferrihydrite showed that the inner-sphere species increase concomitantly with decreasing pH, surface Sb(V) loading and increasing solid concentration. The outer-sphere species distribute over a wider range of pH conditions and are more important at lower ionic strengths. Additionally, the outer-sphere species are dominant for pH>5, whereas the inner-sphere species are dominant for pH<5.

While the adsorption of Sb(III) on ferrihydrite constant over a broad range of pH, and ionic strength shown no effect on the Sb(III) adsorption efficiency. The ETLM analysis of the adsorption date suggest that Sb(III) adsorbs to ferrihydrite mainly via formation of binuclear inner-species, as shown below:

$$2>FeOH + Sb(OH)_3 => (FeO)_2Sb(OH)_2 + 2H_2O$$

$$2>FeOH + Sb(OH)_3 => (FeO)_2SbO^- + H^+ + 2H_2O$$

$$>FeOH + Sb(OH)_3 => FeOH_2^+\_SbO(OH)_2^-$$

The prediction of the surface speciation of Sb(III) on ferrihydrite showed that the inner-sphere species dominate a wide range of pH, surface Sb(III) loading and increasing with solid concentration. These formation behaviors of surface species are consistent with those found from spectroscopic studies. The agreements strongly confirm the validity of the present approach, not only for the integration of spectroscopic and bulk adsorption data of Sb on ferrihydrite, but also for making predictions of surface speciation over wide ranges of conditions of relevance to the migration of Sb species in the environment.

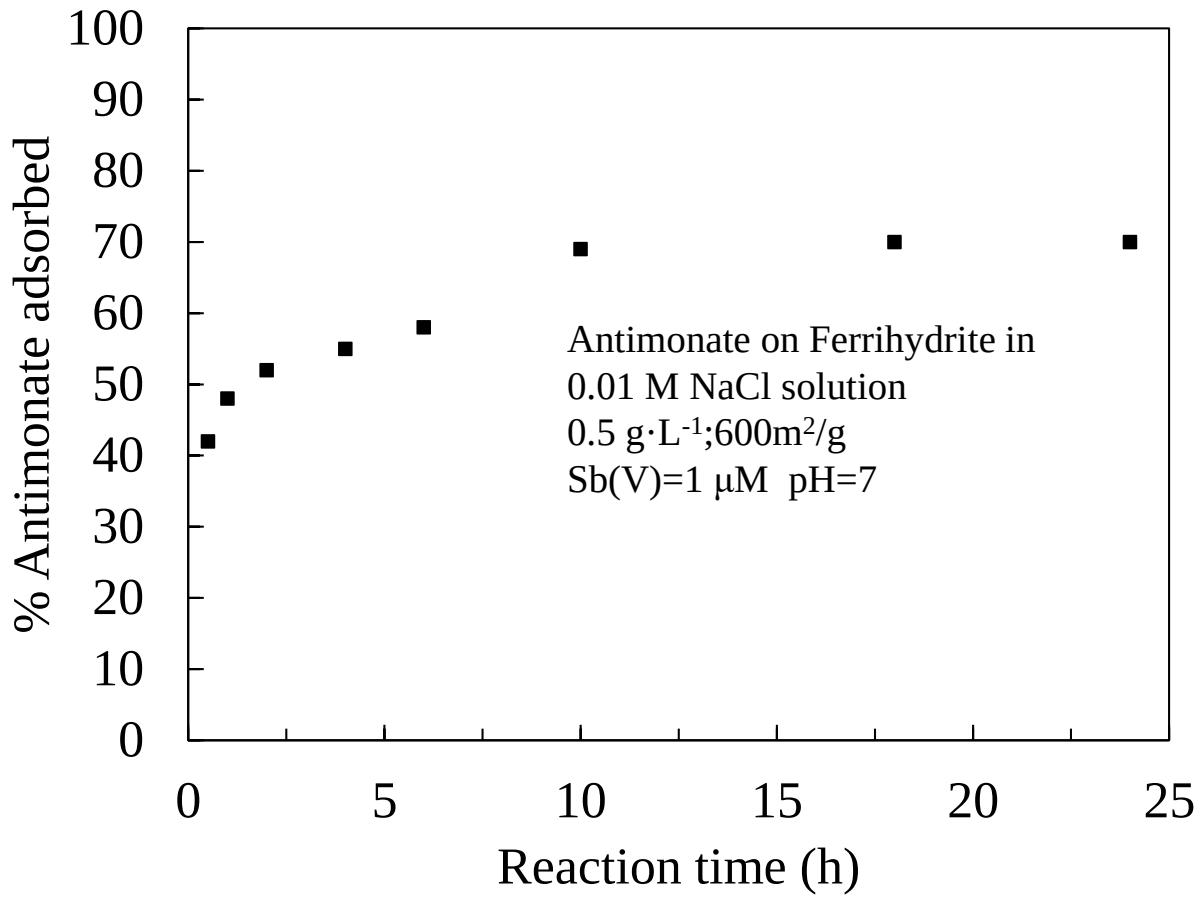

Figure 4-1 Kinetics of antimonate adsorption on ferrihydrite in 0.01 M NaCl solution at 25℃.

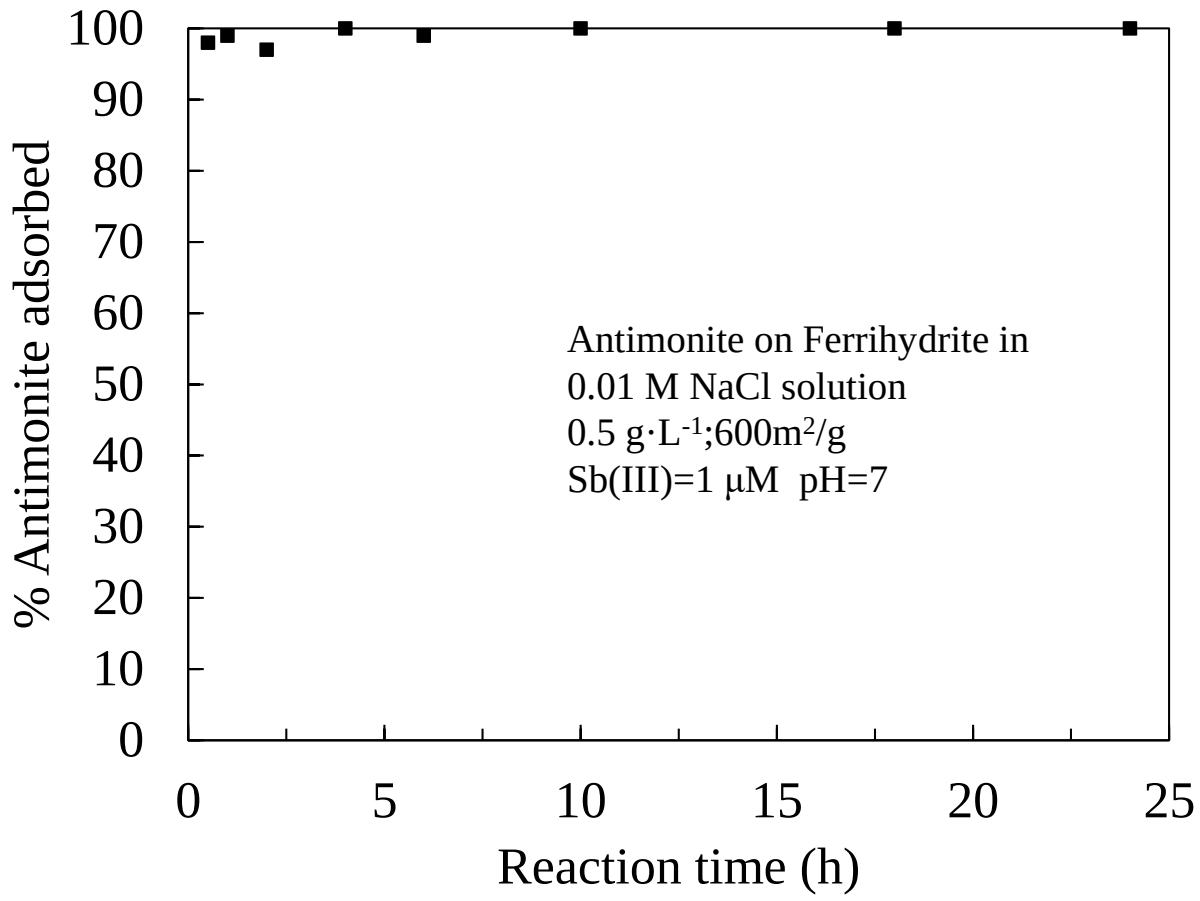

Figure 4-2 Kinetics of antimonite adsorption on ferrihydrite in 0.01 M NaCl solution at 25°C.

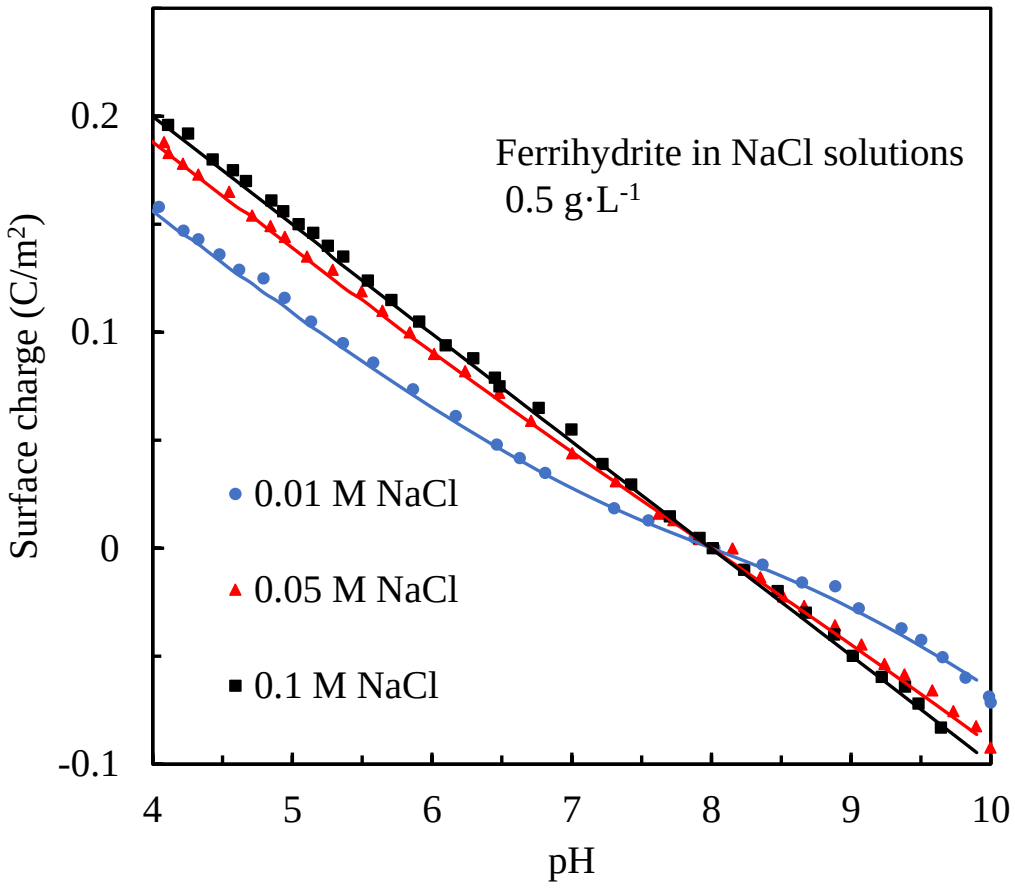

Figure 4-3 Surface charge data of ferrihydrite as a function of pH and ionic strength in NaCl electrolyte solutions at 25°C. Solid lines in the plot are corresponding ETLM calculations based on the parameters presented in **Table 4-1**.

Table 4-1 Sample characteristics, surface protonation, electrolyte adsorption equilibrium constants, and capacitances used for this study.

Solid	Salt ML	N_s *(site/nm²)*	A_s (m^2/g)	pH_{ZPC}	ΔpK_n^{θ}	$\log K_1^{\theta}$	$\log K_2^{\theta}$	$\log K_1^{0}$	$\log K_2^{0}$	$\log K^{\theta}_{M^+}$	$\log K^{\theta}_{L^-}$	$\log^* K^{0}_{M+}$	$\log^* K^{0}_{L^-}$	C_1 ($\mu F/cm^2$)	C_2 ($\mu F/cm^2$)
Ferrihydrite	NaCl	3.8[c]	600[c]	7.9[c]	5.6[d]	5.1	10.7	3.7	-12.1	4.3[e]	4.5[e]	-7.7	8.2	100	20

Values of $\log K_1^{\theta}$, $\log K_2^{\theta}$, $\log K_{M^+}^{\theta}$ and $\log K_{L^-}^{\theta}$ refer to site-occupancy standard states for the reactions listed below [a]. M^+ stands for Na^+. L^- stands for Cl^- for this study. Values of $\log K_1^{\theta}$ and $\log K_2^{\theta}$ were predicted using the given values of pH_{ZPC} and ΔpK_n^{θ}.Values of $\log K_1^{0}$, $\log K_2^{0}$, $\log^* K_{M^+}^{0}$ and $\log^* K_{L^-}^{0}$ refer to the hypothetical 1.0 M standard state and the reactions listed below [b].

They were calculated from values of $\log K_1^{\theta}$ $\log K_2^{\theta}$ $\log K_{M^+}^{\theta}$ and $\log K_{L^-}^{\theta}$ using Eqs. (9), (10), (15), (16) with the tabulated values of N_s, A_s, pH_{ZPC} and ΔpK_n^{θ}.

[a] $\log K_1^{\theta}: >SOH + H^+ \Rightarrow SOH_2^+$; $\log K_2^{\theta}: >SO^- + H^+ \Rightarrow SOH$; $\log K_{M^+}^{\theta}$:

$>SO^- + M^+ \Rightarrow SO^-\_M^+$; $\log K_{L^-}^{\theta}: >SOH_2^+ + L^- \Rightarrow SOH_2^+\_L^-$.

[b] $\log K_1^{0}: >SOH + H^+ \Rightarrow SOH_2^+$; $\log K_2^{0}: >SO^- + H^+ \Rightarrow SOH$; $\log^* K_{M^+}^{0}$:

$>SOH + H^+ + M^+ \Rightarrow SO^-\_M^+ + H^+$; $\log^* K_{L^-}^{0}: >SOH + H^+ + L^- \Rightarrow SOH_2^+\_L^-$.

[c] (Nagata et al., 2009).

[d] (Sverjensky, 2005).

[e] This study.

Table 4-2 Adsorption equilibrium constants for Sb(V) surface complexes on ferrihydrite

Solid	N_s (site/nm^2)	C_s(g/L)	$\log^* K^0_{>SOH_2^+\_Sb(OH)_6^-}$	$\log K^\theta_{>SOH_2^+\_Sb(OH)_6^-}$	$\log^* K^0_{>Fe_2Sb(OH)_6^+}$	$\log K^\theta_{>Fe_2Sb(OH)_6^+}$	Adsorption data	ETLM parameter
Ferrihydrite	3.8	0.5	10.9	12.3	17.1	21.5	This study	This study
Ferrihydrite	3.8	2	10.9	12.3	16.5	21.5	This study	This study

Values of $\log^* K^0_{>SOH_2^+\_Sb(OH)_6^-}$ and $\log^* K^0_{>Fe_2Sb(OH)_6^+}$ refer to the hypothetical 1.0 M standard states and reactions with

>SOH ($\log^* K^0_{>SOH_2^+\_Sb(OH)_6^-}$: $>FeOH + H^+ + Sb(OH)_6^- => FeOH_2^+\_Sb(OH)_6^-$; $\log^* K^0_{>Fe_2Sb(OH)_6^+}$: $2>FeOH + 2H^+ + Sb(OH)_6^- => Fe_2Sb(OH)_6^+ + 2H_2O$).

Values of $\log K^\theta_{>Fe_2Sb(OH)_6^+}$ and $\log K^\theta_{>SOH_2^+\_Sb(OH)_6^-}$ refer to the site-occupancy standard states and reactions with

>SOH_2^+ ($\log K^\theta_{>Fe_2Sb(OH)_6^+}$: $>FeOH_2^+ + Sb(OH)_6^- => FeOH_2^+\_Sb(OH)_6^-$; $\log K^\theta_{>SOH_2^+\_Sb(OH)_6^-}$: $2>FeOH_2^+ + Sb(OH)_6^- => Fe_2Sb(OH)_6^+ + 2H_2O$).

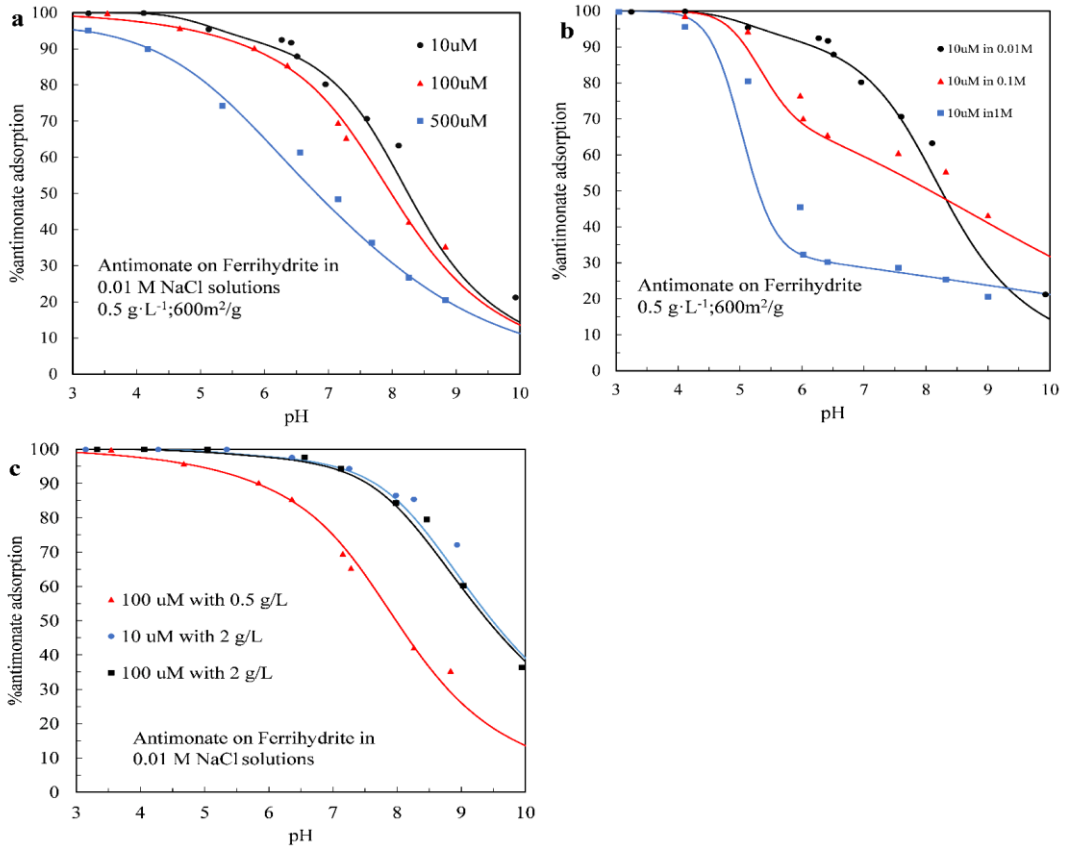

Figure 4-4 Antimonate adsorption edge on ferrihydrite as a function of antimonate loading (a), ionic strength (b) and solid concentrations (c). Solid lines show curves calculated using ETLM.

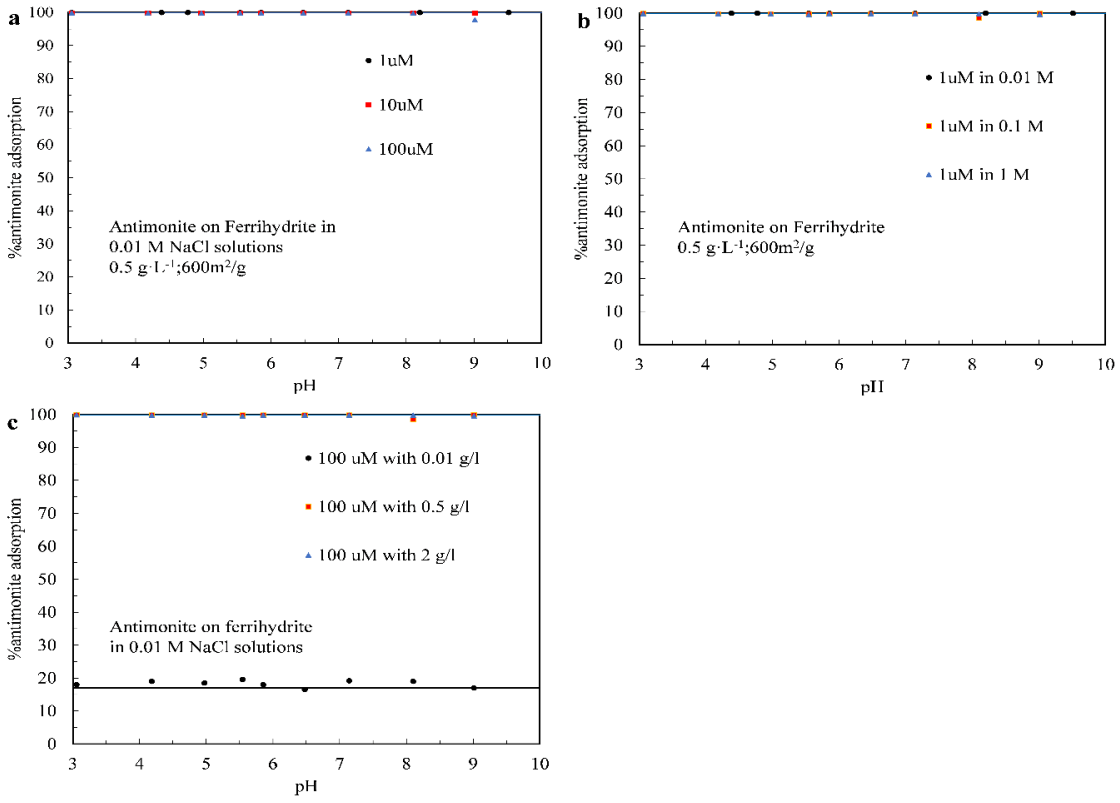

Figure 4-5 Antimonite adsorption edge on ferrihydrite as a function of antimonite loading (a), ionic strength (b) and solid concentrations (c). Solid lines show curves calculated using ETLM.

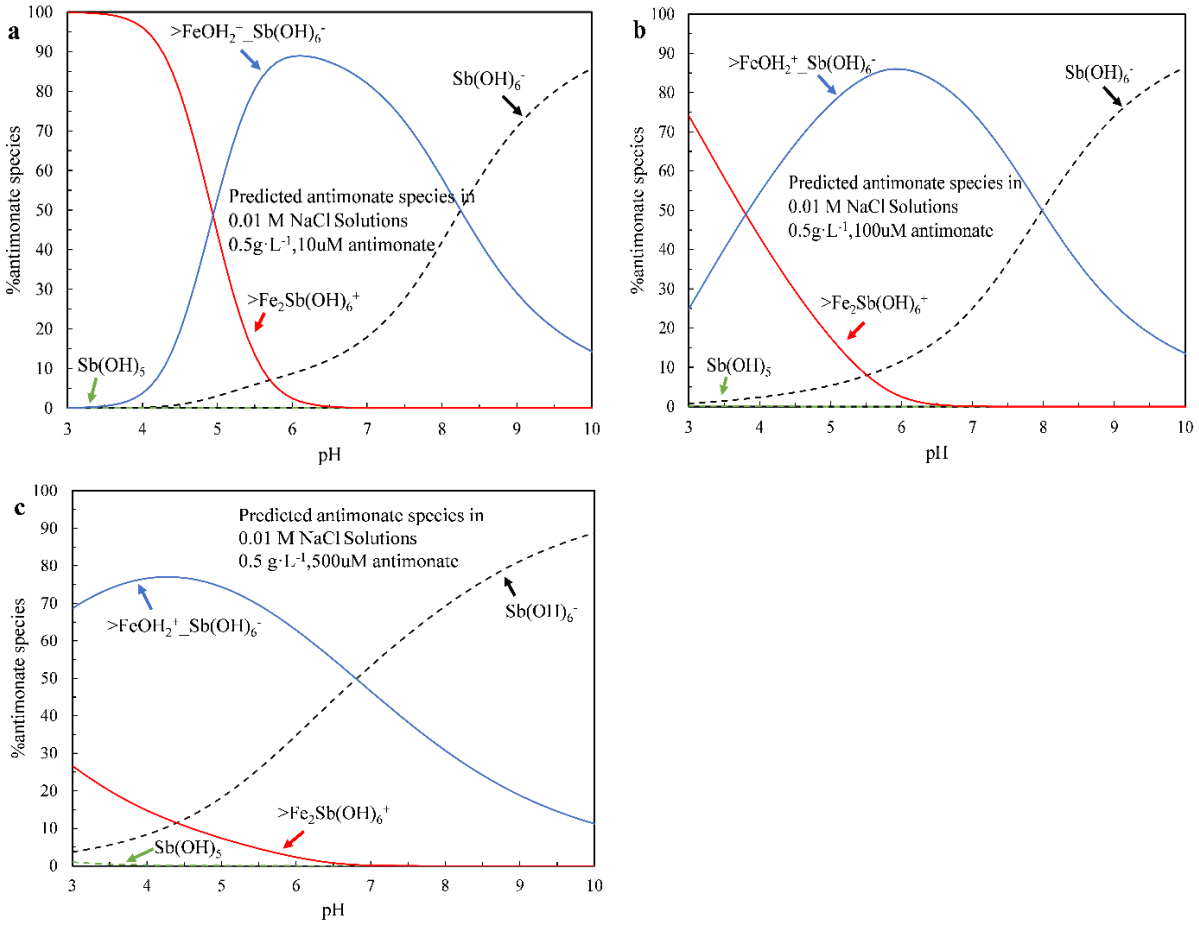

Figure 4-6 Predicted model Sb(V) surface speciation on ferrihydrite in 0.01 M NaCl solutions with different antimonate loadings: (a) 10 μM, (b) 100 μM, and (c) 500 μM.

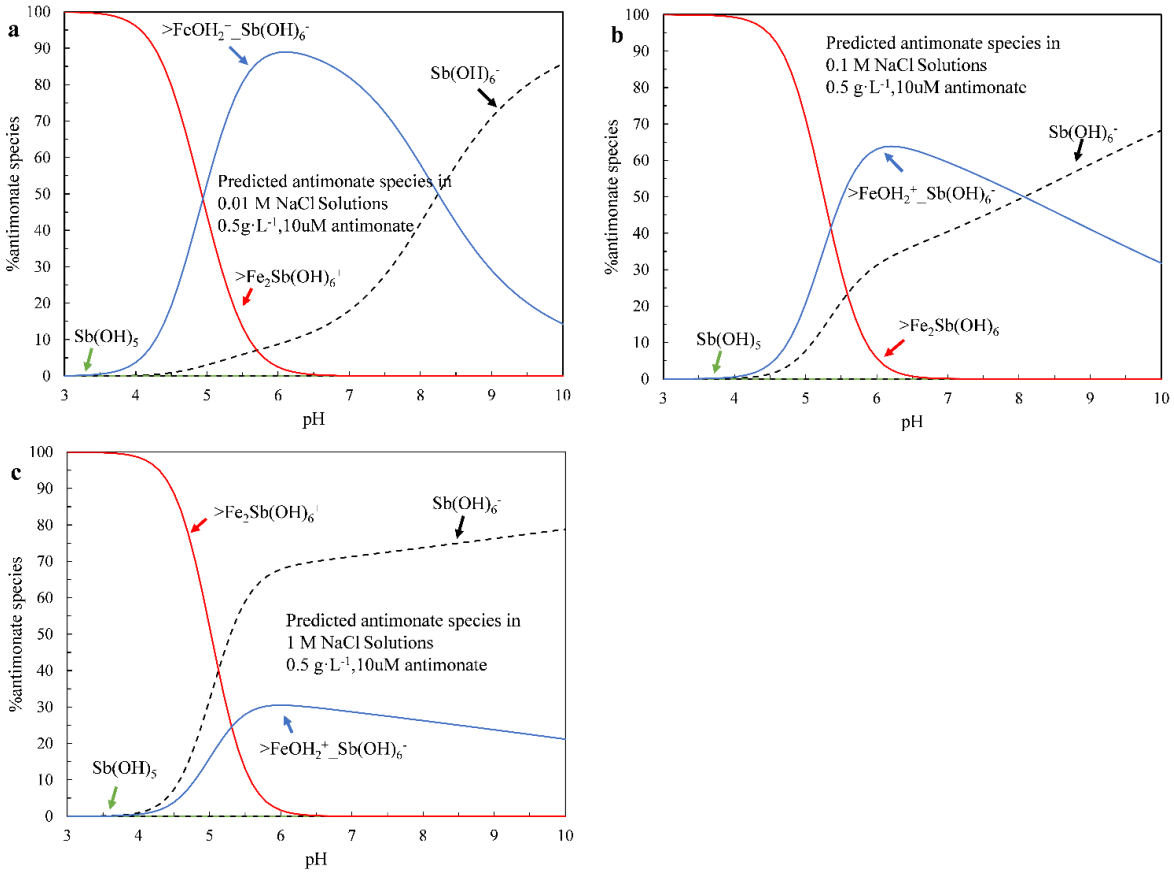

Figure 4-7 Predicted model Sb(V) surface speciation on ferrihydrite in NaCl electrolyte solutions with different electrolyte concentrations in constant Sb(V) concentration (10 μM): (a) 0.01 M, (b) 0.1 M, and (c) 1 M.

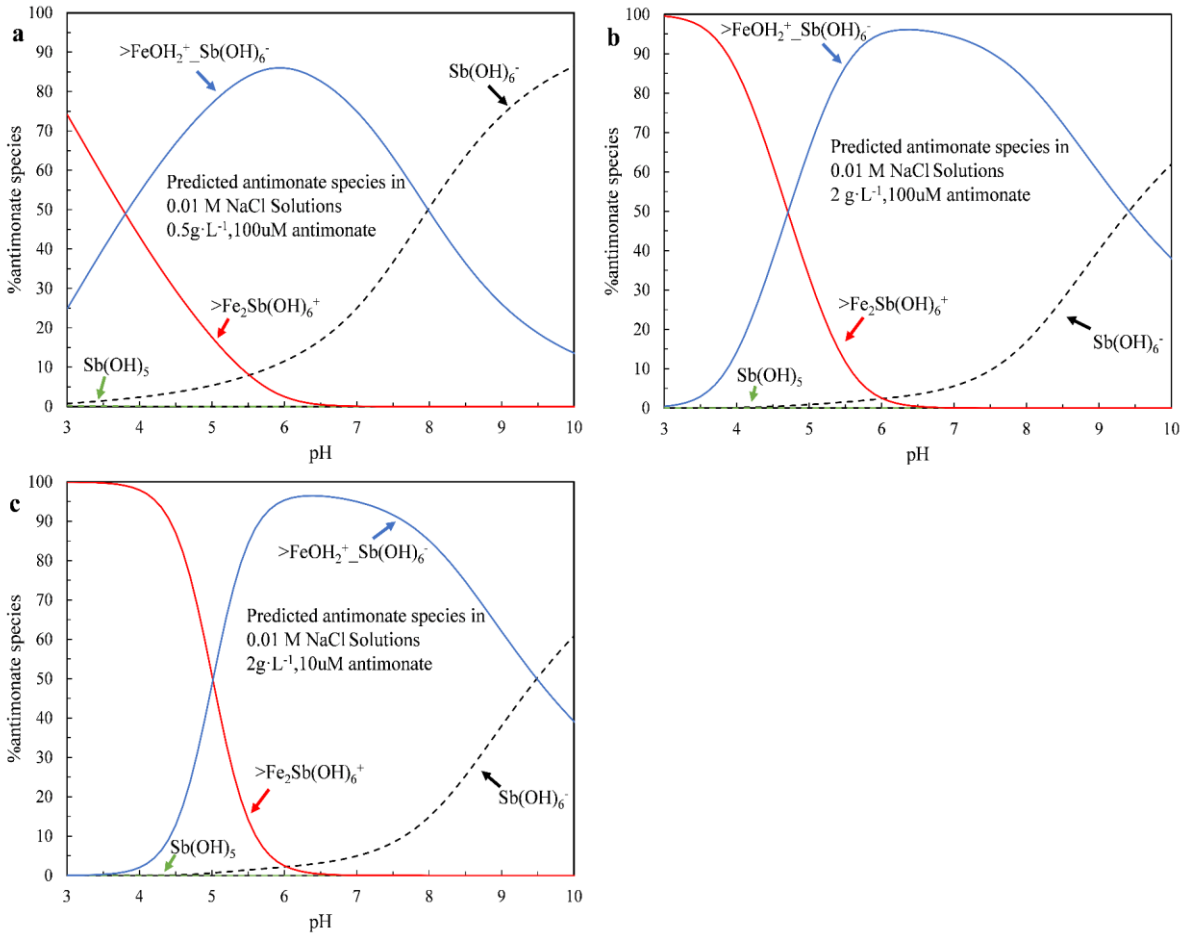

Figure 4-8 Predicted model Sb(V) surface speciation on ferrihydrite in NaCl electrolyte solutions as a function of Sb(V) concentration and solid concentration: (a) 100 μM 0.5 g/L, (b) 100 μM 2 g/L and (c) 10 μM 2 g/L.

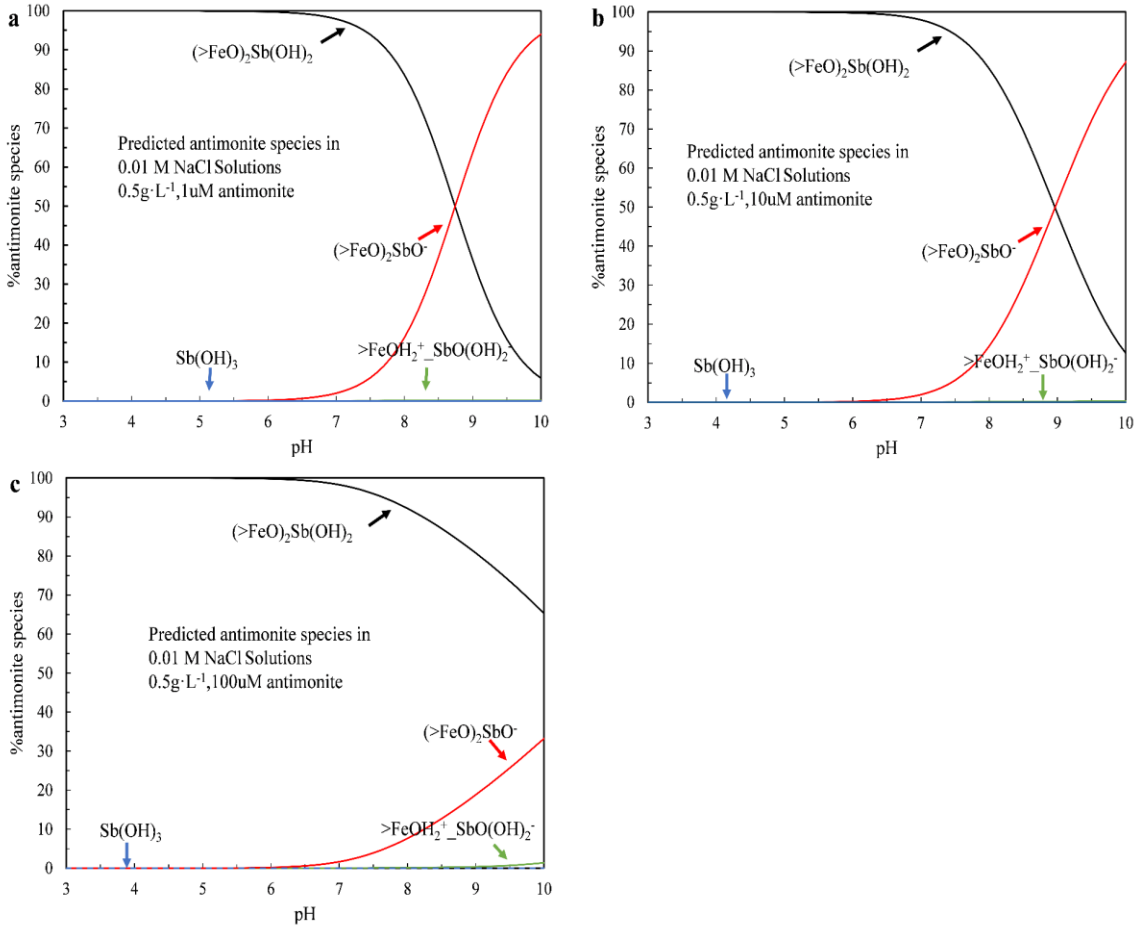

Figure 4-9 Predicted model Sb(III) surface speciation on ferrihydrite in 0.01 M NaCl solutions with different antimonite loadings: (a) 1 μM, (b) 10 μM, and (c) 100 μM.

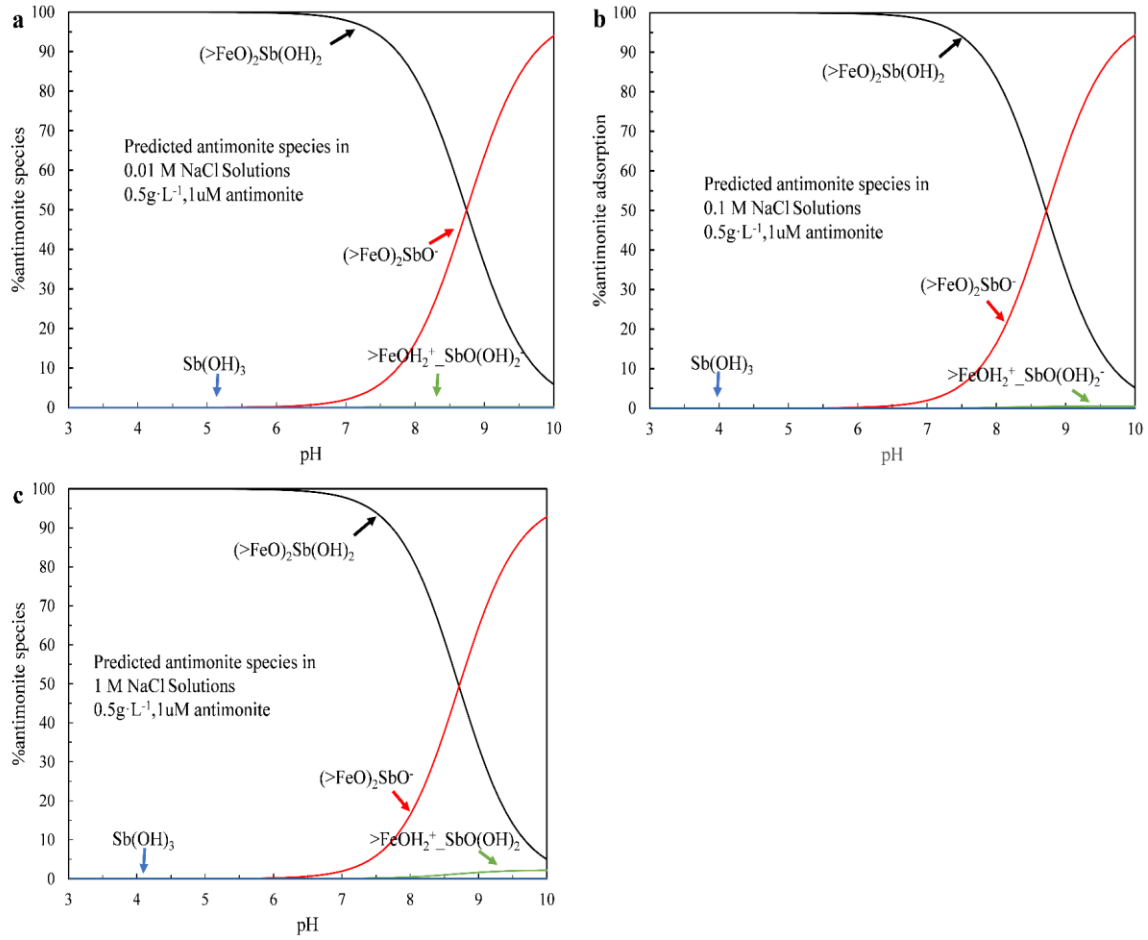

Figure 4-10 Predicted model Sb(III) surface speciation on ferrihydrite in NaCl electrolyte solutions with different electrolyte concentrations in constant Sb(III) concentration (1 μM): (a) 0.01 M, (b) 0.1 M, and (c) 1 M.

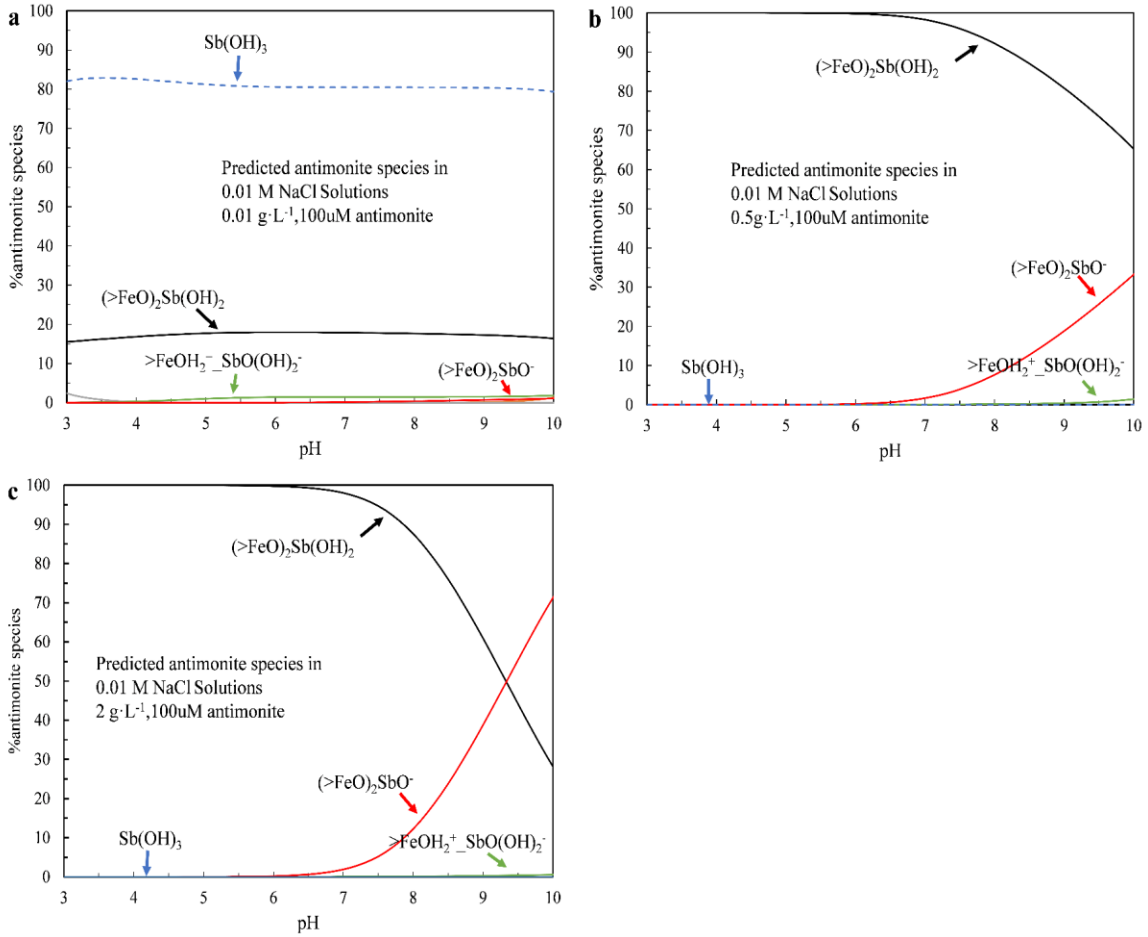

Figure 4-11 Predicted model Sb(III) surface speciation on ferrihydrite in NaCl electrolyte solutions as a function of solid concentration: (a) 100 μM 0.01 g/L, (b) 100 μM 0.5 g/L and (c) 10 μM 2 g/L.

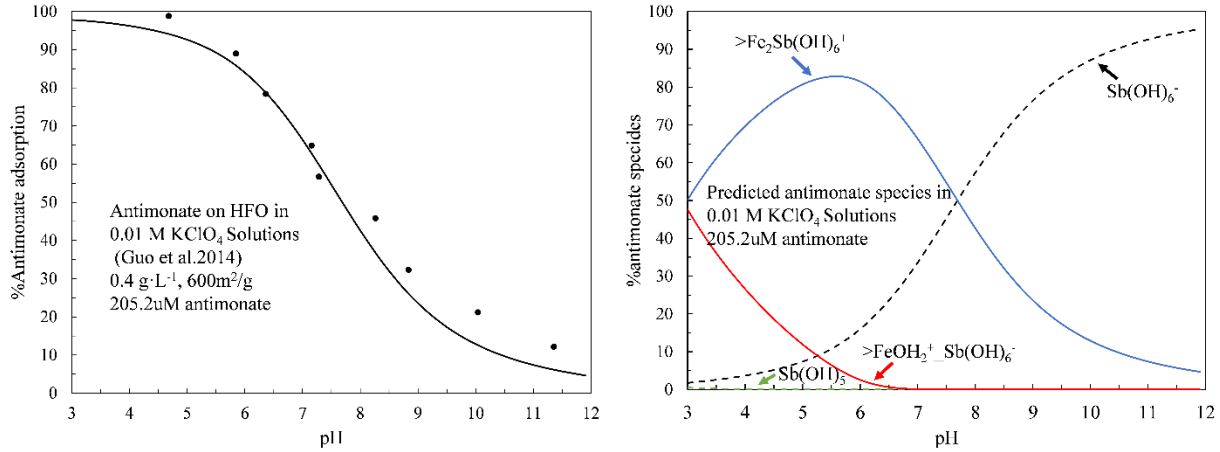

Figure 4-12 The data points represent experimental results for sulfate adsorption on HFO from (Guo et al., 2014). The curves represent regressions calculations with the ETLM.

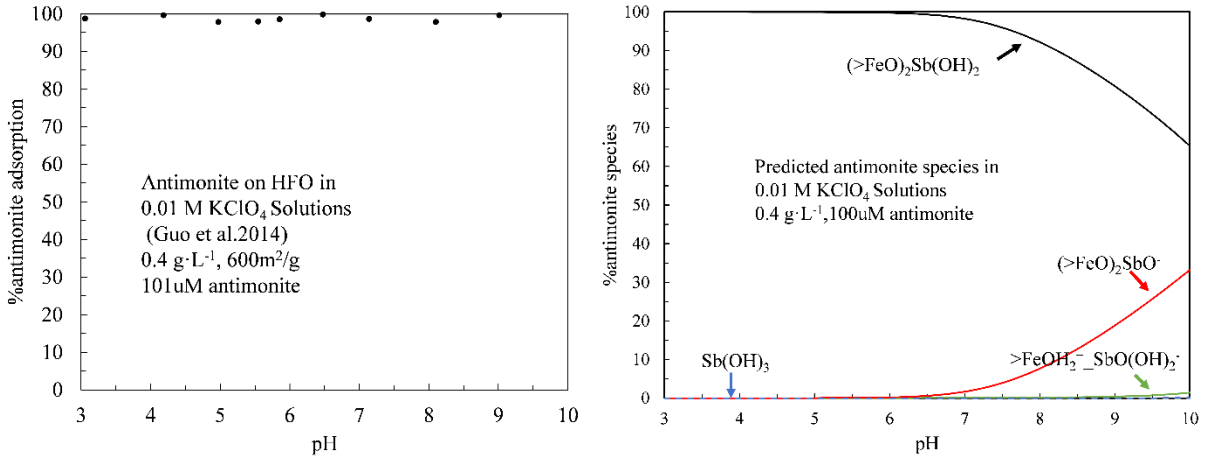

Figure 4-13 The data points represent experimental results for sulfate adsorption on HFO from (Guo et al., 2014). The curves represent regressions calculations with the ETLM.

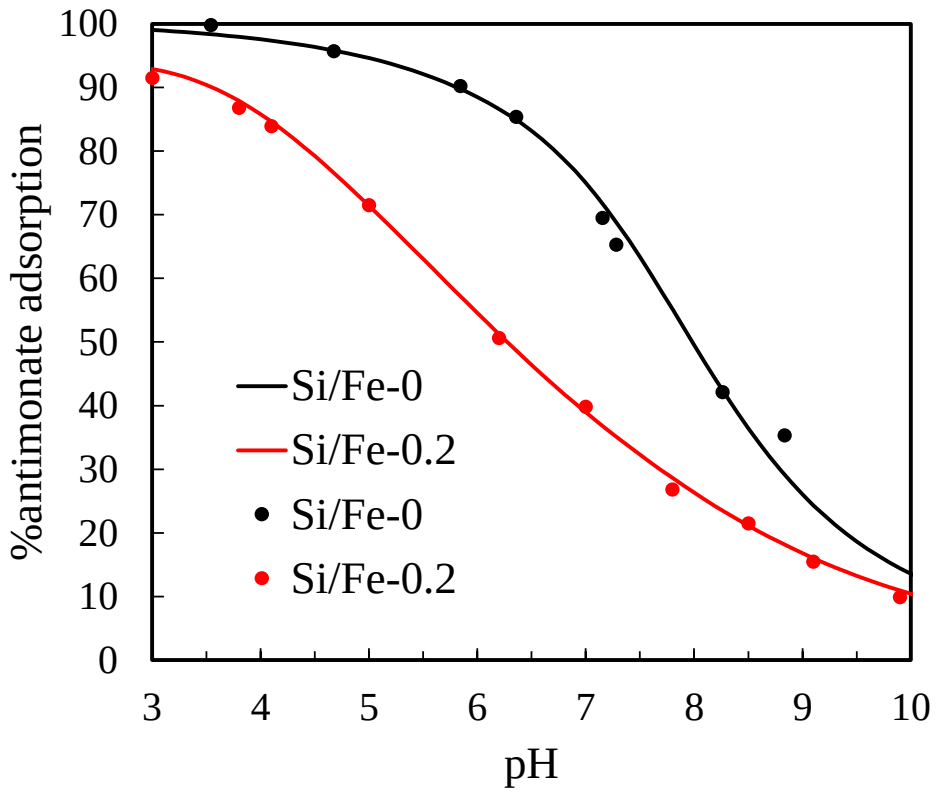

Figure 4-14 Sb(V) adsorption on ferrihydrite under different silica concentration in 0.01 M NaCl as a function of pH. The initial Sb(V) is 100 μM. The data points represent experimental results and the curves represent regressions calculations with the ETLM.

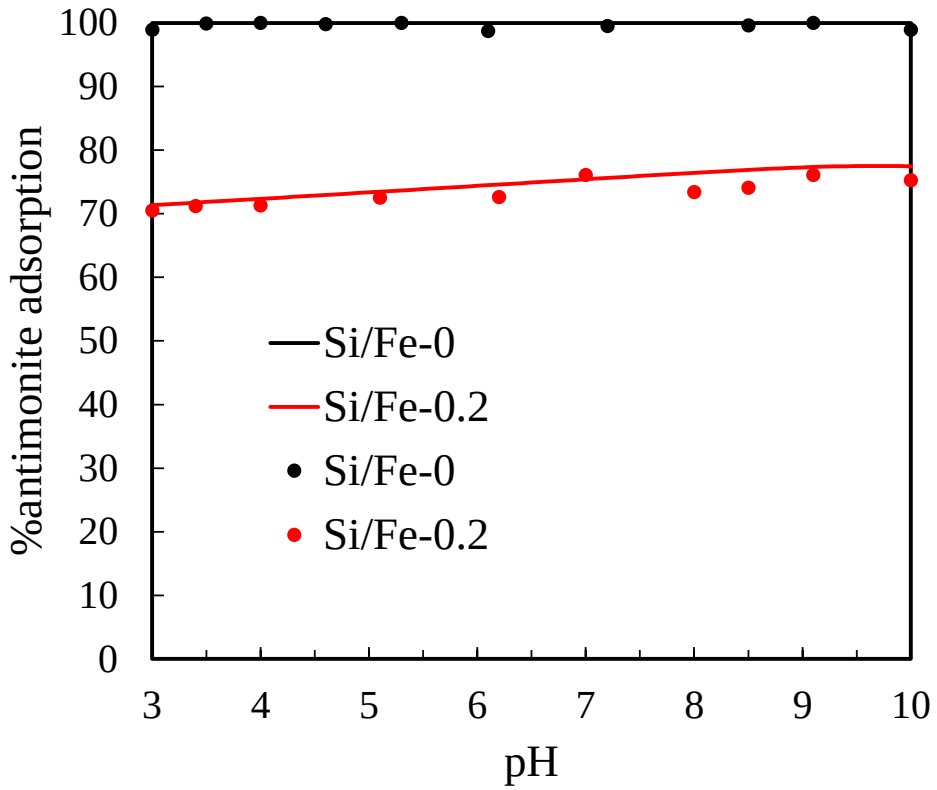

Figure 4-15 Sb(III) adsorption on ferrihydrite under different silica concentration in 0.01 M NaCl as a function of pH. The initial Sb(III) is 100 μM. The data points represent experimental results and the curves represent regressions calculations with the ETLM.

5. Difference between antimony adsorption onto ferrihydrite and antimony co-precipitated with ferrihydrite and their silica effect

Abstract

Elevated antimony concentrations in aqueous environments from anthropogenic sources are becoming of global concern. In this respect iron oxides are known to strongly adsorb aqueous antimony species with different oxidation states, but the effect of silica on the removal characteristics is not well understood despite being a common component in the environment. In this study, ferrihydrite was synthesized at various Si/Fe molar ratios to investigate its adsorption and co-precipitation behaviors with aqueous antimony anionic species, Sb(III) and Sb(V). The X-ray diffraction analyses of the precipitates showed two broad diffraction features at approximately 35° and 62° 2θ, which are characteristics of 2-line ferrihydrite, but no significant shifts in peak positions in the ferrihydrite regardless of the Si/Fe ratios. The infrared spectra showed a sharp band at ~930 cm^{-1}, corresponding to asymmetric stretching vibrations of Si-O-Fe bonds which increased in intensity with increasing Si/Fe molar ratios. Further, the surface charge on the precipitates became more negative with increasing Si/Fe molar ratios. The adsorption experiments indicated that Sb(V) was preferentially adsorbed under acidic conditions which decreased dramatically with increasing pH while the adsorption rate of Sb(III) ions was independent of pH. However, the presence of silica suppressed the adsorption of both Sb(III) and Sb(V) ions. The results showed that Sb(III) and Sb(V) ions were significantly inhibited by co-precipitation with ferrihydrite even in the presence of silica by isomorphous substitution in the ferrihydrite crystal structure.

5.1 Introduction

Antimony (Sb) is widely used in industry as a catalyst in plastics, flame retardants, storage batteries, and ammunition (Filella et al., 2002a)(Carlin Jr, 2000)(Herbst et al., 1985). It is the ninth most mined metal for industrial uses worldwide (Krachler et al., 2001)(Filella et al., 2002b), and one result of this is elevated concentrations of Sb in many soils and waters, especially

around mining and smelting areas (Scheinost et al., 2006)(He, 2007)(Wang et al., 2011)(Westerhoff et al., 2008)(Mitsunobu et al., 2006)(Lichti et al., 2015)(Okkenhaug et al., 2012). There has been a growing concern over the adverse effect of Sb on human health due to its toxicity. Sb has been increasingly identified as a toxic heavy metal with implications for it being a carcinogen (Gebel, 1997). This has caused Sb and its compounds to be listed as a leading pollutant by the United States Environmental Protection Agency (USEPA, 1979) and the Council of the European Union (CEC, 1976).

Sb may be present in a variety of oxidation states (−III, 0, III, V) because of its s^2p^3 outer orbital electron configuration, however it is mainly found in the two oxidation states (III and V) in environmental, biological, and geochemical environments (Filella et al., 2002a)(Filella et al., 2002b). The toxicity of Sb depends strongly on its oxidation state, and reduced Sb(III) species are ten times more poisonous than oxidized Sb(V), similar to the case of arsenic (Oorts et al., 2008). In spite of the widespread usage and the substantial toxicity, the geochemical behaviors of antimony in soil and aquatic systems are poorly understood (Krupka and Serne, 2002)(Mitsunobu et al., 2010).

Recent studies have shown that both Sb(III) and Sb(V) appear to adsorb strongly onto iron oxides (Mitsunobu et al., 2006)(Mitsunobu et al., 2010) (Leuz et al., 2006)(Okkenhaug et al., 2013), which thereby strongly influence the speciation, mobility, and final states of Sb in the environment. Sb is preferentially associated with iron(III) oxyhydroxide in soils and sediments on the basis of direct evidence using extended X-ray absorption fine structure spectroscopy (EXAFS) (Scheinost et al., 2006)(Mitsunobu et al., 2006)(Ackermann et al., 2009). This would suggest that adsorption and incorporation processes into the iron(III) (oxyhydr)oxide phases would be able to control the mobility of Sb in natural environments. Several experimental studies have investigated the Sb adsorption mechanism on iron(III) oxyhydroxides, focusing on Sb speciation at the solid-liquid (water) interface using EXAFS (Mitsunobu et al., 2006)(Guo et al., 2014). However, the surface structure of Sb(III) and Sb(V) binding with iron(III) oxyhydroxides is still unclear. A further important process, co-precipitation with iron(III) (oxyhydr)oxides, does not appear to have been reported. In natural systems, iron(III)(hydro)oxides are often identified in precipitates from the oxidation of iron(II) in the presence of the relevant anions. Thus, the precipitation process may be as important as adsorption, as a sequestration process of Sb species

by iron (III) (oxyhdr)oxides when groundwater with natural or added Fe comes in contact with air or oxygenated water takes place.

Further, as iron minerals are closely associated with silica, one of the most common ligands present in natural environments, pure ferrihydrite is not, strictly speaking, present in nature. Silica always associates with ferrihydrite in the structure or on the ferrihydrite surface. This could mean that silica may affect the crystallization behavior as well as the capacity of ferrihydrite to regulate hazardous element recycling. The effect of silica on arsenic adsorption has been reported for ferrihydrite (Swedlund and Webster, 1999), but no reports of the effect of silica on Sb adsorption or co-precipitation have been reported for other oxides.

Based on the above, the objectives of this study were to (1) to compare the relative adsorption capabilities of Sb(III) and Sb(V) onto ferrihydrite; (2) to evaluate the effect of dissolved silica during the adsorption and co-precipitation of Sb(III) and Sb(V) on ferrihydrite; and also (3) to better understand the differences between the adsorption and co-precipitation processes of Sb.

5.2 Materials and methods

5.2.1 Synthesis

A stock solution of ferric iron (Fe(III), 0.05 mol/L), was prepared by dissolving reagent grade $Fe(NO_3)_3 \cdot 9H_2O$ (Kanto,99%, Tokyo, Japan) in ultrapure water (18M·W·cm). Tetraethylorthosilicate (TEOS; Alfa Aesar, 98%, Heysham, United Kingdom) was then added to 500 mL of the Fe solution to achieve silica concentrations of 0 to 20×10^{-3} mol/L (i.e., Si/Fe = 0.4). These solutions containing both silica and Fe(III) were stirred for about 30 min to dissolve the TEOS completely before pH adjustment. The initial pH of the solution was about 1.8, which was adjusted to about 7.0 ± 0.1 by titrating 1.0 M NaOH (Kanto, 97%, Tokyo, Japan). Addition of the NaOH hydrolyzes the Fe(III) in the solution resulting in formation of a slurry of dark brown precipitate. The slurries were stirred for an additional 15 min to allow the pH to stabilize. The resulting 500 mL slurries were then equally divided into 50 mL polypropylene bottles and then washed in the bottles at least four times with deionized water to remove the salts and freeze-dried for at least 24 h. Samples with different silica concentrations were replicated to evaluate the reproducibility of the experimental results.

5.2.2 Adsorption experiments

Stock solutions of Sb(V) were prepared by dissolving $KSb(OH)_6$ powder (Wako, 50%, Tokyo, Japan) into deionized water, and of Sb(III) by dissolving Sb_2O_3 powder (Wako, 98%, Tokyo, Japan) into 2 mol/L HCl (Kanto, 37%, Tokyo, Japan) solution. The initial concentration of both the Sb(III) and Sb(V) was 100 μM. A control experiment showed that neither Sb(III) nor Sb(V) precipitated under this initial concentration. The adsorption experiments with both Sb(III) and Sb(V) were conducted at a solid concentration of 0.5 g/L with a background ionic strength of 0.01 M NaCl. Triplicates of 40 mL suspensions with a fixed amount of solids (20 mg) and 100 μM solute concentrations were prepared in 50 mL polypropylene bottles. The experiments were conducted at a pH range of 3-12. The pH of the suspensions was adjusted using small volumes of 0.5 M HCl or 0.5 M NaOH during the experiments. Suspensions were agitated on a rotary shaker (110 rpm) for 24 h at 20.5 °C. After the reaction, the suspensions were centrifuged and then filtered through a 0.2 μm cellulose membrane filter for further analysis.

5.2.3 Co-precipitation experiments

The Sb(III) and Sb(V) co-precipitation experiments were conducted by hydrolysis of silica and Fe(III) solution and either Sb(III) or Sb(V) in deionized water, following the method of Waychunas et al. (Waychunas et al., 1993). Co-precipitated samples were prepared by simultaneous addition either of 100 μM Sb(III) or Sb(V), 0.05 M Fe(III) solution, and TEOS to yield the different Si/Fe ratios of the precipitate (Si/Fe = 0-0.4). In all cases, the Si/Fe ratios of the samples were determined assuming complete precipitation of all added Fe and silica. The 500 mL mixed solutions were maintained at the experimental pH (7.0 ± 0.1) by the addition of 1.0 M NaOH. After precipitation and approximately 30 min of pH stabilization, the co-precipitates were washed at least four times with deionized water by centrifugation with a 50 mL plastic tube, then the suspensions were filtered through a 0.2 μm cellulose membrane filter for further analysis.

5.2.4 Analytical methods

The powder X-ray diffraction (XRD) analyses were conducted to determine the mineralogy of the dark brown precipitates. Synthesized precipitates were analyzed by XRD using a Rigaku RINT2000 (Rigaku Co., Tokyo, Japan) X-ray diffractometer operated at 40 kV and 40 mA,

equipped with a Cu target and graphite monochromator, and diffraction profiles were collected from 10° to 70° 2θ.

To measure the concentration of Sb, Inductively Coupled Plasma (ICP)-Atomic Emission Spectroscopy (AES) analyses were conducted. Filtrates were analyzed for Sb(III) and Sb(V) as total Sb by ICP-AES (ICPE-9000). The detection limit of this method was 0.1 µg/L. The pH of the solutions was measured with a pH meter (HORIBA, D-55) calibrated by using commercial pH 4.0, 7.0, and 10.0 buffer solutions. The amount of solute adsorbed was calculated using the difference between the initial and final dissolved solute concentrations.

The XRD data were processed by Match (version 3.3.0) software (Crystal Impact. Bonn, Germany), All the graphs were exported by Sma4 (Version 1.47) software (T. Suzuki, Kyoto, Japan) and Microsoft office 2013.

5.3 Results and discussion

5.3.1 Sb(III) and Sb(V) adsorption with different Si/Fe ratios

The adsorbed ratios of Sb(III) and Sb(V) ions onto ferrihydrite in 0.01 M NaCl solutions is shown as a function of pH in **Figure 5-1**. The adsorption rate of Sb(V) was over 90% between pH 3 and 6. With increasing pH, from 6 to 12, the adsorption rate of Sb(V) rapidly decreased from 90% to 10%. A strong pH dependence on Sb(V) adsorption was reported when goethite and ferrihydrite were used as adsorbents ((Guo et al., 2014)(Qi and Pichler, 2016)). The effect of pH on Sb(III) adsorption however was much weaker, showing a constant adsorbed fraction ~95% over the whole of the pH range investigated here, from 3 to 12. This is in good agreement with earlier studies (Leuz et al., 2006)(Guo et al., 2014). The difference in adsorption efficiency of Sb(III) and Sb(V) ions may mainly be due to differences in the electrostatic interactions between the sorbent surface and Sb oxyanions present in the solutions. The $Sb(OH)_6^-$ is the dominant Sb(V) species over the wide pH range, here pH 3-10 (Filella et al., 2002a). The surface charge of ferrihydrite is positive below pH ~8.2, pH_{pzc} (point of zero charge), and electrostatic attraction between the $Sb(OH)_6^-$ and the surface of ferrihydrite can be expected to be stronger under acidic conditions since $Sb(OH)_6^-$ is negatively charged under the conditions here, leading to electrostatic forces playing an important role in the Sb(V) adsorption. For Sb(III), a trihydroxy

neutral species, $Sb(OH)_3$, is the dominant species over a wide pH range of 2-11 (Filella et al., 2002a), and only minor or no electrostatic effects may be expected for the Sb(III) adsorption. A specific interaction (so-called surface complexation) may also play an important role between the adsorbate and adsorbent in addition to the electrostatic effect.

The effect of silica on the adsorption of Sb was investigated by varying the Si/Fe ratio of the precipitates at pH 7. The results demonstrated that both Sb(III) and Sb(V) are significantly affected by the presence of silica, with the adsorbed fraction decreasing with increasing Si/Fe ratios (**Figure 5-2**). Both Sb(III) and Sb(V) adsorption were suppressed in the presence of silica. The adsorbed fractions of Sb(III) and Sb(V) ions decreased from >96% at Si/Fe = 0 to 60% at Si/Fe = 0.4 and from >75% at Si/Fe = 0 to 30% at Si/Fe = 0.4, respectively. This shows that Sb(V) was affected more significantly by silica than Sb(III). The drop in Sb(V) adsorption efficiency is likely a result of decreased electrostatic interactions between Sb(V) ions and the surface of ferrihydrite by the decreased surface charge of ferrihydrite due to the presence of silica on the ferrihydrite surface. Swedlund (Swedlund and Webster, 1999) also suggested that the decreasing surface charge of ferrihydrite by increasing silica concentrations could be an important factor in inhibiting As adsorption. Besides the effect of silica to decrease the surface charge, silica may also suppress adsorption of Sb by occupying surface sites by inner sphere complexation.

5.3.2 Sb(III) and Sb(V) co-precipitation with different Si/Fe ratios

The co-precipitation efficiencies were calculated using the difference between the initial and final dissolved solute concentrations. **Figure 5-3** shows the co-precipitated ratios of Sb(III) and Sb(V) ions onto ferrihydrite as a function of pH. The co-precipitated rate of both Sb(III) and Sb(V) was over 96% for the whole range of pH. Moreover, the co-precipitation of Sb(III) and Sb(V) with ferrihydrite shown no pH-dependency, which is different from that of adsorption.

Figure 5-4 shows the co-precipitation rates of Sb(III) and Sb(V) ions with different Si/Fe ratios of ferrihydrite at pH 7. The co-precipitation efficiencies were ~100% for both Sb(III) and Sb(V) in the absence of silica (Si/Fe = 0). No effect of silica was observed even at the highest Si/Fe ratio in this study (Si/Fe = 0.4). Here the Sb(V) octahedra may replace Fe octahedrals due to their structural compatibility. By using EXAFS analysis, Scheinost (Scheinost et al., 2006) reported

that the Sb(V) can form both edge-sharing and corner-sharing of inner-sphere complexes to iron oxides in shooting range soils, which would be consistent with our findings.

In the case of Sb(III) co-precipitation, with octahedral or tetrahedral structures absent in Sb(III), the Sb(III) ions could alternatively be surrounded by Fe hydroxides, which would increase the co-precipitation efficiency. However, there is little previous study regarding the co-precipitation mechanism of Sb(III) with ferrihydrite, more specific evidence is necessary to discuss issues related to this.

The absence of any effect of silica on the Sb(III) and Sb(V) co-precipitation process may be because of isomorphous substitution during the simultaneous addition of silica and Sb to the co-precipitation system. Specifically, the Si occupies a tetrahedral environment, being surrounded by four oxygen centers. These tetrahedral structures may share corners with two adjacent edge-sharing Fe octahedral. This has been proposed by Pokrovski (Pokrovsky et al., 2012) on the basis of Fe K-edge studies of Fe(III) hydrolyzed in the presence of silica. In addition, the tetrahedral Si could also coordinate with Fe tetrahedral structures since the ferrihydrite also has a tetrahedral structure as was demonstrated by a previous study (Michel et al., 2007). If so, the silica may incorporate into the ferrihydrite structure during the co-precipitation process, which makes it more likely to have only a minor effect on the Sb retention.

Significant differences were observed in the results of the adsorption and co-precipitation experiments. The co-precipitation of Sb(III) and Sb(V) with ferrihydrite is much more effective than that of the adsorption with or without Sb(III) and Sb(V) in aqueous environments. Intuitively, the adsorption process in our experiments was solely due to adsorption onto the ferrihydrite surface, a surface complexation reaction. The co-precipitation process in principle could include the formation of phases containing Sb(III) and Sb(V) in the structure as well as adsorbing Sb(III) and Sb(V) as an impurity onto the surface of ferrihydrite. This implies that Fe minerals can act as effective scavengers of Sb in natural environments where ferrihydrite is formed.

5.3.3 XRD analyses of adsorption and co-precipitation samples

Both adsorption and co-precipitation samples were analyzed by XRD for mineralogical characterization. In the adsorption samples of the ferrihydrite series, all of the XRD patterns

were almost identical to that of pure two-line ferrihydrite, and any other peaks and peak shift were not observed with both Sb(III) and Sb(V) loading (**Figure 5-5**, **Figure 5-6**). These findings indicate that other Sb and Fe hosting minerals such as Fe antimonate are not formed at all Sb loading levels in the Si-ferrihydrite series. In co-precipitation samples, the peak around 30° and 60° gradually shifted to a lower angle in Si/Fe varies ratios for both Sb(III) and Sb(V). In addition to these noticeable features, broadening of both peaks was also observed in Sb(III) and Sb(V) co-precipitation samples. Similar shifts and/or broadening of peaks were reported in incorporation of metals such as Cr, Zn, Pb, and Ce into Fe(III) oxides as a solid solution (Mohapatra et al., 2005)(Kaur et al., 2009). They suggest that the shift and broadening can be attributed to the differences in ionic radius and charge between Fe(III) and guest metals in Fe(III) oxides. These differences may lead to a change in *d*-spacing and distortion of the structure when the substitution occurs. Moreover, no other peak additions to the peaks related to ferrihydrite were observed in the co-precipitation series at all Si/Fe ratios, indicating that other Sb and Fe hosting minerals were not formed or their abundances were negligible in present system.

5.3.4 XPS analyses of adsorption and co-precipitation samples

XPS spectra of ferrihydrite before and after Sb adsorption and co-precipitation are presented in **Figure 5-7**. Since the binding energy of Sb $3d_{5/2}$ was slightly lower than O 1s, the O 1s + Sb $3d_{5/2}$ was shifted to higher positions after adsorption and co-precipitation because more Sb was bonded to ferrihdyrite, this confirms that the detected antimony species was chemically distinct from the adsorbate. A previous study from Vithanage (Vithanage et al., 2013) found that the Sb $3d_{3/2}$ peaks appeared clearly after Sb(V) and Sb(III) adsorption on iron-oxide-rich red earth soils, which consist with our results. But the difference between the adsorption and co-precipitation samples were not significant. Most importantly, strong and relatively weak Sb $3d_{3/2}$ peaks appeared clearly after Sb(V/III) co-precipitation with ferrihydrite and Sb(III) adsorption on ferrihydrite, respectively, duo to the higher binding affinity of ferrihydrite for Sb(III) than for Sb(V). The increasing intensity of Sb $3d_{3/2}$ after Sb(V) and Sb(III) co-precipitation, which also provided direct evidence that Sb precipitated with ferrihydrite rather than reacted surface ferrihydrite groups. These could further confirm that the co-precipitation process including the structure incorporation to ferrihydrite other than the adsorption only happened on the surface of ferrihydrite.

5.3.5 TEM analyses of adsorption and co-precipitation samples

TEM analyses of ferrihydrite before and after Sb adsorption and co-precipitation are presented in **Figure 5-8** and **Figure 5-9.** The morphologies of adsorption samples were almost identical to that of the 2-line ferrihydrite, which appeared to be granular-like morphologies with several nm in size, while the co-precipitation samples specimens have grape-like aggregates which are composed of granular-like particles. The similar morphologies could indicate that other Sb and Fe hosting minerals such as Fe antimonate or antimonite are not formed at all Sb loading levels in the adsorption and co-precipitation sample series, which is consist with the XRD results. However, the granular-like particles in the co-precipitation samples are less distinct than those in the adsorption samples. It could infer that Sb be associated with ferrihydrite, which may be located between the ferrihydrite particles as well. These could further confirm that the co-precipitation process including the structure incorporation to ferrihydrite other than the adsorption only happened on the surface of ferrihydrite.

5.4 Conclusions

This study examined dissolved silica effects on the adsorption and co-precipitation of Sb(III) and Sb(V) with ferrihydrite. The Sb(V) adsorption onto ferrihydrite increased under more acidic conditions. Overall, Sb(III) adsorption was constant over a broad pH range. The adsorption of Sb(III) and Sb(V) appeared to be significantly affected by the presence of silica, while co-precipitation of Sb(III) and Sb(V) with ferrihydrite was not inhibited by silica. Further, the co-precipitation process took place with higher efficiency than that of the adsorption.

Our findings on the behavior of Sb(III) and Sb(V) adsorption and co-precipitation with ferrihydrite and Si-ferrihydrite have important implications for determining the role of ferrihydrite in controlling the final state of Sb in the environments in which it is released. Although ferrihydrite is an excellent substance for capturing Sb, its use as a medium in a natural Si-rich system should be considered with caution because it will tend towards inhibition of Sb capture induced by the Si-rich environment. However, this may be different in the case of co-precipitation processes. In the present study, we found that silica and Sb(III) and Sb(V) can be incorporated into ferrihydrite and that these three are structurally compatible with ferrihydrite. The co-precipitation process of Sb(III) and Sb(V) would not be greatly influenced by the silica

factor. Thus, Sb(III) and Sb(V) co-precipitation with ferrihydrite would be more efficient than Sb(III) and Sb(V) adsorption by ferrihydrite. This finding will be important when making predictions of the final state of Sb associated with ferrihydrite in natural Si-rich systems.

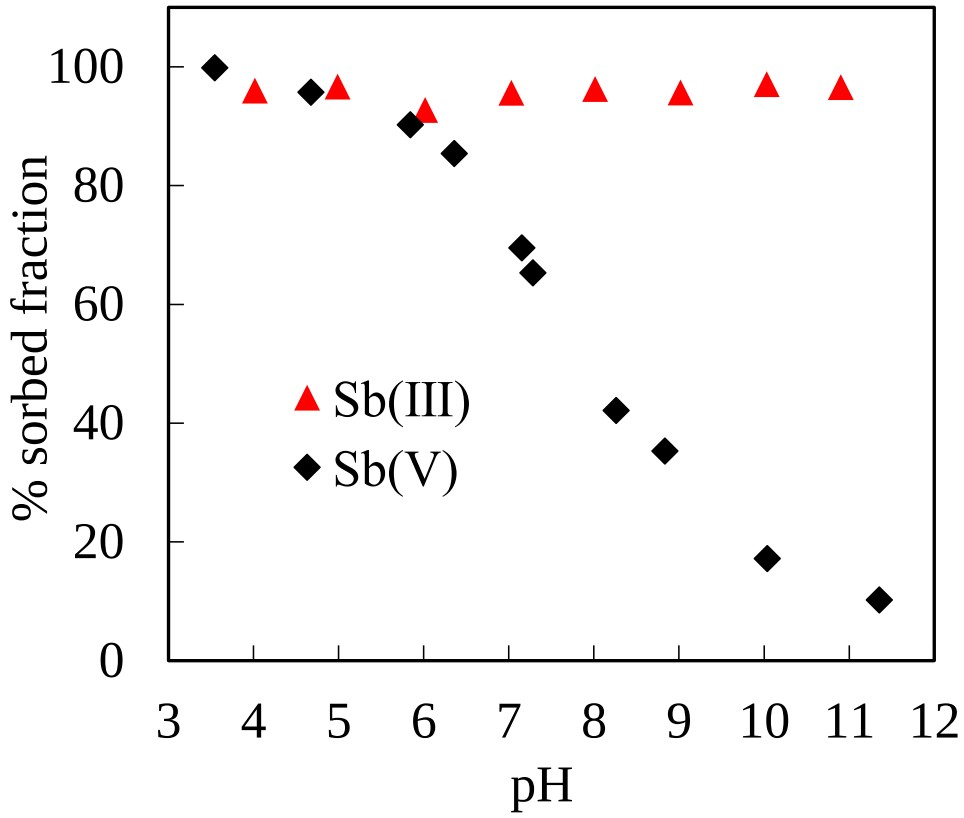

Figure 5-1 Adsorption of Sb(III/V) on ferrihydrite as a function of the pH in 0.01 M NaCl solutions. The initial Sb(III/V) concentration were 100 µM for each sample. The concentrations of suspended solids were 0.5 g/L.

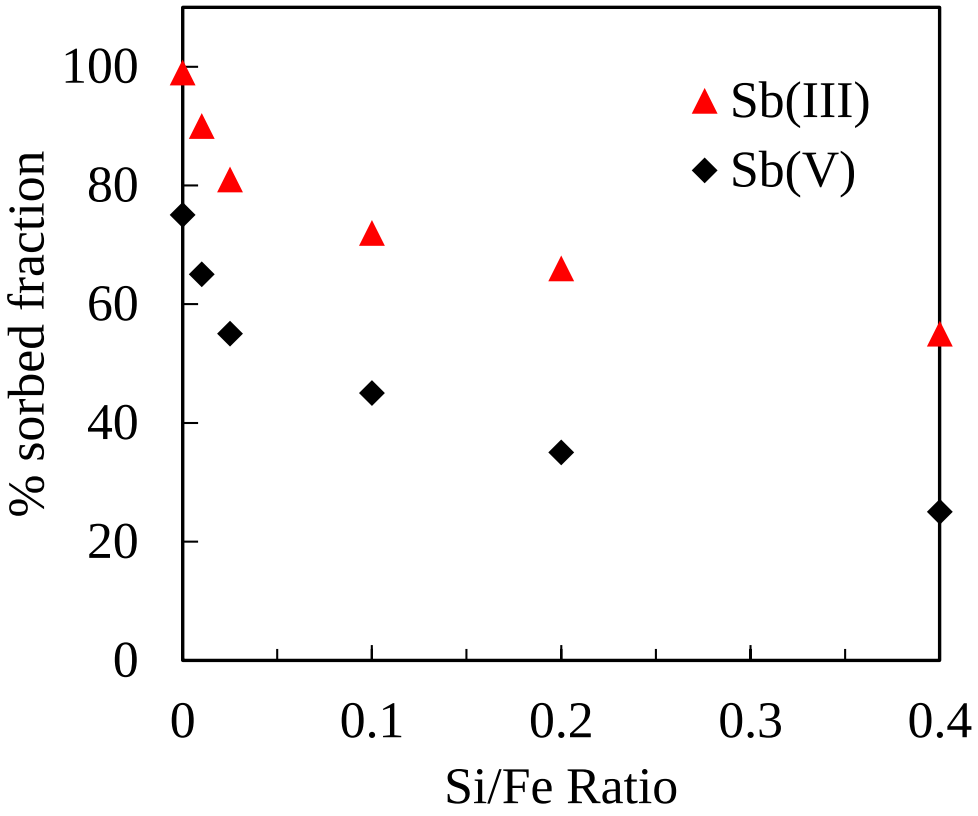

Figure 5-2 Adsorption of Sb(III/V) with different Si/Fe ratios of ferrihydrite at pH 7. The initial Sb(III/V) concentrations were 100 µM for all samples.

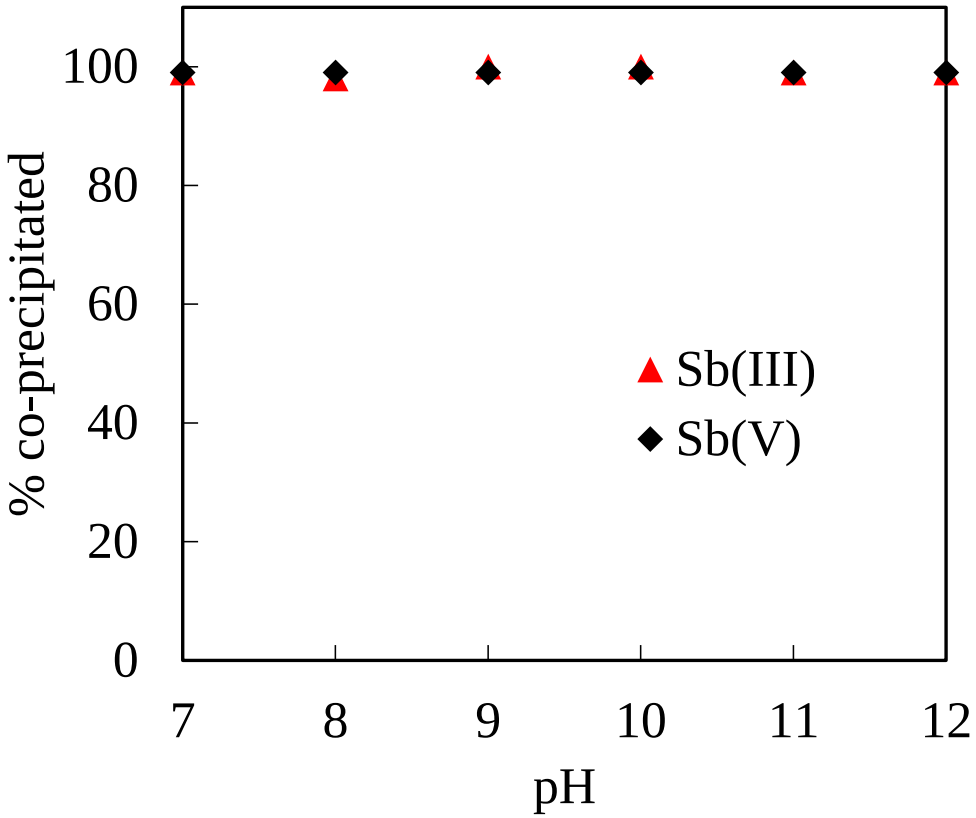

Figure 5-3 Co-precipitation of Sb(III/V) on ferrihydrite as a function of the pH in 0.01 M NaCl solutions. The initial Sb(III/V) concentration were 100 µM for each sample.

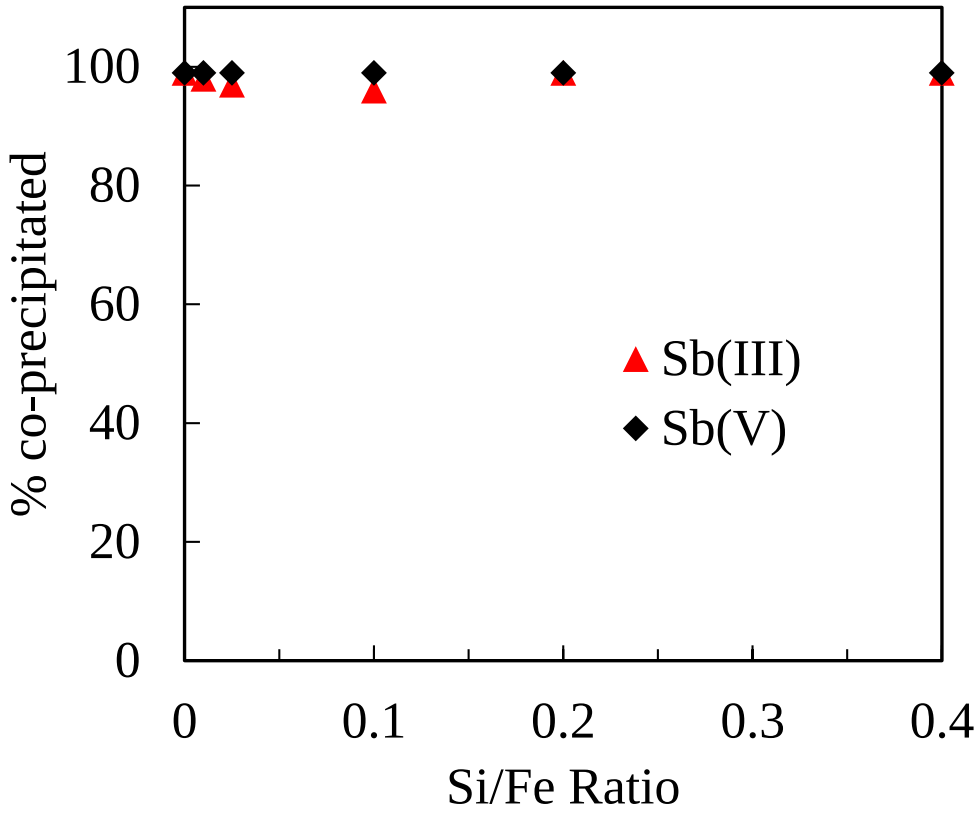

Figure 5-4 Co-precipitation of Sb(III/V) with different Si/Fe ratios of ferrihydrite at pH 7. The initial Sb(III/V) concentrations were 100 µM for all samples.

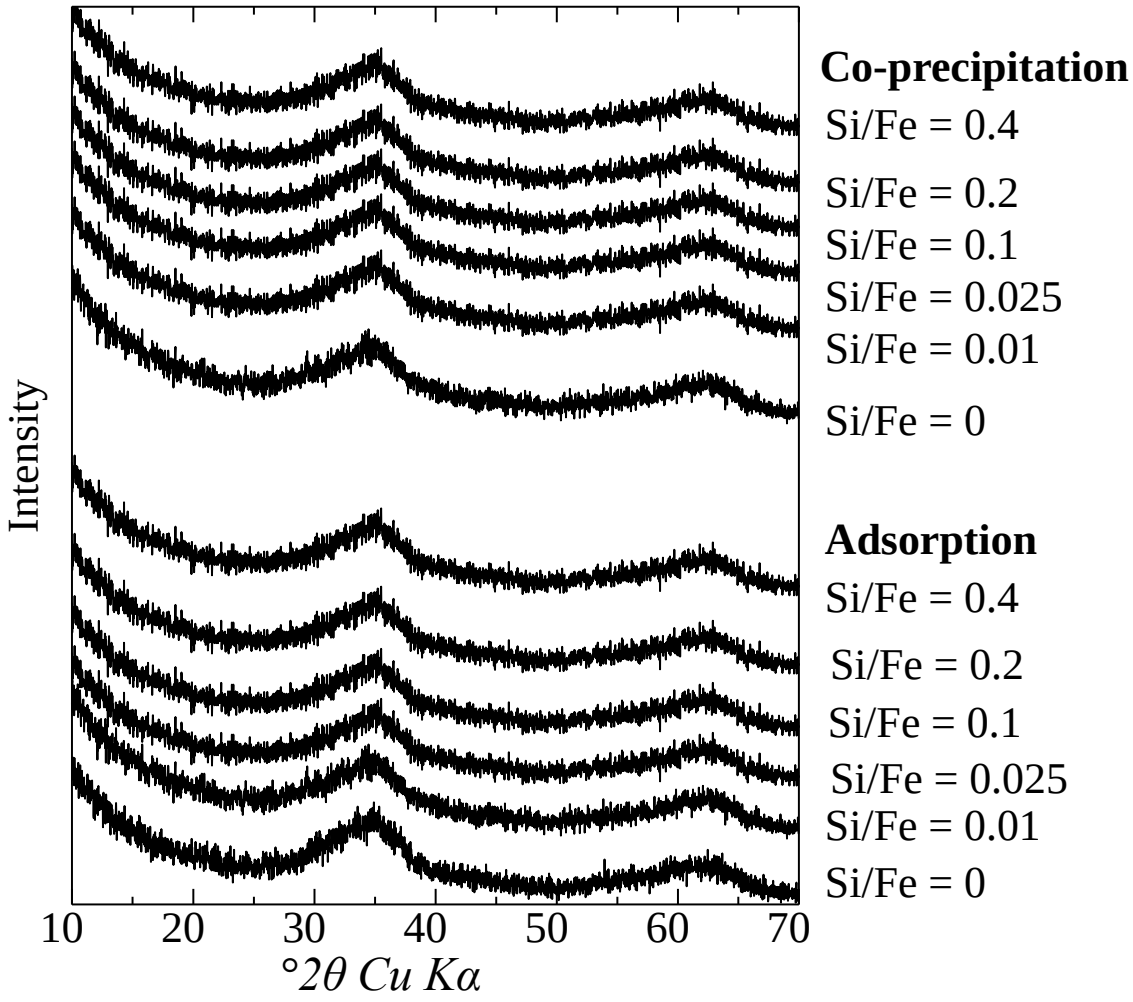

Figure 5-5 XRD patterns of Sb(III)-adsorbed and co-precipitated ferrihydrite.

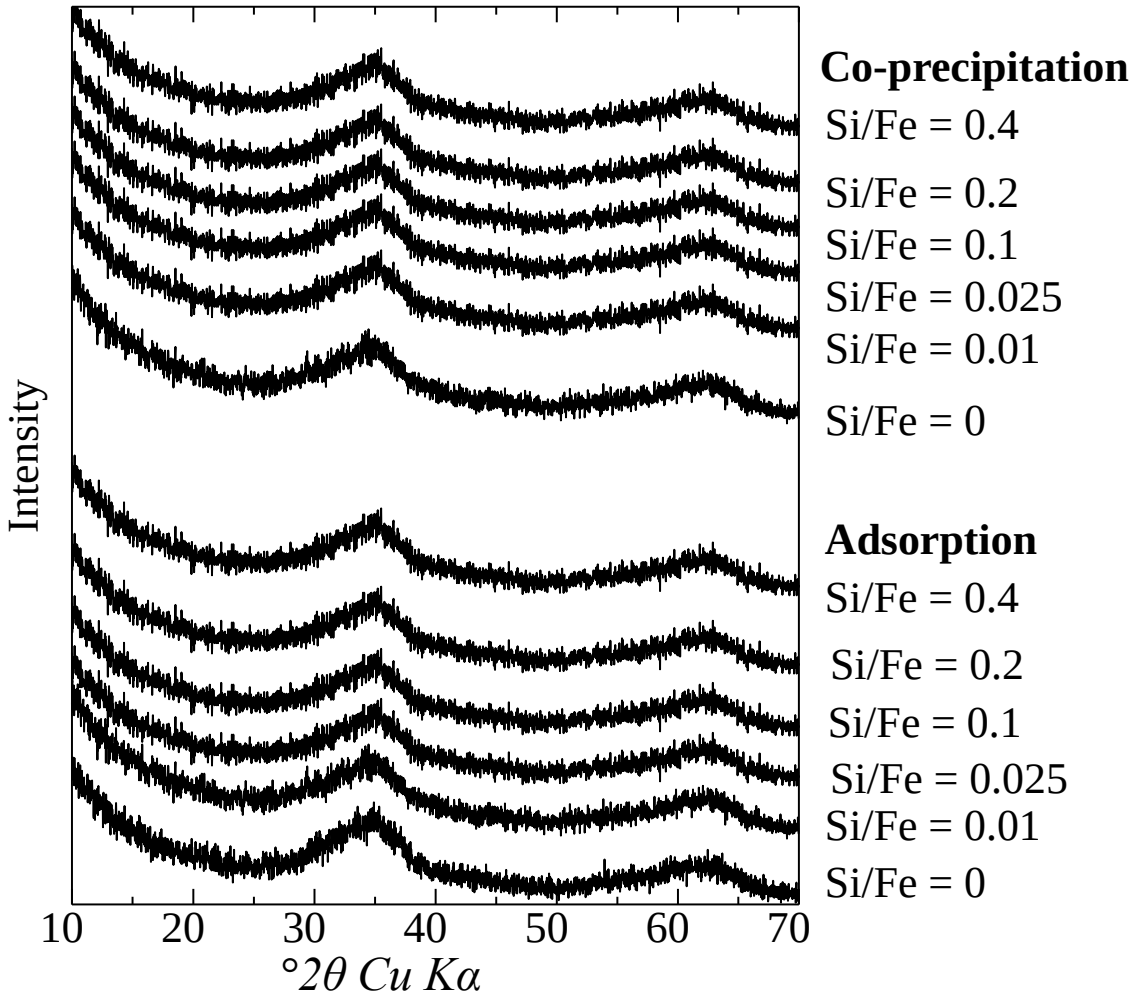

Figure 5-6 XRD patterns of Sb(V)-adsorbed and co-precipitated ferrihydrite.

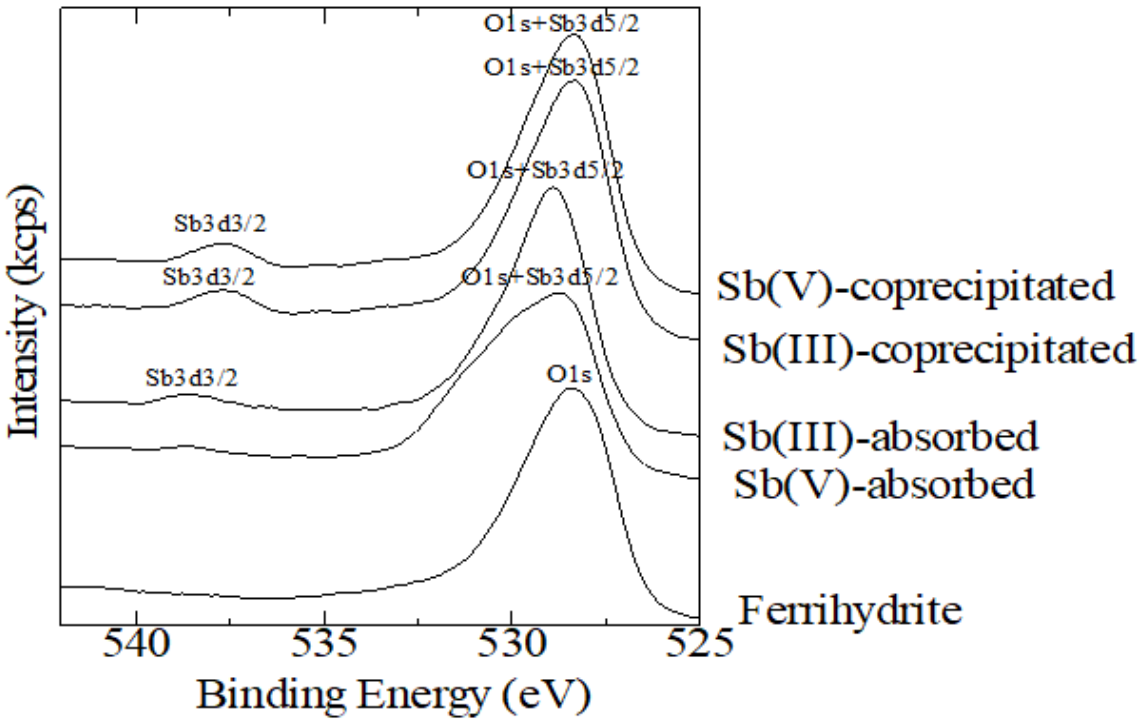

Figure 5-7 XPS spectra analyses of ferrihydrite and Sb(III/V)-adsorbed and co-precipitated ferrihydrite.

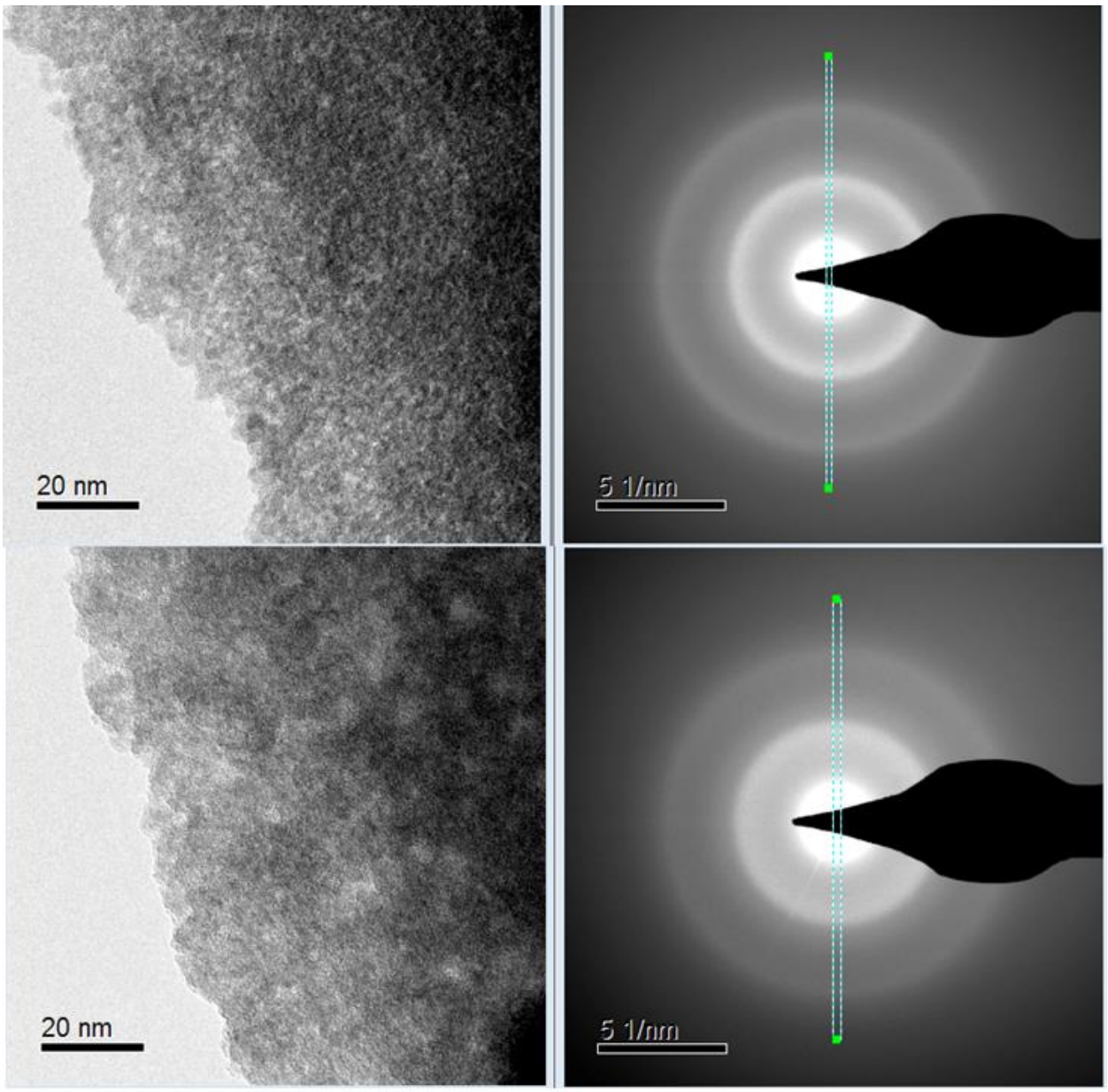

Figure 5-8 TEM analyses of Sb(III)-adsorbed (upper) and co-precipitated ferrihydrite (lower).

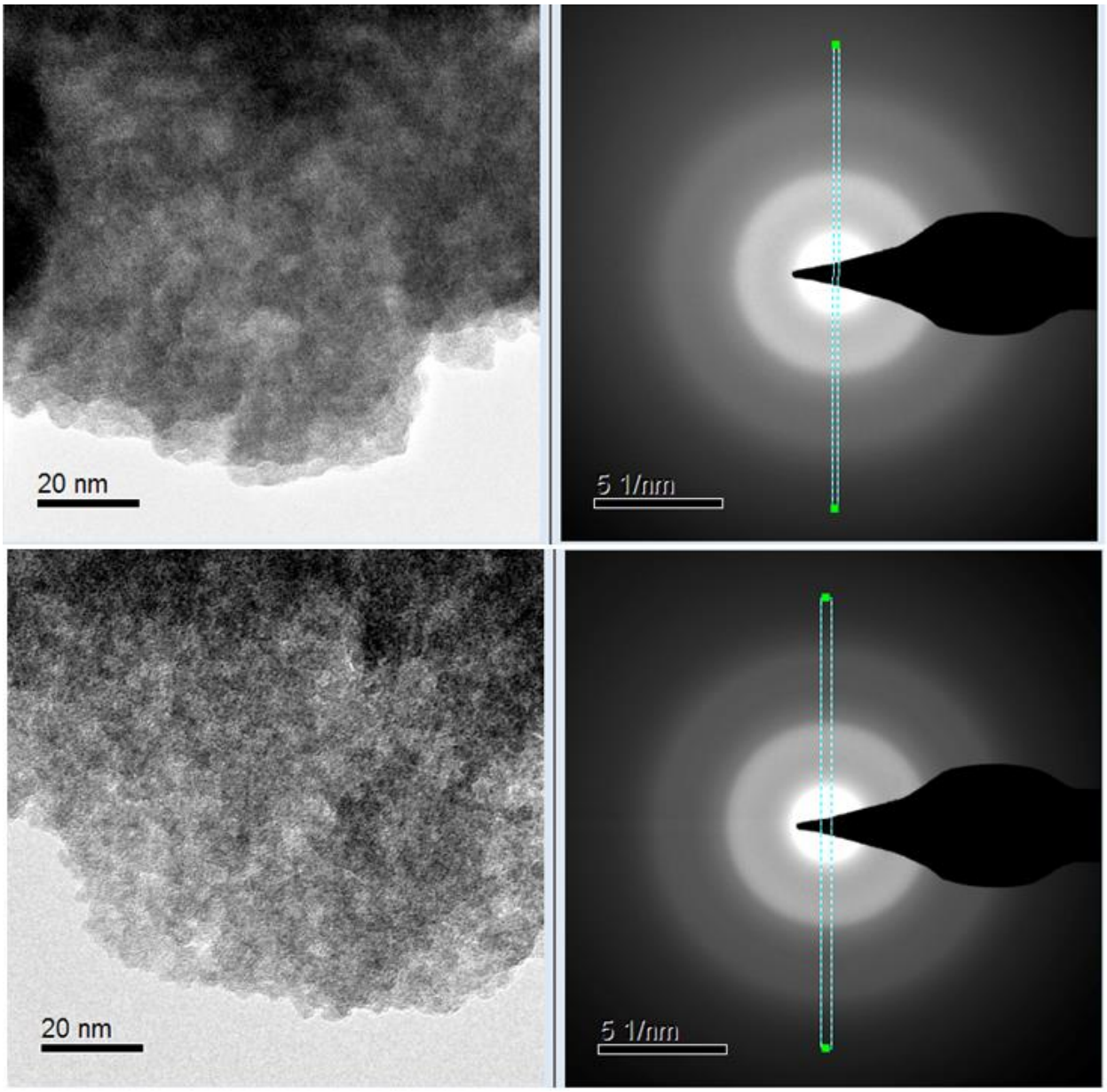

Figure 5-9 TEM analyses of Sb(V)-adsorbed (upper) and co-precipitated ferrihydrite (lower).

6. Conclusions and outlook

6.1 Conclusions

Currently, a number of studies have been carried out concerning the adsorption behavior of Sb(III) and Sb(V) on Fe hydroxides. However, the effect of dissolved silica and the co-precipitation of Sb with ferrihydrite under the Si-rich condition in natural environment have never been studied. Therefore, in this study, the adsorption and co-precipitation of Sb(III) and Sb(V) with ferrihydrite under dissolved silica effect was studied. More importantly, the ETLM was used for analyzing the Sb(III) and Sb(V) adsorption data, which provide a basis for the understanding and prediction of Sb surface speciation on ferrihydrite. To the best of our knowledge, this is the first time it has been considered applying the ETLM for prediction of Sb adsorption. This study presented that both adsorption and co-precipitation methods could be a feasible method for removing Sb from wastewater in terms of the high efficiency and regeneration capability. The main results and general conclusions are summarized as follow:

(1) The X-ray diffraction (XRD) analyses of the precipitates showed two broad diffraction features at approximately 35° and 62° 2θ, which are characteristics of 2-line ferrihydrite, but no significant shifts in peak positions in the ferrihydrite regardless of the Si/Fe ratios. The infrared spectra showed a sharp band at ~930 cm^{-1}, corresponding to asymmetric stretching vibrations of Si-O-Fe bonds which increased in intensity with increasing Si/Fe molar ratios. Further, the surface charge on the precipitates became more negative with increasing Si/Fe molar ratios. The adsorption experiments indicated that Sb(V) was preferentially adsorbed under acidic conditions which decreased dramatically with increasing pH while the adsorption rate of Sb(III) ions was independent of pH. However, the presence of silica suppressed the adsorption of both Sb(III) and Sb(V) ions.

(2) The adsorption data of Sb(V) on ferrihydrite were obtained from this study, conducted under widely various pH, Sb(V) loadings, ionic strength and solid concentrations in NaCl solutions, which were analyzed using ETLM. The adsorption of Sb(V) on ferrihydrite decreased concomitantly with pH, which is consistent with other anionic species on iron oxides, and decreased with ionic strength. The ETLM analysis of the adsorption date suggest that Sb(V)

adsorbs to ferrihydrite via formation of monodentate, mononuclear outer-sphere species and bidentate binuclear inner-species, as shown below:

$$>FeOH + H^+ + Sb(OH)_6^- = > FeOH_2^+\_Sb(OH)_6^-$$

$$2>FeOH + 2H^+ + Sb(OH)_6^- = > Fe_2Sb(OH)_6^+ + 2H_2O$$

The prediction of the surface speciation of Sb(V) on ferrihydrite showed that the inner-sphere species increase concomitantly with decreasing pH, surface Sb(V) loading and increasing solid concentration. The outer-sphere species distribute over a wider range of pH conditions and are more important at lower ionic strengths. Additionally, the outer-sphere species are dominant for pH>5, whereas the inner-sphere species are dominant for pH<5.

While the adsorption of Sb(III) on ferrihydrite constant over a broad range of pH, and ionic strength shown no effect on the Sb(III) adsorption efficiency. The ETLM analysis of the adsorption date suggest that Sb(III) adsorbs to ferrihydrite mainly via formation of binuclear inner-species, as shown below:

$$2>FeOH + Sb(OH)_3 = > (FeO)_2Sb(OH)_2 + 2H_2O$$

$$2>FeOH + Sb(OH)_3 = > (FeO)_2SbO^- + H^+ + 2H_2O$$

$$>FeOH + Sb(OH)_3 = > FeOH_2^+\_SbO(OH)_2^-$$

The prediction of the surface speciation of Sb(III) on ferrihydrite showed that the inner-sphere species dominate a wide range of pH, surface Sb(III) loading and increasing with solid concentration. These formation behaviors of surface species are consistent with those found from spectroscopic studies. The agreements strongly confirm the validity of the present approach, not only for the integration of spectroscopic and bulk adsorption data of Sb on ferrihydrite, but also for making predictions of surface speciation over wide ranges of conditions of relevance to the migration of Sb species in the environment.

(3) This study examined dissolved silica effects on the adsorption and co-precipitation of Sb(III) and Sb(V) with ferrihydrite. The Sb(V) adsorption onto ferrihydrite increased under more acidic conditions. Overall, Sb(III) adsorption was constant over a broad pH range. The adsorption of

Sb(III) and Sb(V) appeared to be significantly affected by the presence of silica, while co-precipitation of Sb(III) and Sb(V) with ferrihydrite was not inhibited by silica. Further, the co-precipitation process took place with higher efficiency than that of the adsorption.

Our findings on the behavior of Sb(III) and Sb(V) adsorption and co-precipitation with ferrihydrite and Si-ferrihydrite have important implications for determining the role of ferrihydrite in controlling the final state of Sb in the environments in which it is released. Although ferrihydrite is an excellent substance for capturing Sb, its use as a medium in a natural Si-rich system should be considered with caution because it will tend towards inhibition of Sb capture induced by the Si-rich environment. However, this may be different in the case of co-precipitation processes. In the present study, we found that silica and Sb(III) and Sb(V) can be incorporated into ferrihydrite and that these three are structurally compatible with ferrihydrite. The co-precipitation process of Sb(III) and Sb(V) would not be greatly influenced by the silica factor. Thus, Sb(III) and Sb(V) co-precipitation with ferrihydrite would be more efficient than Sb(III) and Sb(V) adsorption by ferrihydrite. This finding will be important when making predictions of the final state of Sb associated with ferrihydrite in natural Si-rich systems.

6.2 Outlook

The contamination of Sb in aqueous environment is a big challenge for scientists. More efforts are required to well understand the adsorption and co-precipitation of Sb with ferrihydrite, and it would be of interest to study it according to the following aspects:

1) Spectroscopy evidences are required to further identify the adsorption and co-precipitation of Sb(III) and Sb(V) on ferrihydrite.

2) There are several limitations in the laboratory experiments compared to the natural aquatic environment. The efficiency of ferrihydrite to remove Sb should be studied in different water matrices since the natural environment is a more complex condition. It also would be interesting to apply co-precipitation process of ferrihydrite into the real Sb contaminated waters.

References

Ackermann, S., Gieré, R., Newville, M., Majzlan, J., 2009. Antimony sinks in the weathering crust of bullets from Swiss shooting ranges. Sci. Total Environ. 407, 1669–1682. doi:10.1016/j.scitotenv.2008.10.059

ADAMS, W.A., KASSIM, J.K., 1984. Iron oxyhydroxides in soils developed from Lower Palaeozoic sedimentary rocks in mid-Wales and implications for some pedogenetic processes. J. Soil Sci. doi:10.1111/j.1365-2389.1984.tb00266.x

Ainsworth, N., Cooke, J.A., Johnson, M.S., 1990. Distribution of antimony in contaminated grassland: 1- vegetation and soils. Environ. Pollut. doi:10.1016/0269-7491(90)90165-9

Aksoy, N., Şimşek, C., Gunduz, O., 2009. Groundwater contamination mechanism in a geothermal field: A case study of Balcova, Turkey. J. Contam. Hydrol. doi:10.1016/j.jconhyd.2008.08.006

Ali, I., Gupta, V.K., 2007. Advances in water treatment by adsorption technology. Nat. Protoc. doi:10.1038/nprot.2006.370

Anderson, C.G., 2012. The metallurgy of antimony. Chemie der Erde. doi:10.1016/j.chemer.2012.04.001

Andreae, M.O., Asmodé, J.F., Foster, P., Van't deck, L., 1981. Determination of antimony(III), antimony(V), and methylantimony species in natural waters by atomic absorption spectrometry with hydride generation. Anal. Chem. 53, 1766–1771. doi:10.1021/ac00235a012

Andreae, M.O., Byrd, J.T., Froellch, P.N., 1983. Arsenic, Antimony, Germanium, and Tin in the Tejo Estuary, Portugal: Modeling a Polluted Estuary. Environ. Sci. Technol. doi:10.1021/es00118a008

Appelo, C.A.J., Postma, D., 2004. Geochemistry, groundwater and pollution. CRC press.

Arimoto, R., Duce, R.A., Ray, B.J., Ellis, W.G., Cullen, J.D., Merrill, J.T., 1995. Trace elements in the atmosphere over the North Atlantic. J. Geophys. Res. doi:10.1029/94JD02618

Asami, T., Kubota, M., Saito, S., 1992. Simultaneous determination of antimony and bismuth in

soils by continuous hydride generation-atomic absorption spectrometry. Water, Air, Soil Pollut. doi:10.1007/BF00480266

Baes, C.F., Mesmer, R.E., 1976. The Hydrolysis of Cations. Wiley:New York.

Biswas, B.K., Inoue, J., Kawakita, H., Ohto, K., Inoue, K., 2009. Effective removal and recovery of antimony using metal-loaded saponified orange waste. J. Hazard. Mater. 172, 721–728. doi:10.1016/j.jhazmat.2009.07.055

Brannon, J., Patrick, J.W., 1985. Fixation and mobilization of antimony in sediments. Environ. Pollut. Ser. B Chem. Phys. 9, 107–124. doi:10.1016/0143-148X(85)90027-8

Carlin Jr, J.F., 2000. Antimony. US Geol. Surv. Miner. Commod. Summ. 295–306.

Carlson, L., Schwertmann, U., 1981. Natural ferrihydrites in surface deposits from Finland and their association with silica. Geochim. Cosmochim. Acta 45. doi:10.1016/0016-7037(81)90250-7

CEC, 1976. Council Directive 76/substances discharged into Aquatic Environment of the Community. Off. J. L. 129, 23–29.

Ceriotti, G., Amarasiriwardena, D., 2009. A study of antimony complexed to soil-derived humic acids and inorganic antimony species along a Massachusetts highway. Microchem. J. 91, 85–93. doi:10.1016/j.microc.2008.08.010

Cheng, Z.L., Lam, K.S., Chan, L.Y., Wang, T., Cheng, K.K., 2000. Chemical characteristics of aerosols at coastal station in Hong Kong. I. Seasonal variation of major ions, halogens and mineral dusts between 1995 and 1996. Atmos. Environ. doi:10.1016/S1352-2310(99)00343-X

Ching-kuo Daniel Hsi, Langmuir, D., 1985. Adsorption of uranyl onto ferric oxyhydroxides: Application of the surface complexation site-binding model. Geochim. Cosmochim. Acta 49, 1931–1941. doi:10.1016/0016-7037(85)90088-2

Cismasu, A.C., Michel, F.M., Tcaciuc, A.P., Brown, G.E., 2014. Properties of impurity-bearing ferrihydrite III. Effects of Si on the structure of 2-line ferrihydrite. Geochim. Cosmochim. Acta 133, 168–185. doi:10.1016/j.gca.2014.02.018

Cooper, R., Harrison, A., 2009. The exposure to and health effects of antimony. Indian J. Occup. Environ. Med. doi:10.4103/0019-5278.50716

Cornell, R.M., Schwertmann, U., 2003. The iron oxides: structure, properties, reactions, occurrences and uses. John Wiley & Sons.

Criscenti, L.J., Sverjensky, D.A., 2002. A single-site model for divalent transition and heavy metal adsorption over a range of metal concentrations. J. Colloid Interface Sci. 253, 329–352. doi:10.1006/jcis.2002.8529

Criscenti, L.J., Sverjensky, D.A., 1999. The role of electrolyte anions (ClO-4, NO-3, and Cl-) in divalent metal (M2+) adsorption on oxide and hydroxide surfaces in salt solutions. Am. J. Sci. doi:10.2475/ajs.299.10.828

Cutter, G.A., 1993. METALLOIDS IN WET DEPOSITION ON BERMUDA - CONCENTRATIONS, SOURCES, AND FLUXES. J. Geophys. Res. doi:10.1029/93jd01689

Daus, B., Wennrich, R., 2014. Investigation on stability and preservation of antimonite in iron rich water samples. Anal. Chim. Acta. doi:10.1016/j.aca.2014.08.019

Davis, J., James, R., Leckie, J., 1978. Surface Ionization and Complexation at the Oxide / Water Interface. J. Colloid Interface Sci. 63, 480–499. doi:10.1016/S0021-9797(78)80009-5

Davis, J.A., Kent, D.B., 1990. Surface Complexation Modeling ,in Aqueous Geochemistry. Miner. Interface Geochemistry 23, 177–260.

Dodd, M., Grundy, S.L., Reimer, K.J., Cullen, W.R., 1992. Methylated antimony(V) compounds: Synthesis, hydride generation properties and implications for aquatic speciation. Appl. Organomet. Chem. doi:10.1002/aoc.590060215

Doelsch, E., Masion, A., Rose, J., Stone, W.E.E., Bottero, J.Y., Bertsch, P.M., 2003. Chemistry and structure of colloids obtained by hydrolysis of Fe(III) in the presence of SiO4 ligands. Colloids Surfaces A Physicochem. Eng. Asp. 217, 121–128. doi:10.1016/S0927-7757(02)00566-6

Drever, J.I., 1997. The Geochemistry of Natural Waters: Surface and Groundwater Environments,

436 pp.

Duester, L., Diaz-Bone, R.A., Kösters, J., Hirner, A. V., 2005. Methylated arsenic, antimony and tin species in soils, in: Journal of Environmental Monitoring. doi:10.1039/b508206d

Duester, L., van der Geest, H.G., Moelleken, S., Hirner, A. V., Kueppers, K., 2011. Comparative phytotoxicity of methylated and inorganic arsenic- and antimony species to Lemna minor, Wolffia arrhiza and Selenastrum capricornutum. Microchem. J. 97, 30–37. doi:10.1016/j.microc.2010.05.007

Dyer, L., Fawell, P.D., Newman, O.M.G., Richmond, W.R., 2010. Synthesis and characterisation of ferrihydrite/silica co-precipitates. J. Colloid Interface Sci. 348, 65–70. doi:10.1016/j.jcis.2010.03.056

Dzombak, D.A., Morel, F.M.M., 1990. Surface complexation modeling: hydrous ferric oxide. John Wiley & Sons.

Ellwood, M.J., Maher, W.A., 2002. Arsenic and antimony species in surface transects and depth profiles across a frontal zone: The Chatham Rise, New Zealand. Deep. Res. Part I Oceanogr. Res. Pap. doi:10.1016/S0967-0637(02)00115-2

Filella, M., Belzile, N., Chen, Y.W., 2002a. Antimony in the environment: A review focused on natural waters I. Occurence. Earth-Science Rev. 57, 125–176. doi:10.1016/S0012-8252(01)00070-8

Filella, M., Belzile, N., Chen, Y.W., 2002b. Antimony in the environment: A review focused on natural waters II. Relevant solution chemistry. Earth-Science Rev. 59, 265–285. doi:10.1016/S0012-8252(02)00089-2

Filella, M., Williams, P.A., Belzile, N., 2009. Antimony in the environment: Knowns and unknowns. Environ. Chem. doi:10.1071/EN09007

Fukushi, K., Aoyama, K., Yang, C., Kitadai, N., Nakashima, S., 2013. Surface complexation modeling for sulfate adsorption on ferrihydrite consistent with in situ infrared spectroscopic observations. Appl. Geochemistry 36, 92–103. doi:10.1016/j.apgeochem.2013.06.013

Fukushi, K., Sverjensky, D.A., 2007a. A predictive model (ETLM) for arsenate adsorption and

surface speciation on oxides consistent with spectroscopic and theoretical molecular evidence. Geochim. Cosmochim. Acta 71, 3717–3745. doi:10.1016/j.gca.2007.05.018

Fukushi, K., Sverjensky, D.A., 2007b. A surface complexation model for sulfate and selenate on iron oxides consistent with spectroscopic and theoretical molecular evidence. Geochim. Cosmochim. Acta 71, 1–24. doi:10.1016/j.gca.2006.08.048

Fuller, C.C., Davis, J.A., 1989. Influence of coupling of sorption and photosynthetic processes on trace element cycles in natural waters. Nature. doi:10.1038/340052a0

Gebel, T., 1997. Aresnic and antimony: Comparative approach on mechanistic toxicology. Chem. Biol. Interact. doi:10.1016/S0009-2797(97)00087-2

Grimanis, A.P., Vassilaki-Grimani, M., Griggs, G.B., 1977. Pollution studies of trace elements in sediments from the Upper Saronikos Gulf, Greece. J. Radioanal. Chem. doi:10.1007/BF02519388

Grossl, P.R., Eick, M., Sparks, D.L., Goldberg, S., Ainsworth, C.C., 1997. Arsenate and chromate retention mechanisms on goethite. 2. Kinetic evaluation using a pressure-jump relaxation technique. Environ. Sci. Technol. 31, 321–326. doi:10.1021/es950654l

Guo, X., Wu, Z., He, M., 2009. Removal of antimony(V) and antimony(III) from drinking water by coagulation-flocculation-sedimentation (CFS). Water Res. 43, 4327–4335. doi:10.1016/j.watres.2009.06.033

Guo, X., Wu, Z., He, M., Meng, X., Jin, X., Qiu, N., Zhang, J., 2014. Adsorption of antimony onto iron oxyhydroxides: Adsorption behavior and surface structure. J. Hazard. Mater. 276, 339–345. doi:10.1016/j.jhazmat.2014.05.025

Gürleyük, H., Van Fleet-Stalder, V., Chasteen, T.G., 1997. Confirmation of the Biomethylation of Antimony Compounds. Appl. Organomet. Chem. doi:10.1002/(SICI)1099-0739(199706)11:6<471::AID-AOC590>3.3.CO;2-8

Hayes, K.F., Papelis, C., Leckie, J.O., 1988. Modeling ionic strength effects on anion adsorption at hydrous oxide/solution interfaces. J. Colloid Interface Sci. 125, 717–726. doi:10.1016/0021-9797(88)90039-2

Hayes, K.F., Redden, G., Ela, W., Leckie, J.O., 1991. Surface complexation models: An evaluation of model parameter estimation using FITEQL and oxide mineral titration data. J. Colloid Interface Sci. doi:10.1016/0021-9797(91)90075-J

He, M., 2007. Distribution and phytoavailability of antimony at an antimony mining and smelting area, Hunan, China. Environ. Geochem. Health 29, 209–219. doi:10.1007/s10653-006-9066-9

He, M., Wang, X., Wu, F., Fu, Z., 2012. Antimony pollution in China. Sci. Total Environ. doi:10.1016/j.scitotenv.2011.06.009

He, Z., Liu, R., Liu, H., Qu, J., 2015. Adsorption of Sb(III) and Sb(V) on Freshly Prepared Ferric Hydroxide (FeOxHy). Environ. Eng. Sci. doi:10.1089/ees.2014.0155

Herbst, K.A., Rose, G., Hanusch, K., Schumann, H., Wolf, H.U., 1985. Antimony and antimony compounds. Ullmann's Encycl. Ind. Chem. 3, 55–76.

Hiemstra, T., Barnett, M.O., van Riemsdijk, W.H., 2007. Interaction of silicic acid with goethite. J. Colloid Interface Sci. 310, 8–17. doi:10.1016/j.jcis.2007.01.065

Hiller, E., Lalinská, B., Chovan, M., Jurkovič, Ľ., Klimko, T., Jankulár, M., Hovorič, R., Šottník, P., Fľaková, R., Ženišová, Z., Ondrejková, I., 2012. Arsenic and antimony contamination of waters, stream sediments and soils in the vicinity of abandoned antimony mines in the Western Carpathians, Slovakia. Appl. Geochemistry. doi:10.1016/j.apgeochem.2011.12.005

Ilgen, A.G., Trainor, T.P., 2012. Sb(III) and Sb(V) sorption onto al-rich phases: Hydrous al oxide and the clay minerals kaolinite KGa-1b and oxidized and reduced nontronite NAu-1. Environ. Sci. Technol. doi:10.1021/es203027v

Jackson, T.A., Keller, W.D., 1970. A comparative study of the role of lichens and “inorganic” processes in the chemical weathering of Recent Hawaiian lava flows. Am. J. Sci. doi:10.2475/ajs.269.5.446

Jenkins, R.O., Craig, P.J., Miller, D.P., Stoop, L.C.A.M., Ostah, N., Morris, T.A., 1998. Antimony Biomethylation by Mixed Cultures of Micro-organisms under Anaerobic Conditions. Appl. Organomet. Chem. doi:10.1002/(SICI)1099-0739(199806)12:6<449::AID-AOC719>3.0.CO;2-4

Johnson, C.A., Moench, H., Wersin, P., Kugler, P., Wenger, C., 2005. Solubility of antimony and other elements in samples taken from shooting ranges. J. Environ. Qual. doi:10.2134/jeq2005.0248

Jordan, N., Marmier, N., Lomenech, C., Giffaut, E., Ehrhardt, J.J., 2009. Competition between selenium (IV) and silicic acid on the hematite surface. Chemosphere 75, 129–134. doi:10.1016/j.chemosphere.2008.11.018

Kanematsu, M., Young, T.M., Fukushi, K., Green, P.G., Darby, J.L., 2010. Extended Triple Layer Modeling of Arsenate and Phosphate Adsorption on a Goethite-based Granular Porous Adsorbent. Environ. Sci. Technol. 44, 3388–3394. doi:10.1021/es903658h

Kang, M., Kawasaki, M., Tamada, S., Kamei, T., Magara, Y., 2000. Effect of pH on the removal of arsenic and antimony using reverse osmosis membranes. Desalination. doi:10.1016/S0011-9164(00)90027-4

Kaur, N., Gräfe, M., Singh, B., Kennedy, B., 2009. Simultaneous incorporation of Cr, Zn, Cd, and Pb in the goethite structure. Clays Clay Miner. 57, 234–250. doi:10.1346/CCMN.2009.0570210

Kersten, M., Kriews, M., Förstner, U., 1991. Partitioning of trace metals released from polluted marine aerosols in coastal seawater. Mar. Chem. doi:10.1016/S0304-4203(09)90060-3

Kolbe, F., Weiss, H., Morgenstern, P., Wennrich, R., Lorenz, W., Schurk, K., Stanjek, H., Daus, B., 2011. Sorption of aqueous antimony and arsenic species onto akaganeite. J. Colloid Interface Sci. doi:10.1016/j.jcis.2011.01.095

Koparal, S.S., Özgür, R., Öğütveren, Ü.B., Bergmann, H., 2004. Antimony removal from model acid solutions by electrodeposition. Sep. Purif. Technol. doi:10.1016/j.seppur.2003.09.001

Koretsky, C., 2000. The significance of surface complexation reactions in hydrologic systems: A geochemist's perspective. J. Hydrol. doi:10.1016/S0022-1694(00)00215-8

Krachler, M., Emons, H., Zheng, J., 2001. Speciation of antimony for the 21st century: Promises and pitfalls. TrAC - Trends Anal. Chem. 20, 79–90. doi:10.1016/S0165-9936(00)00065-0

Krupka, K.M., Serne, R.J., 2002. Geochemical Factors Affecting the Behavior of Antimony,

Cobalt, Europium , Technetium, and Uranium in Vadose Sediments, PNNL-14126.

Leuz, A.K., Johnson, C.A., 2005. Oxidation of Sb(III) to Sb(V) by O2 and H2O2 in aqueous solutions. Geochim. Cosmochim. Acta 69, 1165–1172. doi:10.1016/j.gca.2004.08.019

Leuz, A.K., Mönch, H., Johnson, C.A., 2006. Sorption of Sb(III) and Sb(V) to goethite: Influence on Sb(III) oxidation and mobilization. Environ. Sci. Technol. 40, 7277–7282. doi:10.1021/es061284b

Lichti, K. a., Ko, M., Wallis, L., 2015. Galvanic corrosion study of carbon steel to arsenic and antimony couples. Geothermics 58, 15–21. doi:10.1016/j.geothermics.2015.07.006

Manceau, A., 2012. Critical evaluation of the revised akdalaite model for ferrihydrite - Reply. Am. Mineral. 97, 255–256. doi:10.2138/am.2012.3954

Mathys, R., Dittmar, J., Johnson, C.A., Krähenbühl, P., fédéral de l'environnement, S.O., 2007. Antimony in Switzerland: a substance flow analysis. Federal Office for the Environment FOEN.

McComb, K.A., Craw, D., McQuillan, A.J., 2007. ATR-IR spectroscopic study of antimonate adsorption to iron oxide. Langmuir. doi:10.1021/la7012667

Michel, F.M., Ehm, L., Antao, S.M., Lee, P.L., Chupas, P.J., Liu, G., Strongin, D.R., Schoonen, M.A.A., Phillips, B.L., Parise, J.B., 2007. The Structure of Ferrihydrite, a Nanocrystalline Material. Science (80-.). 316, 1726–1729. doi:10.1126/science.1142525

Mitsunobu, S., Harada, T., Takahashi, Y., 2006. Comparison of antimony behavior with that of arsenic under various soil redox conditions. Environ. Sci. Technol. 40, 7270–7276. doi:10.1021/es060694x

Mitsunobu, S., Muramatsu, C., Watanabe, K., Sakata, M., 2013. Behavior of antimony(V) during the transformation of ferrihydrite and its environmental implications. Environ. Sci. Technol. 47, 9660–9667. doi:10.1021/es4010398

Mitsunobu, S., Takahashi, Y., Terada, Y., Sakata, M., 2010. Antimony(V) incorporation into synthetic ferrihydrite, goethite, and natural iron oxyhydroxides. Environ. Sci. Technol. 44, 3712–3718. doi:10.1021/es903901e

Mittal, V.K., Bera, S., Narasimhan, S. V., Velmurugan, S., 2013. Adsorption behavior of antimony(III) oxyanions on magnetite surface in aqueous organic acid environment. Appl. Surf. Sci. doi:10.1016/j.apsusc.2012.12.010

Mohapatra, M., Sahoo, S.K., Mohanty, C.K., Das, R.P., Anand, S., 2005. Effect of Ce(IV) doping on formation of goethite and its transformation to hematite. Mater. Chem. Phys. 94, 417–422. doi:10.1016/j.matchemphys.2005.05.024

Morel, F.M.M., Hering, J.G., Hering, J.G., others, 1993. Principles and applications of aquatic chemistry. John Wiley & Sons.

Nagata, T., Fukushi, K., 2010. Prediction of iodate adsorption and surface speciation on oxides by surface complexation modeling. Geochim. Cosmochim. Acta 74, 6000–6013. doi:10.1016/j.gca.2010.08.002

Nagata, T., Fukushi, K., Takahashi, Y., 2009. Prediction of iodide adsorption on oxides by surface complexation modeling with spectroscopic confirmation. J. Colloid Interface Sci. 332, 309–316. doi:10.1016/j.jcis.2008.12.037

Nakamura, Y., Tokunaga, T., 1996. Antimony in the aquatic environment in North Kyushu district of Japan, in: Water Science and Technology. doi:10.1016/S0273-1223(96)00734-2

Navarro, P., Alguacil, F.J., 2002. Adsorption of antimony and arsenic from a copper electrorefining solution onto activated carbon. Hydrometallurgy. doi:10.1016/S0304-386X(02)00108-1

Okkenhaug, G., Amstätter, K., Lassen Bue, H., Cornelissen, G., Breedveld, G.D., Henriksen, T., Mulder, J., 2013. Antimony (Sb) contaminated shooting range soil: Sb mobility and immobilization by soil amendments. Environ. Sci. Technol. 47, 6431–6439. doi:10.1021/es302448k

Okkenhaug, G., Zhu, Y.G., He, J., Li, X., Luo, L., Mulder, J., 2012. Antimony (Sb) and Arsenic (As) in Sb mining impacted paddy soil from Xikuangshan, China: Differences in mechanisms controlling soil sequestration and uptake in Rice. Environ. Sci. Technol. 46, 3155–3162. doi:10.1021/es2022472

Oorts, K., Smolders, E., Degryse, F., Buekers, J., Gascó, G., Cornelis, G., Mertens, J., 2008.

Solubility and toxicity of antimony trioxide (Sb2O3) in soil. Environ. Sci. Technol. 42, 4378–4383. doi:10.1021/es703061t

Organization, W.H., 2004. Guidelines for drinking-water quality: recommendations. World Health Organization.

Pakzadeh, B., Batista, J.R., 2011. Surface complexation modeling of the removal of arsenic from ion-exchange waste brines with ferric chloride. J. Hazard. Mater. 188, 399–407. doi:10.1016/j.jhazmat.2011.01.117

Papakostidis, G., Grimanis, A.P., Zafiropoulos, D., Griggs, G.B., Hopkins, T.S., 1975. Heavy metals in sediments from the Athens sewage outfall area. Mar. Pollut. Bull. doi:10.1016/0025-326X(75)90170-8

Pokrovski, G.S., Schott, J., Farges, F., Hazemann, J.-L., 2003. Iron (III)-silica interactions in aqueous solution: insights from X-ray absorption fine structure spectroscopy. Geochim. Cosmochim. Acta 67, 3559–3573.

Pokrovsky, O.S., Probst, A., Leviel, E., Liao, B., 2012. Interactions between cadmium and lead with acidic soils: Experimental evidence of similar adsorption patterns for a wide range of metal concentrations and the implications of metal migration. J. Hazard. Mater. 199–200, 358–366. doi:10.1016/j.jhazmat.2011.11.027

Qi, P., Pichler, T., 2016. Sequential and simultaneous adsorption of Sb(III) and Sb(V) on ferrihydrite: Implications for oxidation and competition. Chemosphere 145, 55–60. doi:10.1016/j.chemosphere.2015.11.057

Rakshit, S., Sarkar, D., Datta, R., 2015. Surface complexation of antimony on kaolinite. Chemosphere 119, 349–354. doi:10.1016/j.chemosphere.2014.06.070

Rakshit, S., Sarkar, D., Punamiya, P., Datta, R., 2011. Antimony sorption at gibbsite-water interface. Chemosphere. doi:10.1016/j.chemosphere.2011.03.028

Reimann, C., Matschullat, J., Birke, M., Salminen, R., 2010. Antimony in the environment: Lessons from geochemical mapping. Appl. Geochemistry. doi:10.1016/j.apgeochem.2009.11.011

Ritchie, V.J., Ilgen, A.G., Mueller, S.H., Trainor, T.P., Goldfarb, R.J., 2013. Mobility and chemical fate of antimony and arsenic in historic mining environments of the Kantishna Hills district, Denali National Park and Preserve, Alaska. Chem. Geol. doi:10.1016/j.chemgeo.2012.10.016

Riveros, P.A., 2010. The removal of antimony from copper electrolytes using amino-phosphonic resins: Improving the elution of pentavalent antimony. Hydrometallurgy. doi:10.1016/j.hydromet.2010.08.008

Russell, J.D., 1979. Infrared spectroscopy of ferrihydrite: Evidence for the presence ofstructural hydroxyl groups. Clay Miner. 14, 109–114. doi:10.1180/claymin.1979.014.2.03

S. Korichi, A. Elias, A. Mefti, 2009. Characterization of smectite after acid activation with microwave irradiation. Appl. Clay Sci. 42, 432–438. doi:10.1016/j.clay.2008.04.014

Sahai, N., Sverjensky, D.A., 1998. GEOSURF: A computer program for modeling adsorption on mineral surfaces from aqueous solution. Comput. Geosci. 24, 853–873.

Scheinost, A.C., Rossberg, A., Vantelon, D., Xifra, I., Kretzschmar, R., Leuz, A.K., Funke, H., Johnson, C.A., 2006. Quantitative antimony speciation in shooting-range soils by EXAFS spectroscopy. Geochim. Cosmochim. Acta 70, 3299–3312. doi:10.1016/j.gca.2006.03.020

Schindler, P.W., 1990. Co-adsorption of metal ions and organic ligands; formation of ternary surface complexes. Rev. Mineral. Geochemistry 23, 281–307.

Schwertmann, U., Cornell, R.M., 2008. Iron oxides in the laboratory. John Wiley & Sons.

Schwertmann, U., Schulze, D.G., Murad, E., 1982. Identification of Ferrihydrite in Soils by Dissolution Kinetics, Differential X-ray Diffraction, and Mossbauer Spectroscopy. Soil Sci .Soc.Am.J. doi:10.2136/sssaj1982.03615995004600040040x

Seehra, M.S., Roy, P., Raman, A., Manivannan, A., 2004. Structural investigations of synthetic ferrihydrite nanoparticles doped with Si. Solid State Commun. 130, 597–601. doi:10.1016/j.ssc.2004.03.022

Shan, C., Ma, Z., Tong, M., 2014. Efficient removal of trace antimony(III) through adsorption by hematite modified magnetic nanoparticles. J. Hazard. Mater.

doi:10.1016/j.jhazmat.2014.01.020

Sposito, G., 1990. Molecular models of iron adsorption on mineral surfaces. Rev. Mineral. Geochemistry 23, 261–279.

Sposito, G., others, 1984. The surface chemistry of soils. Oxford university press.

Steinnes, E., 1990. Lead, cadmium and other metals in scandinavian surface waters, with emphasis on acidification and atmospheric deposition. Environ. Toxicol. Chem. doi:10.1002/etc.5620090702

Stemmer, K.L., 1976. Pharmacology and toxicology of heavy metals: Antimony. Pharmacol.Ther.Ser.a 1, 157–160. doi:10.1016/0362-5478(76)90005-X

Stumm, W., 1992. Chemistry of the solid-water interface. Wiley, New York.

Stumm, W., Morgan, J.J., 2012. Aquatic chemistry: chemical equilibria and rates in natural waters. John Wiley & Sons.

Sun, Y.C., Yang, J.Y., Tzeng, S.R., 1999. Rapid determination of molybdate in natural waters by coprecipitation and neutron activation analysis. Analyst 124, 421–424. doi:10.1039/a809596e

Sverjensky, D.A., 2005. Prediction of surface charge on oxides in salt solutions: Revisions for 1:1 (M+L-) electrolytes. Geochim. Cosmochim. Acta 69, 225–257. doi:10.1016/j.gca.2004.05.040

Sverjensky, D.A., 2003. Standard states for the activities of mineral surface sites and species. Geochim. Cosmochim. Acta 67, 17–28. doi:10.1016/S0016-7037(02)01074-8

Sverjensky, D.A., Fukushi, K., 2006a. Anion adsorption on oxide surfaces: Inclusion of the water dipole in modeling the electrostatics of ligand exchange. Environ. Sci. Technol. 40, 263–271. doi:10.1021/es051521v

Sverjensky, D.A., Fukushi, K., 2006b. A predictive model (ETLM) for As(III) adsorption and surface speciation on oxides consistent with spectroscopic data. Geochim. Cosmochim. Acta 70, 3778–3802. doi:10.1016/j.gca.2006.05.012

Swedlund, P.J., Miskelly, G.M., McQuillan, A.J., 2010. Silicic acid adsorption and

oligomerization at the ferrihydrite - Water interface: Interpretation of ATR-IR spectra based on a model surface structure. Langmuir 26, 3394–3401. doi:10.1021/la903160q

Swedlund, P.J., Miskelly, G.M., McQuillan, A.J., 2009. An attenuated total reflectance IR study of silicic acid adsorbed onto a ferric oxyhydroxide surface. Geochim. Cosmochim. Acta 73, 4199–4214. doi:10.1016/j.gca.2009.04.007

Swedlund, P.J., Webster, J.G., 1999. Adsorption and polymerisation of silicic acid on ferrihydrite, and its effect on arsenic adsorption. Water Res. 33, 3413–3422. doi:10.1016/S0043-1354(99)00055-X

Tella, M., Pokrovski, G.S., 2009. Antimony(III) complexing with O-bearing organic ligands in aqueous solution: An X-ray absorption fine structure spectroscopy and solubility study. Geochim. Cosmochim. Acta. doi:10.1016/j.gca.2008.10.014

Tighe, M., Lockwood, P., Wilson, S., 2005. Adsorption of antimony(v) by floodplain soils, amorphous iron(III) hydroxide and humic acid, in: Journal of Environmental Monitoring. doi:10.1039/b508302h

Tipping, E., Woof, C., Cooke, D., 1981. Iron oxide from a seasonally anoxic lake. Geochim. Cosmochim. Acta. doi:10.1016/0016-7037(81)90275-1

UNEP, 2001. BASEL CONVENTION on the The Basel Convention on the Control of Transboundary Movements of Hazardous Wastes and Their Disposal: Protocol on Liability and Compensation. Ecol. Law Q. 28, 120. doi:10.2307/24114136

Ungureanu, G., Santos, S., Boaventura, R., Botelho, C., 2015. Arsenic and antimony in water and wastewater: Overview of removal techniques with special reference to latest advances in adsorption. J. Environ. Manage. doi:10.1016/j.jenvman.2014.12.051

USEPA, 1979. Water Related Fate of the 129 Priority Pollutants. USEPA, Washington, DC 1, DOC. 745-R-00-007.

Vithanage, M., Rajapaksha, A.U., Dou, X., Bolan, N.S., Yang, J.E., Ok, Y.S., 2013. Surface complexation modeling and spectroscopic evidence of antimony adsorption on iron-oxide-rich red earth soils. J. Colloid Interface Sci. 406, 217–24. doi:10.1016/j.jcis.2013.05.053

Wang, H., Chen, F., Mu, S., Zhang, D., Pan, X., Lee, D.J., Chang, J.S., 2013. Removal of antimony (Sb(V)) from Sb mine drainage: Biological sulfate reduction and sulfide oxidation-precipitation. Bioresour. Technol. doi:10.1016/j.biortech.2013.08.002

Wang, L., Wan, C., Zhang, Y., Lee, D.-J., Liu, X., Chen, X., Tay, J.-H., 2015. Mechanism of enhanced Sb(V) removal from aqueous solution using chemically modified aerobic granules. J. Hazard. Mater. 284, 43–49. doi:10.1016/j.jhazmat.2014.10.041

Wang, X., He, M., Lin, C., Gao, Y., Zheng, L., 2012. Antimony(III) oxidation and antimony(V) adsorption reactions on synthetic manganite. Chemie der Erde - Geochemistry 72, 41–47. doi:10.1016/j.chemer.2012.02.002

Wang, X., He, M., Xi, J., Lu, X., 2011. Antimony distribution and mobility in rivers around the world's largest antimony mine of Xikuangshan, Hunan Province, China. Microchem. J. 97, 4–11. doi:10.1016/j.microc.2010.05.011

Waychunas, G.. A., Rea, B.. A., Fuller, C.. C., Davis, J.. A., 1993. Surface chemistry of ferrihydrite: Part 1.EXAFS studies ongeometrie of coprecipitated and adsorbed arsenate. Geochim. Cosmochim. Acta 57, 2251–2269. doi:10.1016/0016-7037(93)90567-G

Westerhoff, P., Prapaipong, P., Shock, E., Hillaireau, A., 2008. Antimony leaching from polyethylene terephthalate (PET) plastic used for bottled drinking water. Water Res. 42, 551–556. doi:10.1016/j.watres.2007.07.048

Wilson, N.J., Craw, D., Hunter, K., 2004. Antimony distribution and environmental mobility at an historic antimony smelter site, New Zealand. Environ. Pollut. doi:10.1016/j.envpol.2003.10.014

Wu, Z., He, M., Guo, X., Zhou, R., 2010. Removal of antimony (III) and antimony (V) from drinking water by ferric chloride coagulation: Competing ion effect and the mechanism analysis. Sep. Purif. Technol. doi:10.1016/j.seppur.2010.10.006

Xi, J., He, M., Lin, C., 2011. Adsorption of antimony(III) and antimony(V) on bentonite: Kinetics, thermodynamics and anion competition. Microchem. J. doi:10.1016/j.microc.2010.05.017

Xi, J., He, M., Zhang, G., 2014. Antimony adsorption on kaolinite in the presence of competitive

anions. Environ. Earth Sci. 71, 2989–2997. doi:10.1007/s12665-013-2673-8

Xu, Y.-H., Ohki, A., Maeda, S., 2001. Adsorption and removal of antimony from aqueous solution by an activated Alumina: 1. Adsorption capacity of adsorbent and effect of process variables. Toxicol. Environ. Chem. 80, 133–144.

Zhang, P., Sparks, D.L., 1990. Kinetics of Selenate and Selenite Adsorption/Desorption at the Goethite/Water Interface. Environ. Sci. Technol. 24, 1848–1856. doi:10.1021/es00082a010

Zhao, X., Dou, X., Mohan, D., Pittman, C.U., Ok, Y.S., Jin, X., 2014. Antimonate and antimonite adsorption by a polyvinyl alcohol-stabilized granular adsorbent containing nanoscale zero-valent iron. Chem. Eng. J. doi:10.1016/j.cej.2014.02.096

Zhou, S., Sato, T., Otake, T., 2018. Dissolved Silica Effects on Adsorption and Co-Precipitation of Sb(III) and Sb(V) with Ferrihydrite. Minerals 8, 101. doi:10.3390/min8030101

Zhu, J., Wu, F., Pan, X., Guo, J., Wen, D., 2011. Removal of antimony from antimony mine flotation wastewater by electrocoagulation with aluminum electrodes. J. Environ. Sci. doi:10.1016/S1001-0742(10)60550-5